29B X-732-66-147 END

NASA TM X- 55711

3 BALLOON SOLAR OBSERVATORY SYSTEM 6 pg

9 APRIL 1966 10

GODDARD SPACE FLIGHT CENTER
GREENBELT, MARYLAND 3

RQ 743967

BALLOON SOLAR OBSERVATORY SYSTEM

Date: April 1966

The design and development of the Balloon Solar Observatory was accomplished through the efforts of the following people.

6 Paul Fahlstrom ET AL 12-1	Project Engineer
Walter Nagel	Asst. Project Engineer & Servo Design
Robert Fulcher	Logic, Systems Engineering & Test
Robert Estes	Equatorial Computer
Lawrence Draper	Sun Sensor
Frank Cepollina	Structure & Mechanical Design
Gene Lapura	Mechanical Design and Layout
Robert Sava	Electronic Technician and Fabrication
Edward Lewis	Design and Drafting

The authors wish to acknowledge the significant contributions of the following: William Hibbard for the initial equatorial computer concept; William Limberis for the filter design; Clarence Cantor, William Palmer, David Small and Ralph Harms for their technical assistance; and the experimenters - Kenneth Frost, Dr. Henry Horstman and Ed Rothe - for their guidance and support. The authors are also indebted to many additional Goddard personnel in Fabrication, Test and Evaluation and elsewhere for their support.

TABLE OF CONTENTS

I. Introduction

Balloon borne payloads are used for conducting aerospace experiments primarily because of their relatively low cost. Pointed experiments do require some form of attitude control, however, and the design and development of such a system can become expensive. This paper describes the design, development and testing of a relatively inexpensive balloon solar observatory system suitable for scientific experiments where pointing accuracy is not paramount. The system functions in two primary modes: solar and computer. The solar mode is used to point an experiment to the center of the sun and has an accuracy of better than ± 1 degree. The computer mode is used to point an experiment toward any selected points in the celestial sphere, without benefit of radiating stimuli, and has an accuracy of better than ± 3 degrees over a period of 10 hours. In addition to the primary modes of operation, there are a number of secondary modes such as back-azimuth, launch-recovery, etc. Photographs of the system are shown at the end of this report.

II. System Description

A typical balloon system is shown in Figure 1. The gondola is attached to the balloon via a parachute (multifilar suspension). The spreader plates and ring provide the proper stiffness to the multifilar suspension for experiment pointing. Recovery is made by separation of the release mechanism, the parachute providing a reasonable descent. Ground impact loads are absorbed by a shock mitigator fabricated from a frangible material. The azimuth bearing precludes overworking of the azimuth control loop in the event the balloon is rotating rapidly during ascent; it is also required to aid pointing stability. The gondola itself is made up of a gondola assembly, inertia ring assembly and a mast assembly. The gondola assembly is mated to the inertia ring and mast assemblies by ball bearings. Azimuth and elevation control of the experiment enables instrument pointing to any desired direction. The proper angles are generated by a computer. The azimuth servo drive, which is attached to the gondola assembly, torques against the mast and inertia ring assemblies to provide azimuthal motion of the experiment using magnetic north as a reference. The elevation servo torques against the gondola assembly to obtain elevation motion using the pendulosity of the suspension system to provide an elevation reference. The pointing of the experiment during flight is pre-programmed by means of a rotating cam programmer. The balloon system is powered by batteries. Experiment data, along with some key system operation data, is recorded on board, using a tape recorder.

In order to accomplish the experimenters' objectives, the system operates in the following modes:

1. Launch-Recovery
2. Solar Tracking
3. Stellar Tracking
4. Back-Azimuth
5. Elevation Command

These modes are not independent. For example, mode 4 occurs while the system is in mode 2 or 3. A description of each mode follows:

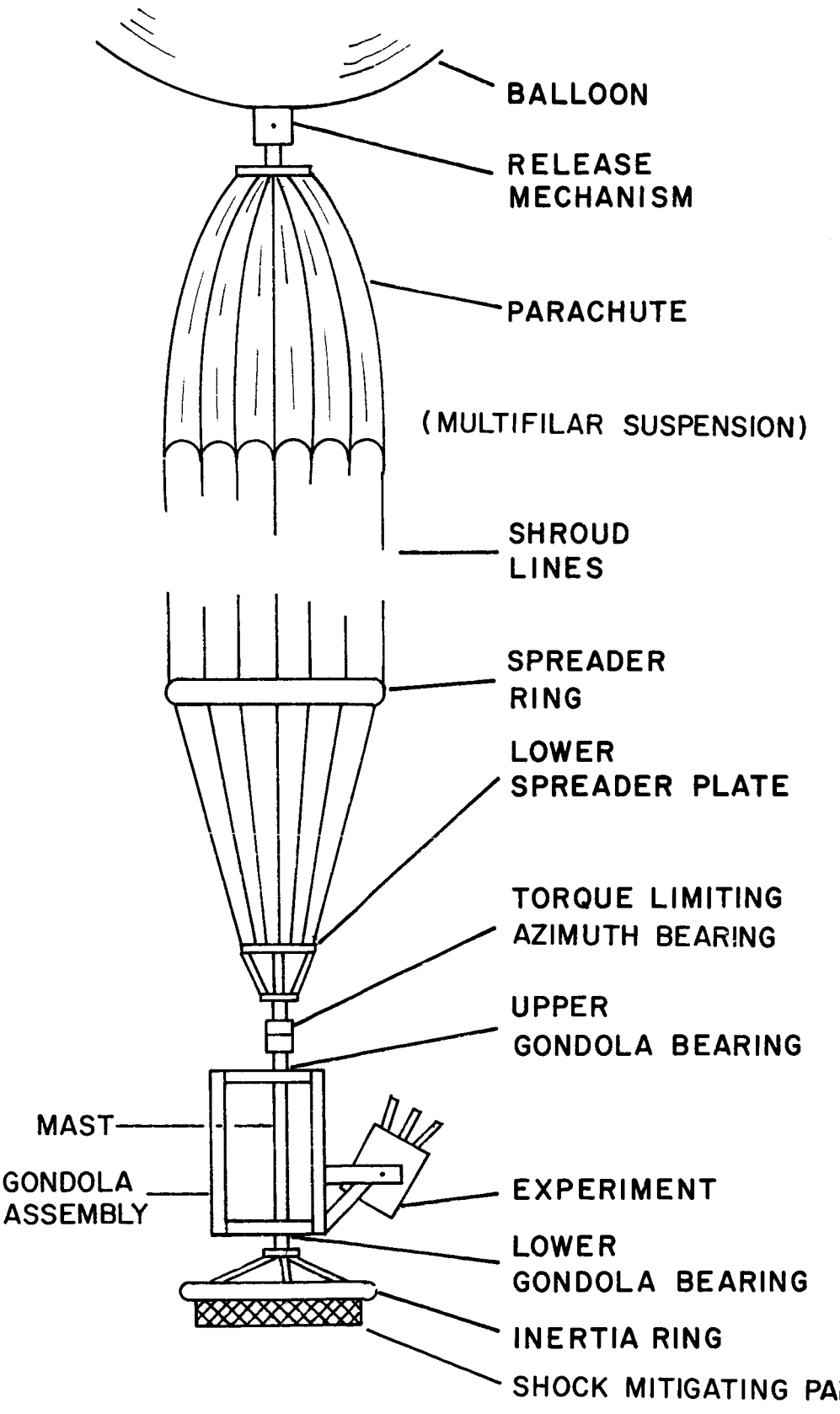

FIGURE 1 TYPICAL BALLOON SYSTEM

Launch-Recovery

This mode is used when the system is either being launched or recovered. The launch and recovery phases of the mode have the same implementation, and the system status during recovery is the same as during launch. The launch phase of this mode is begun on the ground and terminates with the pointing modes (modes 2 through 5 above) beginning at approximately 80,000 feet altitude. Following the desired flight time, the recovery phase of this mode is initiated. During this mode, the system is essentially de-energized.

Solar Tracking

In this mode, the experiment is pointed to the center of the sun. Error signals for azimuth and elevation control are provided by a sun sensor using matched silicon detectors.

Stellar Tracking

In this mode, the experiment is pointed, open loop, to any desired point in the celestial sphere. This is accomplished by resolving the right ascension and declination angles through the angular variables associated with the balloon's geographic position and earth's rotation into experiment azimuth and elevation angles. This is performed with a chain of electrical induction resolvers.

Back Azimuth

In this mode, the gondola slews 180 degrees in azimuth from its solar or stellar mode target, while elevation is maintained at its last value prior to the initiation of the mode.

Elevation Command

In this mode, the experiment is commanded to point up, down, or horizontal, relative to the gondola. This is accomplished by placing the system in the stellar tracking mode and supplying reference voltages to the elevation resolver.

III. Control System

A. Logic

Introduction

The logic required to select and control system modes is implemented by relays located appropriately throughout the system. These relays are primarily controlled by a motor-driven cam programmer which consists of 16 adjustable cams and their associated switches. (Eight of these cams and switches are for experimenter usage.) Additional logic hardware consists of a "time zero" switch, a barometric switch and 24 hour launch-recovery cam, a logic solar cell and ultra-sensitive relay, and a "cam rotating" light. A discussion of the functioning of these components to accomplish the system modes follows. Figure 2 is a complete diagram of the system logic.

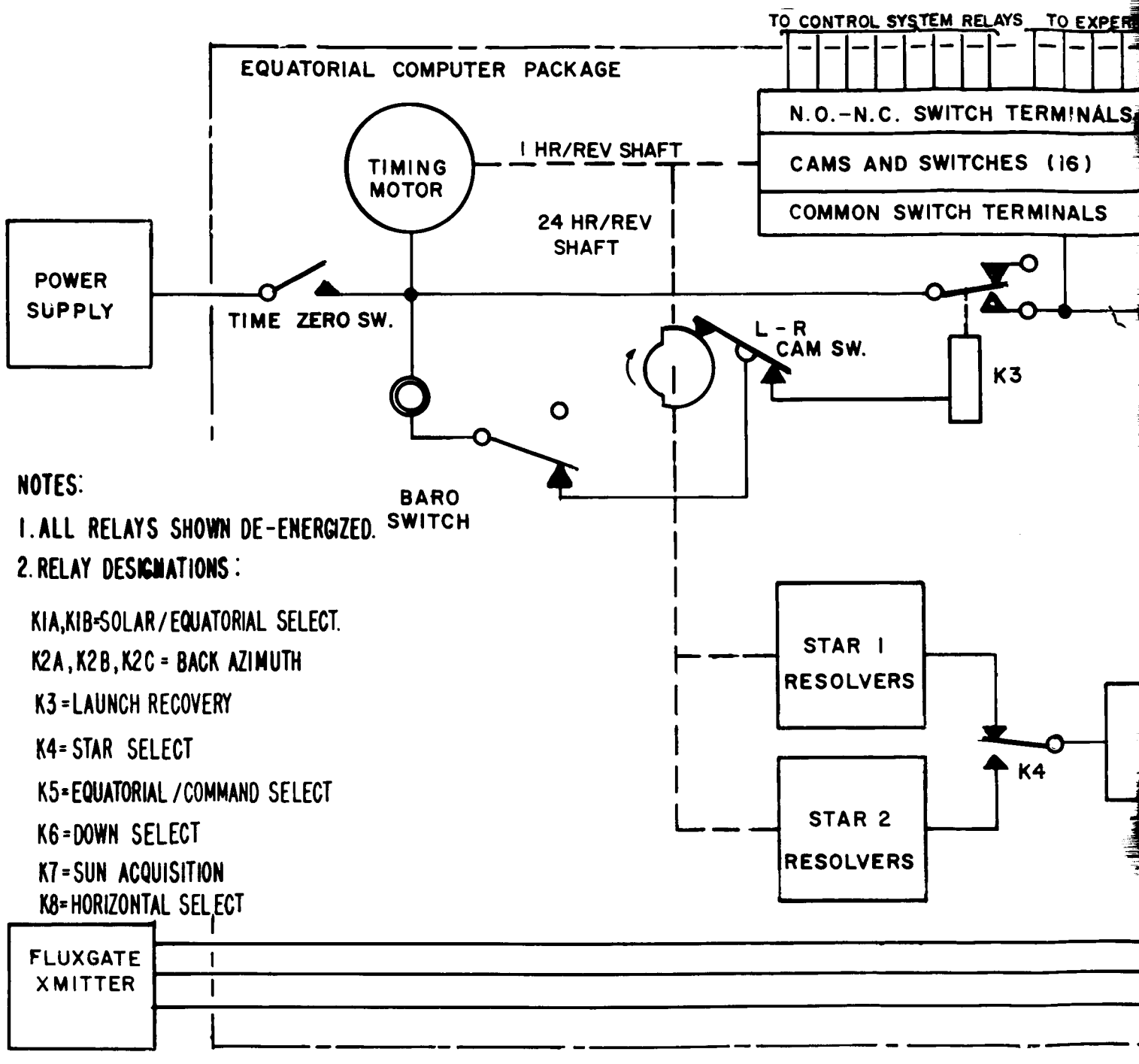

BALLOON SOLA

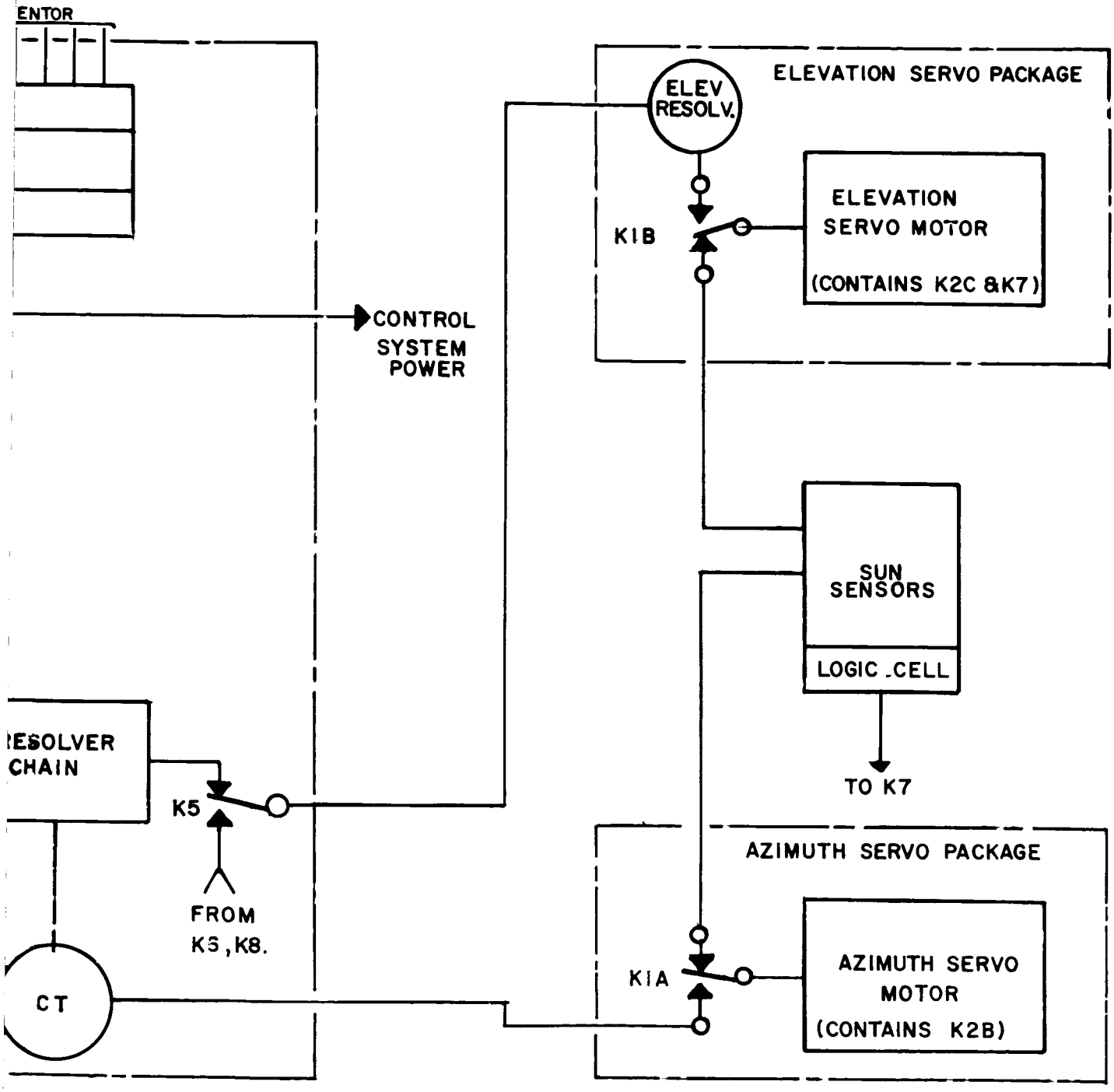

R OBSERVATORY SYSTEM

FIGURE 2

Mode Logic

Launch-Recovery

The launch phase of this mode is begun by closing the "time zero" switch. This provides battery power to the cam programmer motor which rotates the 16 cams, the launch-recovery cam, and the earth rate resolvers in the computing resolver chain. This latter function requires that the closing of the switch be precisely coordinated with some time reference such as WWV (National Bureau of Standards radio station). When the "time zero" switch is closed, the launch recovery relay energizes, preventing electrical power from being distributed to the system. The launch-recovery relay is energized through both the closed barometric switch and the switch associated with the launch-recovery cam, since these switches are in series with the relay coil. Only one switch, of the 16 associated with the cam programmer, is effective at this time. This switch, and the cam associated with it, is used to alternately turn off or on the "cam rotating" light. Monitoring of this light until the instant of launch assures that all cams are rotating and that the earth rate resolvers are being driven properly. The launch phase of this mode is terminated by the opening of the barometric switch when the balloon reaches altitude. (In the event that the barometric switch fails to open, the launch-recovery relay will be de-energized a short time later by the launch-recovery cam switch.) Once the launch-recovery relay is de-energized, power is distributed throughout the system, and the cam programmer switches become effective in sequencing the system through the pre-programmed flight modes. The cam programmer rotates at a nominal rate of one revolution per hour, so the mode sequence pre-programmed on its cams repeats itself each hour. The launch-recovery cam switch is set to close just prior to the end of the flight, so that when approximately 80,000 feet is reached, the launch-recovery relay will be energized by the closing of the barometric switch. When the relay is energized, power is again removed from the system and the system is prepared for recovery. During the recovery phase, as in the launch phase of this mode, the cam programmer motor continues to operate. It should be noted that when the cam programmer switches become effective, following the launch phase, the pre-programmed sequence may be at any point in its cycle.

Solar Tracking

In this mode, no relays are energized. The solar/stellar relays connect the elevation and azimuth solar cells to their respective servo loops, resulting in solar tracking. The control field of the elevation loop servo motor is kept open in this mode, until the sun is adequately acquired in azimuth. This is accomplished by a logic solar cell connected directly to an ultra-sensitive relay. The ultra-sensitive relay in turn controls 28 volts DC to the sun acquisition relay in the elevation loop. During this mode, the de-energized state of the solar/stellar relay connects a phase shifting capacitor into the elevation servo loops, to improve servo performance.

Stellar Tracking

In this mode, the solar/stellar relays are energized, connecting the azimuth control transformer and the elevation resolver to their respective servo loops. The state of the star select relay, controlled by the cam programmer, determines which of two pre-set star targets is tracked.

Back Azimuth

Back azimuth is accomplished with "back azimuth relays" in the elevation and azimuth servo loops and in the azimuth resolver nulling loop. Whether back azimuth is called for in the solar or stellar mode, elevation is maintained by opening of the elevation servo motor control field with the back azimuth relay located in the elevation servo loop. There is a difference in implementation for the solar and stellar modes in the azimuth case, however. When back azimuth occurs in the solar mode, the signal polarity is switched on the control field of the azimuth servo motor, and a small bias voltage is added to drive off any null which may exist. This is accomplished by the "back azimuth relay" located in the azimuth servo loop, and results in the gondola stable null shifting 180°, producing the desired azimuth reorientation. When back azimuth occurs in the stellar mode, the same concept is used, but the polarity reversal and bias is introduced in the loop which nulls the azimuth resolver. This is accomplished by the "back azimuth relay" located in the azimuth resolver nulling loop. In the stellar mode case, the "back azimuth relay" in the azimuth servo is inhibited from operating because the two reversals would cancel. In the case of back azimuth in the solar mode, both reversals are allowed, since the reversal in the resolver nulling loop has no effect.

Elevation Command

Elevation command is accomplished by switching fixed voltages to the stator windings of the elevation resolver while the system is in the stellar tracking mode. Azimuth orientation during elevation commands is that corresponding to the stellar target selected. When the stellar/ command relay is energized, the normal resolver chain input to the elevation resolver stator windings is removed and replaced by a reference voltage on one winding and a short on the other. This results in the experiment pointing up. Pointing down is accomplished by energizing the down select relay, which reverses the polarity of the voltage being applied to the winding not shorted. Pointing horizontal is accomplished by returning to the case of only the stellar/command relay energized, but further energizing the horizontal select relay. This results in the reference voltage now being applied to the stator winding which is shorted when only the stellar/command relay is energized, and shorts the other stator winding.

Pre-Programmed Experimenter's Sequences

The modes discussed are available to allow the experimenters to set up pre-programmed sequences on the cam programmer to achieve their scientific objectives. The use of these modes on three typical sequences is illustrated in Figure 3. The corresponding relay duty cycles are shown in Figure 4.

Special Logic Notes

This section describes some of the more detailed features of the balloon system logic. Included are discussions of setting the launch-recovery cam, cam overlap, back azimuth cams, ratio change gears, elevation blind spot, and cam-resolver drive motor.

Setting the Launch-Recovery Cam

The use of this cam in implementing the launch-recovery mode was mentioned in the section on modes of operation. As stated there, the launch-recovery cam switch is in series with the barometric switch for controlling the state of the launch-recovery relay. The function of the cam and its associated switch are to back-up the barometric switch. However, certain considerations must be taken in setting it. First, the cam should be set to open its switch some safe time after the barometric switch has actuated during the launch. This requires that an estimate be made of how long the balloon will be on the ground after the "time zero" switch is closed and how long it will take for the ascent to 80,000 feet. If this estimate is too short, premature operation of the system will occur. If it is too long, valuable flight time will be lost in the event that the barometric switch fails to open. Initiation of the recovery phase requires that both the cam switch and the barometric switch are closed. Therefore, prior to launch, it should be estimated how long the flight will last, so that the cam switch can be set to close some safe time before the barometric switch will close on the descent. Too short an estimate will result in loss of valuable flight time if the barometric switch fails to open during the flight. Too long an estimate will result in failure to initiate recovery at 80,000 ft by the barometric switch. It should be noted that an "open" failure of either the launch-recovery switch or barometric switch will result in the recovery phase not being initiated. Also, if balloon recovery is not accomplished by the time the launch-recovery cam recycles to its "open" position, system operation will resume on the ground. This is a consequence of the continuous operation of the drive motor whenever the "time zero" switch is closed. Any precise setting of the launch-recovery cam is complicated by its being a 24-hour cycle on a small cam.

Cam Overlap

Since the cams on the cam programmer are set independently, the relay actuations to accomplish the experimenter's sequences will not, in general, occur precisely together. From an operational standpoint, there is only one possible serious consequence of this in the case of the elevation command mode when looking horizontal. If the sequence of the commanded elevations is not carefully selected, an overlap of the down select relay time will cause elevation to attempt to point into the gondola. This can, and should, be avoided by never commanding "look horizontal" immediately before or after "look down".

Back Azimuth Cams

Two cams in the cam programmer are designated for back azimuth. This is to accommodate two back azimuth modes in one sequence. Otherwise, one cam with two adjustable notches would be required. In sequences where only one back azimuth mode is required in a cycle, the other cam is available as a spare.

Ratio Change Gears

As noted previously, the pre-programmed sequence cycles at a nominal rate of one revolution per hour. The design is such that two gears in the drive of the cam programmer are replaceable by gears of other ratios, thus providing several possible cycle times.

Elevation Blind Spot

The solar cells for the elevation servo have a space in their field of view, such that if elevation is pointed downward, the sun at very high elevation angles would not be acquired. To preclude this, elevation must be pointed upward prior to launch. Another requirement is that commanded elevation sequence must not terminate pointed down. This, along with the constraint discussed under cam overlap, dictates that the best sequence for elevation command is down-up-horizontal.

Cam-Resolver Drive Motor

As mentioned, a timing motor drives the cam programmer, the launch-recovery cam, and the earth rate resolvers. It is a chronometrically governed motor running directly from battery voltage. Over a voltage range of 24-30 volts DC, its speed regulation is 3,600 rpm $\pm$0.05%. Any attempt to adjust or measure the speed of this motor should be accomplished only with test instrumentation of much greater accuracy than the regulation of the motor (43 parts in 86,400). Motor life is given as 2,000 hours, and replacement should be considered at this number of operating hours.

Balloon System Logic Equations

As an aid to trouble shooting and understanding the system operation, the following logic equations are given, along with the abbreviations selected. In the equations, an "on" state corresponds to a relay coil energized and a switch closed.

Abbreviations

Modes:
- Launch-Recovery = LR
- Solar Track = SOLT
- Stellar Track = ST
- Back Azimuth Solar = BASOLT
- Back Azimuth Stellar = BAST
- Elevation Command Up = ECU
- Elevation Command Down = ECD
- Elevation Command Horizontal = ECH

Other:
- Barometric Switch = BS
- Launch-Recovery Cam Switch = LRCS
- Time Zero Switch = TO
- Cam Motor Rotating = CMR
- Logic Cell Illuminated = LCI
- Star Target 1 = ST1
- Star Target 2 = ST2
- Relay = K

. Logical and
+ Logical or
- Not

Logic Equations

1) Launch-Recovery

$LR = K3 = BS \cdot LRCS \cdot TO$

where $TO = CMR$

$\overline{K3} = \overline{LRCS} + \overline{BS} + \overline{TO}$

$\overline{LR} = \overline{K3}$

2) Solar Track

$SOLT = \overline{K3} \cdot TO \cdot \overline{K1A} \cdot \overline{K1B} \cdot \overline{K2B} \cdot \overline{K2C} \cdot (K7 + \overline{K7})$

where $K7 = LCI + K1B$

$\overline{K7} = \overline{LCI} \cdot \overline{K1B}$

$LCI = US$

3) Stellar Track

$ST = \overline{K3} \cdot TO \cdot K1A \cdot K1B \cdot \overline{K2A} \cdot \overline{K2B} \cdot \overline{K2C} \cdot \overline{K5} \cdot (K4 + \overline{K4})$

where $K1B = K7$

$K4 = ST2$

$\overline{K4} = ST1$

4) Back Azimuth Solar

$BASOLT = \overline{K3} \cdot TO \cdot \overline{K1A} \cdot \overline{K1B} \cdot K2B \cdot K2C$

$K2C = \overline{K7}$

5) Back Azimuth Stellar

$BAST = \overline{K3} \cdot TO \cdot K1A \cdot K1B \cdot K2A \cdot K2C \cdot (K4 + \overline{K4})$

where $K1A = \overline{K2B}$

6) Elevation Command Up

$ECU = \overline{K3} \cdot TO \cdot K1A \cdot K1B \cdot \overline{K2A} \cdot \overline{K2B} \cdot \overline{K2C} \cdot K5 \cdot (K4 + \overline{K4})$

PRE-PROGRAMMED EXPERIMENTER'S SEQUENCES

	Mode	Time in Mode
Program 1:		
	Launch-Recovery (Launch Phase)	3 hours (approximately)
	Solar Tracking	1/5 cycle time
	Back Azimuth (Solar)	1/5 cycle time
Repeated	Stellar Tracking (Star 1)	1/5 cycle time
Sequence	Back Azimuth (Star 1)	1/5 cycle time
for 8 Hours	Elevation Command Down	1/15 cycle time
	Elevation Command Up	1/15 cycle time
	Elevation Command Horizontal	1/15 cycle time
	Launch-Recovery (Recovery Phase)	13 hours (approx.)
Program 2:		
	Launch-Recovery (Launch Phase)	3 hours (approx.)
	Stellar Tracking (Star 1)	1/5 cycle time
	Back Azimuth (Star 1)	1/5 cycle time
Repeated	Stellar Tracking (Star 2)	1/5 cycle time
Sequence	Back Azimuth (Star 2)	1/5 cycle time
for 8 Hours	Elevation Command Down	1/15 cycle time
	Elevation Command Up	1/15 cycle time
	Elevation Command Horizontal	1/15 cycle time
	Launch-Recovery (Recovery Phase)	13 hours (approx.)
Program 3:		
	Launch-Recovery (Launch Phase)	3 hours (approx.)
	Solar Tracking	2/5 cycle time
Repeated	Back Azimuth (Solar)	2/5 cycle time
Sequence	Elevation Command Down	1/15 cycle time
for 8 Hours	Elevation Command Up	1/15 cycle time
	Elevation Command Horizontal	1/15 cycle time
	Launch-Recovery (Recovery Phase)	13 hours (approx.)

FIGURE 3

7) Elevation Command Down

$$ECD = \overline{K3} \cdot TO \cdot K1A \cdot K1B \cdot \overline{K2A} \cdot \overline{K2B} \cdot \overline{K2C} \cdot K5 \cdot K6 \cdot (K4 + \overline{K4})$$

8) Elevation Command Horizontal

$$ECH = \overline{K3} \cdot TO \cdot K1A \cdot K1B \cdot \overline{K2A} \cdot \overline{K2B} \cdot \overline{K2C} \cdot K5 \cdot K8 \cdot (K4 + \overline{K4})$$

B. Servo Design

In order to adequately and accurately fulfill the gondola pointing requirements as set forth by the experimenters, the following constraints were imposed on the design of the servo systems:

1. The system must be capable of pointing to within $\pm$ one degree of the mean solar disc in both azimuth and elevation while in the solar mode.

2. While in the stellar mode the system must be capable of a pointing accuracy of $\pm$ three degrees of any pre-selected stellar object.

3. The time required to make a 180 degree maneuver will be limited to one minute.

4. The elevation and azimuth servo drive will be required to operate from either of two independent error sources, i.e., the solar sensor or the equatorial computer.

5. The equatorial computer must have a north reference (Fluxgate compass or Magnetometer) with an associated instrument servo follow-up drive.

6. The vertical reference will be provided by the balloon suspension system.

7. There must be the capability of pointing the experiment up, down, and horizontal.

8. The inertia ring and gondola assemblies would be decoupled from the balloon suspension system by means of an in-line bearing. (It was later determined that this assumption was not valid for small pointing errors and the effect of the suspension system dynamics would have to be included in the analysis.)

Based on the above restraints coupled with the fact that ac power is required on the gondola to supply the resolver chain in the equatorial computer, the decision was made to design ac servo drive systems for both elevation and azimuth. The ac servo has the additional advantages of being efficient and inexpensive.

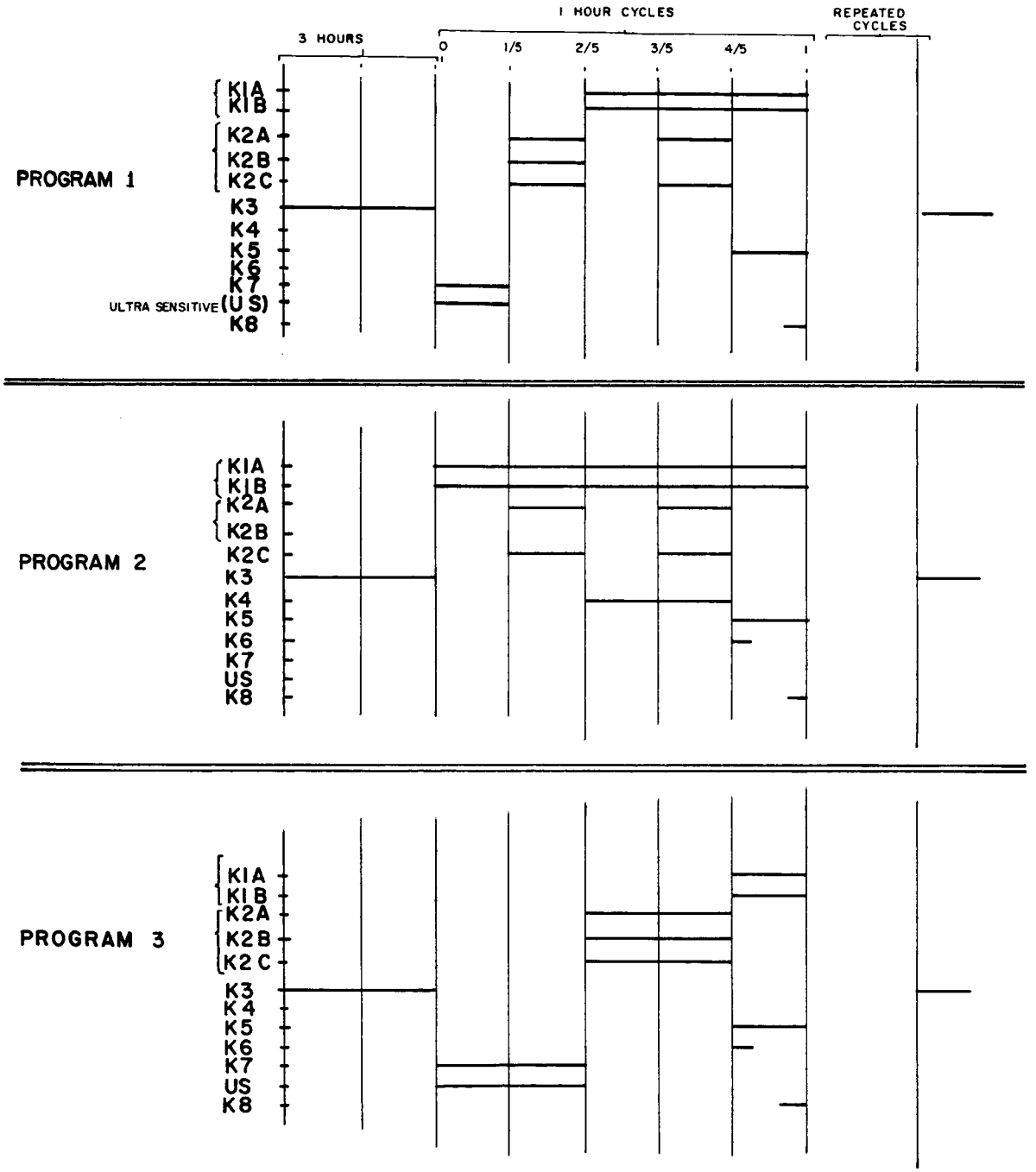

FIG 4. RELAY DUTY CYCLES FOR EXPERIMENTERS' SEQUENCES

The following analysis is based on the large signal case where the in-line bearing has decoupled the shroud dynamics from the gondola and the bearing friction is negligible. From Figure 6 the uncompensated transfer function becomes

$$GH = \frac{K_{ED}\ K_{SA}\ K_M\ J_2}{S\ (J_{eq}/fm\ S+1)\ N\ (J_1 + J_2)\ fm}$$

$$GH = \frac{7.65}{S\ (.38\ S+1)}$$

where fm = .001 in-oz/rad/sec
and $J_{eq} = J_m + J_1/N^2 = 38.0 \times 10^{-5}$ in-oz sec^2

$J_1 = J_2 = 4.0$ ft lb sec^2 (Estimated)

The resulting Bode plot for the uncompensated azimuth control loop is shown in Figure 7. It is obvious from the plot that the system would be lightly damped due to the low phase margin of 30°. Therefore, the addition of the anticipated minor loop tachometer was included in the analysis. In order to achieve a reasonable phase margin and at the same time increasing the bandwidth and the damping of the system, it was necessary to increase the forward loop gain by adjustment of K_{SA}. Figure 8 illustrates the compensated azimuth servo block diagram.

The minor loop is

$$\frac{G'}{1 + G'\ H} \qquad \frac{4.3}{S(S/9.7 + 1)}$$

and the major loop transfer function

$$GH = \frac{3.86}{S(S/9.7 + 1)}$$

The gain of the forward loop has been increased to 426 and the tachometer output amplified by a factor of 42.6. From the open loop Bode diagram, also shown on Figure 7, it is observed that the system now has 65° of phase margin and the corner frequency has been increased from 2.64 radians/second to 9.7 radians/second.

The closed loop Bode plot of the compensated azimuth servo loop is shown in Figure 9.

$$\frac{G}{1 + GH} = \frac{37.4}{S^2 + 9.7S + 37.4}$$

Therefore W_n = 6.1 radians/second
and δ = .795

The servo motor size was based on the maximum power requirements, (i.e., the power required to overcome coulomb friction in addition to that required to accelerate the load under maximum expected velocity).

$$P_{total} = T_{SF}\ \dot{\Psi}_2 + (J_2 + J_M N^2)\ \ddot{\Psi}_2\ \dot{\Psi}_2 \quad 1*$$

where

$T_{SF} = W_T\ R$
$= 200\ (.031)\ (3)\ (16) = 300$ in.oz.$= 1.52$ ft lbs
Maximum relative velocity $\dot{\Psi}_2 = .1$ RPM $= .105$ rad/sec
Maximum relative acceleration $\ddot{\Psi}_2 = .166$ rad/sec^2
$P_{total} = .311$ watts or $.23$ ft lb sec

Allowing sufficient safety margin for system degradation due to environmental conditions a convenient and readily available size 11 motor was selected which has the capability of supplying .95 watts power at the shaft.

Error Source Allotment

In order to achieve a total system, sun pointing accuracy of less than $\pm$ one degree, the following error allotments were made.

Source	Error (arc min)
1. Error detector, including resolution & null shift as a function of temperature & time.	15
2. Gearing errors, including friction clutch, gearhead & final belt drive.	35
3. Servo static error.	10
4. Servo random error due to time & temperature variations.	20
5. Alignment error of sun sensors to experiment package.	5
Total rms Error Per Axis =	44.4 arc min

The open loop gain is determined from the motor characteristics, system inertias, error detector characteristics and required accuracy.

Referring to Figure 5 the uncompensated open loop gain is calculated based on a static servo error of 10 arc minutes.

$$K_{SA} = \frac{T_{SF} + N_{fg}}{E_{min}\ K_{ED}\ K_M\ N}$$

$= 230$ volts/volt uncompensated

where
$N_{fg} = 27$ in-oz
$T_{SF} = 300$ in-oz
$E_{min} = 10$ arc minutes
$K_{ED} = 200$ mv/degree
$K_M = .01575$ in-oz/volt
$N = 2720$

*Abbreviations are shown at the end of this section.

Whereas if no compensation were employed, the system transfer function would be

$$\frac{G}{1 + GH} = \frac{20.2}{S^2 + 2.64 + 20.2}$$

and the resulting W_n = 4.5 radians/second with ζ = .294.

The addition of the tachometer, therefore, raises the bandwidth of the system by 50%, doubles the phase margin, and improves the damping characteristic to yield a high performance system.

The elevation servo system was designed to have essentially the same performance characteristics as the azimuth servo. The only significant difference between the two drives is that the final inertia ratio term in the azimuth block diagram becomes unity for the elevation loop. The forward loop amplifier gain was reduced by one-half to compensate for this term. The only other difference in the two loops is the reflected load inertia term. This difference, however, becomes negligible since the reflected load inertia through the gear train is only about 10% of the motor, tachometer and first gear assembly.

To obtain a north reference system for the azimuth control loop a fluxgate compass system similar to that used in aircraft was utilized. The fluxgate compass can be thought of as a control transmitter - control transformer pair. When the control transmitter (fluxgate) is not physically aligned with magnetic north an electrical error signal will be transmitted to the control transformer. The control transformer then supplies a servo amplifier with an error signal which rotates a servo motor and positions the resolver R4 in the equatorial computer and also positions the mechanical shaft of the control transformer. The shaft will continue to revolve until the control transformer is in electrical agreement with the transmitter. The mechanical rotation of the transformer then represents the physical deviation of the gondola with respect to magnetic north. Since the equatorial computer analysis is based on a true north reference it was necessary to offset the mechanical null of the control transformer equal to the magnetic deviation between true north and magnetic north at the expected launch site. Thus, although the fluxgate system is generating signals referenced to magnetic north, the R4 resolver is being positioned from true north. It is therefore required to mechanically re-position the fluxgate control transformer each time a different launch site is selected.

The design of the small instrument servo used in the equatorial computer to position the fluxgate control transformer is straight forward. It consists of a size 11 servo motor-gearhead arrangement with a gear ratio of 1,720. The block diagram is shown in Figure 10. No compensation is required in this servo loop. The amplifier gain was set to 135 to insure fast response along with high accuracy. The output gearhead shaft positions the rotor of the fluxgate control transformer while rotating the rotor of resolver R4 to its null position. The electrical winding of the rotor of the control

transformer now contains the desired generated angle and becomes the input error signal for the azimuth servo drive loop in the equatorial mode. The open loop Bode diagram for the instrument servo is shown in Figure 11 which indicates an adequate phase margin of 50°.

The above analysis is based on the assumption that the in-line bearing has broken away. This assumption is valid for pointing angles greater than ± one degree since the breakaway friction of the bearing is ten in-oz and the spring restraint of the shroud lines when including the spreader ring is 3.2 ft lbs per radian.

For the region of pointing less than 1° however, the in-line bearing will not decouple the shroud dynamics from the gondola, and this must be included in the analysis. It will be shown that during small angle pointing a low frequency limit cycle condition will exist. However, since the experimenters are not concerned with the pointing behavior at angles less than 1°, there was no attempt to eliminate this limit cycle condition.

The following analysis will describe the behavior of the control system when operating in the small angle region. Figure 12 depicts a typical balloon gondola, including the suspension, without the in-line bearing which will be the case for small angles.

Writing the equations of motion for the gondola and suspension system one obtains:

$$T_1 = J_1 \ddot{\psi}_1$$

$$T_2 = J_2 \ddot{\psi}_2 + F_S \dot{\psi}_2 + K \psi_2 \qquad \text{B (1)}$$

and $T_1 = T_2 = T$ or $\qquad \text{B (2)}$

$$J_1 \ddot{\psi}_1 = (J_2 \ddot{\psi}_2 + F_S \dot{\psi}_2 + K \psi_2) \qquad \text{B (3)}$$

The torque developed by the azimuth servo motor (M) is given by the following equation:

$$T_d = K_m V_C - f_m \dot{\psi}_m = J_m \ddot{\psi}_m + T_L, \quad \text{where}$$

V_c = Control Voltage

$T_L = T/N$ = Reflected Load Torque; therefore

$$N K_m V_c = N J_m \ddot{\psi}_m + N f_m \dot{\psi}_m + T \qquad \text{B (4)}$$

$$T = \begin{cases} T_{SF}, & \text{before breakaway} \\ T_1, & \text{after breakaway} \end{cases}$$

ψ_1 and ψ_2 are related as follows

$$\psi_T = \psi_1 + \psi_2 \approx \psi_m / N$$

$$\psi_m \approx N \left| \psi_1 + \psi_2 \right| \qquad \text{B (5)}$$

Substituting B(1) and B(5) in B(4) we have

$$NK_mV_c = (J_1 + N^2J_m)\ddot{\psi}_1 + N^2f_m\psi_1 + \left(N^2J_m\ddot{\psi}_2 + N^2f_m\dot{\psi}\right) \quad B(6)$$

and now, writing the LaPlace transform of equations B(3) and B(6) we can solve for $\psi_1(S)$ as follows:

$$\begin{bmatrix} 0 & 1 \\ NK_mV_c - T_S & (J_1 + N^2J_m)S^2 + N^2f_mS \end{bmatrix} \begin{bmatrix} J_1S^2 & +J_2S^2+SF_S+K \\ -N^2J_mS^2+Nf_mS & \end{bmatrix} = \begin{bmatrix} \psi_1(S) \\ \psi_2(S) \end{bmatrix}$$

$$\psi_1(S) = \frac{N^KmV_c\,(J_2S^2 + SF_s + K)}{[J_1J_2 + (J_1+J_2)N^2Jm]S^4 + [(J_1+J_2)N^2f_m+(J_1+N^2Jm)Fs]S^3+[(J_1+N^2Jm)K+N^2fmFs]S^2 +N^2fmKs} \quad B(7)$$

Rewriting Equation B7, one obtains the system forward loop transfer function

$$\frac{\psi_{1(s)}}{\psi_{e(s)}} = \frac{NK_mK_{ed}K_{sa}J2}{A} \cdot \frac{S^2 + SF_s/J2 + K/J2}{S\left[S^3 + \frac{(J_1+J_2)N^2f_{eq}+(J_1+N^2J_{eq})Fs}{A}S^2 + \frac{(J1+N^2Jeq)K+N^2feqFs}{A}S + \frac{N^2FeqK}{A}\right]}$$

$V_c = K_{ed}\psi_{e(s)}$

$A = J_1J_2 + (J_1 + J_2)N^2J_{eq}$

J_{eq} = Equivalent inertia of motor and gear train

f_{eq} = Equivalent motor viscous damping including tach feedback

The block diagram of the system is:

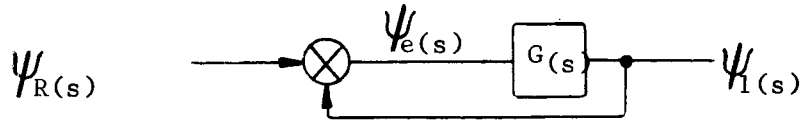

Since the system has unity feedback the closed loop transfer function is:

$$\frac{\psi_1(S)}{\psi_R(S)} = \frac{G(S)^*}{1 + G(S)}$$

The stability of the system can now be analyzed by plotting the root locus of the characteristic equation of $\psi_1(S)/\psi_R(S)$. For the analysis, the values for the system constants were:

$J_1 = 4.0$ lb-ft-sec^2
$J_2 = 1.5$ lb-ft-sec^2
} Actual

$J_{eq} = 1.98 \times 10^{-6}$ lb-ft-sec^2

*Note G and G(S) are used interchangeably in this report.

$N = 2720$
$K_m = .082 \times 10^{-3}$ lb-ft/volt
$K_{ED} = .200$ V/Degree
$K_S = .15$ lb-ft/Rad
$f_{eq} = .052 \times 10^{-4}$ lb-ft/rad/sec (Cases 1 & 2)
$f_{eq} = .068 \times 10^{-4}$ lb-ft/rad/sec (Case 3)

$F_s = 0.1$ (Case 1)
$F_s = 1.0$ (Cases 2 & 3)

Writing $G_{(S)} = K'G'_{(S)}$ we have

$$K' = K_{SA} \frac{NK_m K_{ED} J_2}{4} = .97 \times 10^{-3} K_{SA}$$

$$G'(S) = \frac{S^2 + 0.67S + 0.1}{S[S^3+(.03N^2f_{eq}+.22Fs)S^2 + (.033+N^2F_{eq}F_S)S + N^2f_eK_S}$$

Substituting in the values for F_S and f_{eq} given above, we have the root loci shown in Figures 13 and 14.

We see that for low values of suspension damping the system can be unstable, as the root locus will be on the right half plane.

Increased shroud damping has the greatest effect on stability, as it moves the zeros off the inaginary axis and into the left half plane. Also, the effect of tach feedback is to move the pole on the real axis further to the left, thus also aiding stability.

Abbreviations:

T_{SF} - Azimuth bearing static friction
W_T - Weight of Gondola
n - Azimuth bearing coefficient of friction
R - Radius of lower gondola bearing
$\dot{\Psi}_2$ - Velocity of gondola relative to inertia ring
$\ddot{\Psi}_2$ - Acceleration of gondola relative to inertia ring
f_g - Static friction of gearhead
K_{ED} - Error detector gain
K_{SA} - Servo amplifier gain
N - Gear ratio 2720
f_m - Servo motor = .001 oz-in/rad/sec
J_1 - Inertia of gondola 4.0 slug ft^2
J_2 - Inertia of reaction mass 4.0 slug ft^2
Shroud line coefficient of viscous friction = .04 ft lb/rad/sec
K - Shroud line spring constant = 3.2 ft lb/rad
T_d - Motor developed torque
K_m - Motor torque constant
V_c - Voltage appearing at input of motor
J_m - Servo motor inertia

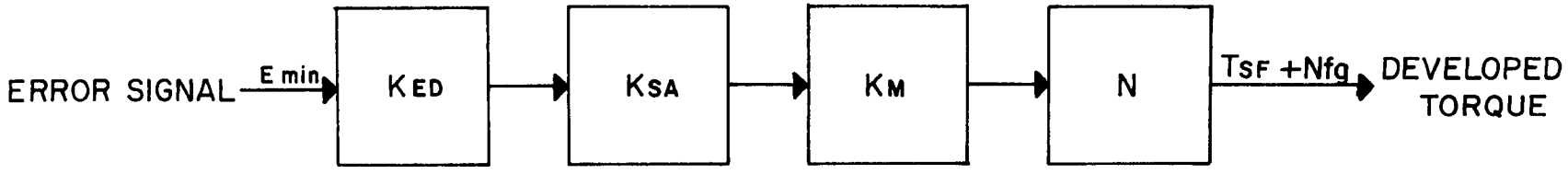

FIGURE 5 FORWARD LOOP BLOCK DIAGRAM

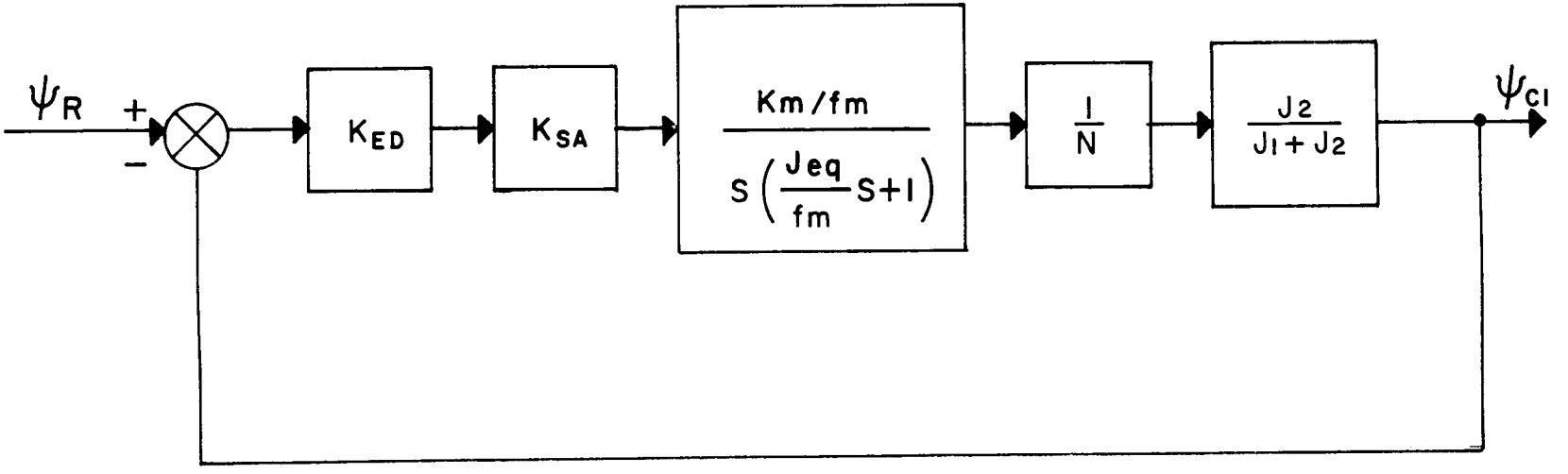

FIGURE 6 UNCOMPENSATED AZIMUTH SERVO LOOP NEGLECTING SUSPENSION SYSTEM DYNAMICS

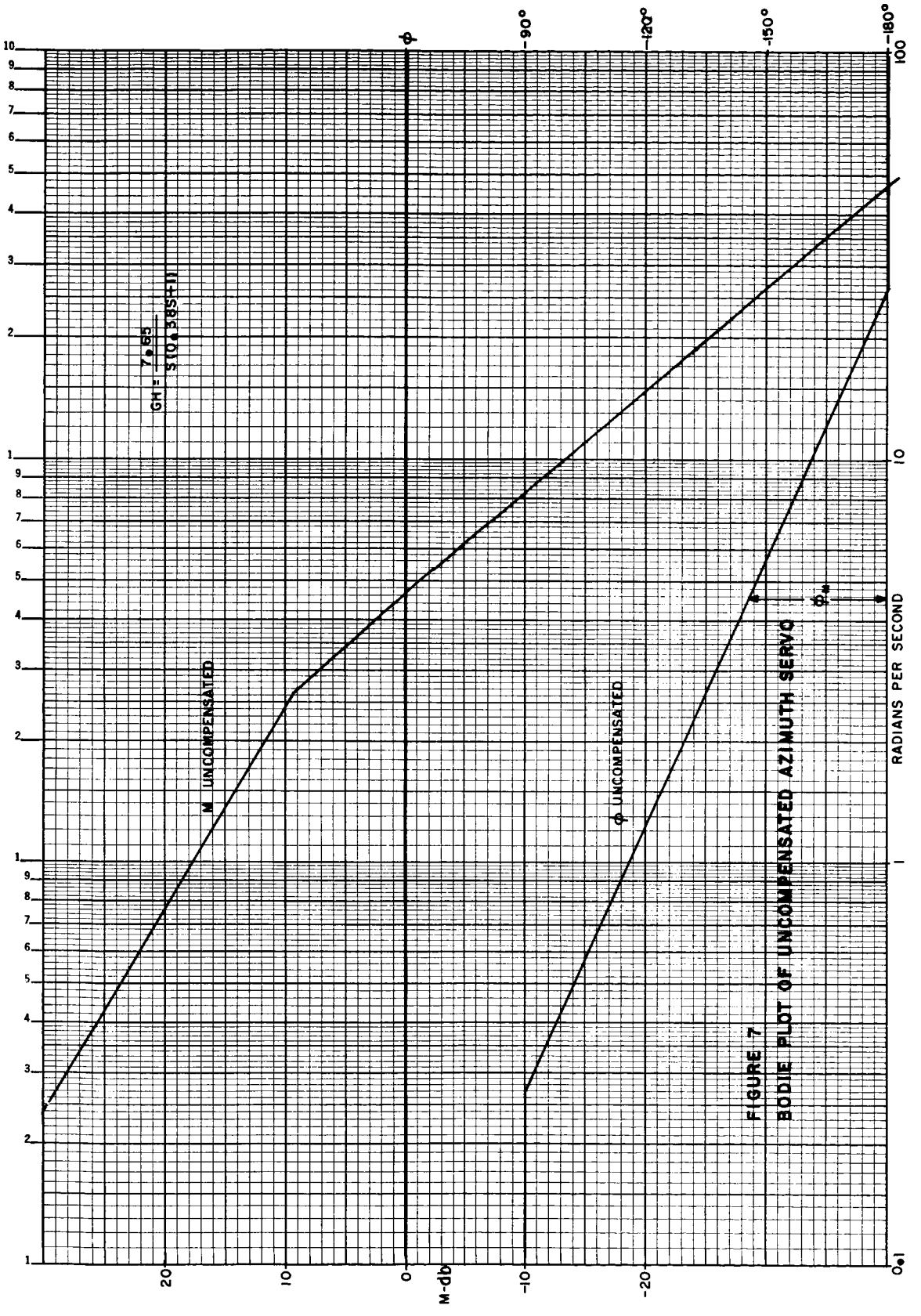

FIGURE 7
BODIE PLOT OF UNCOMPENSATED AZIMUTH SERVO

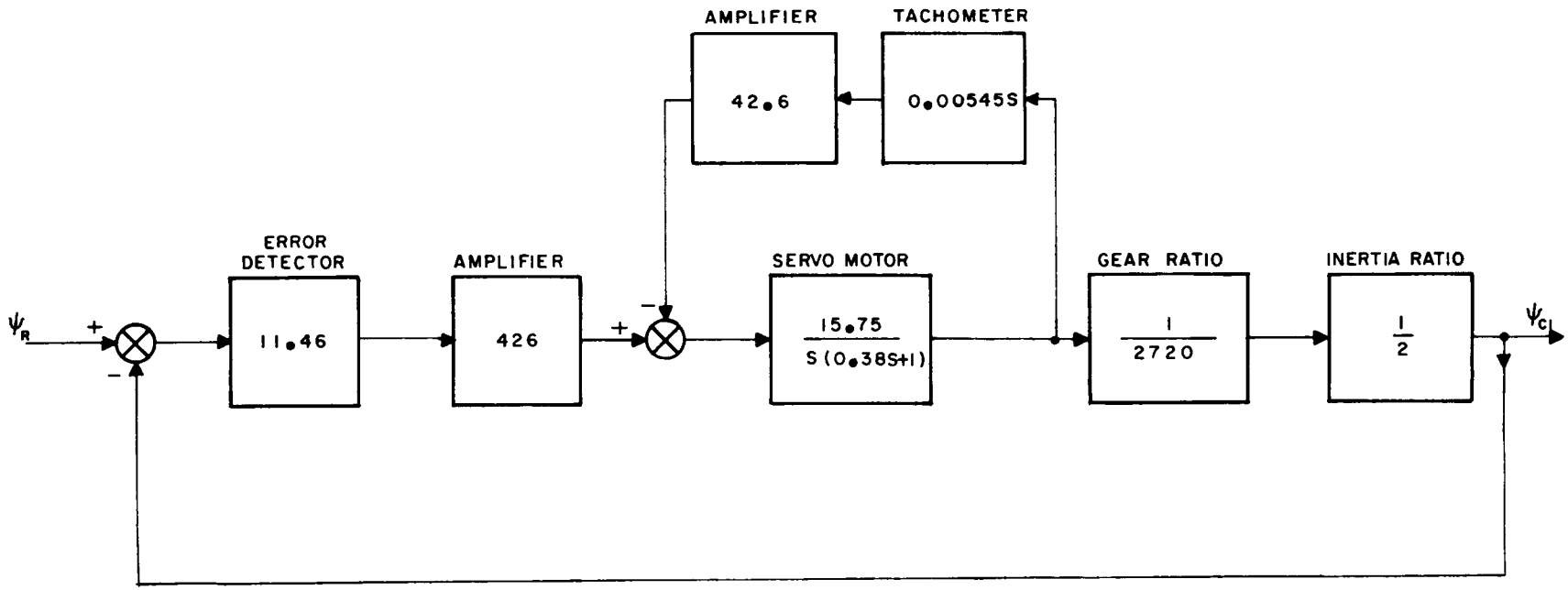

FIGURE 8 COMPENSATED AZIMUTH SERVO LOOP BLOCK DIAGRAM

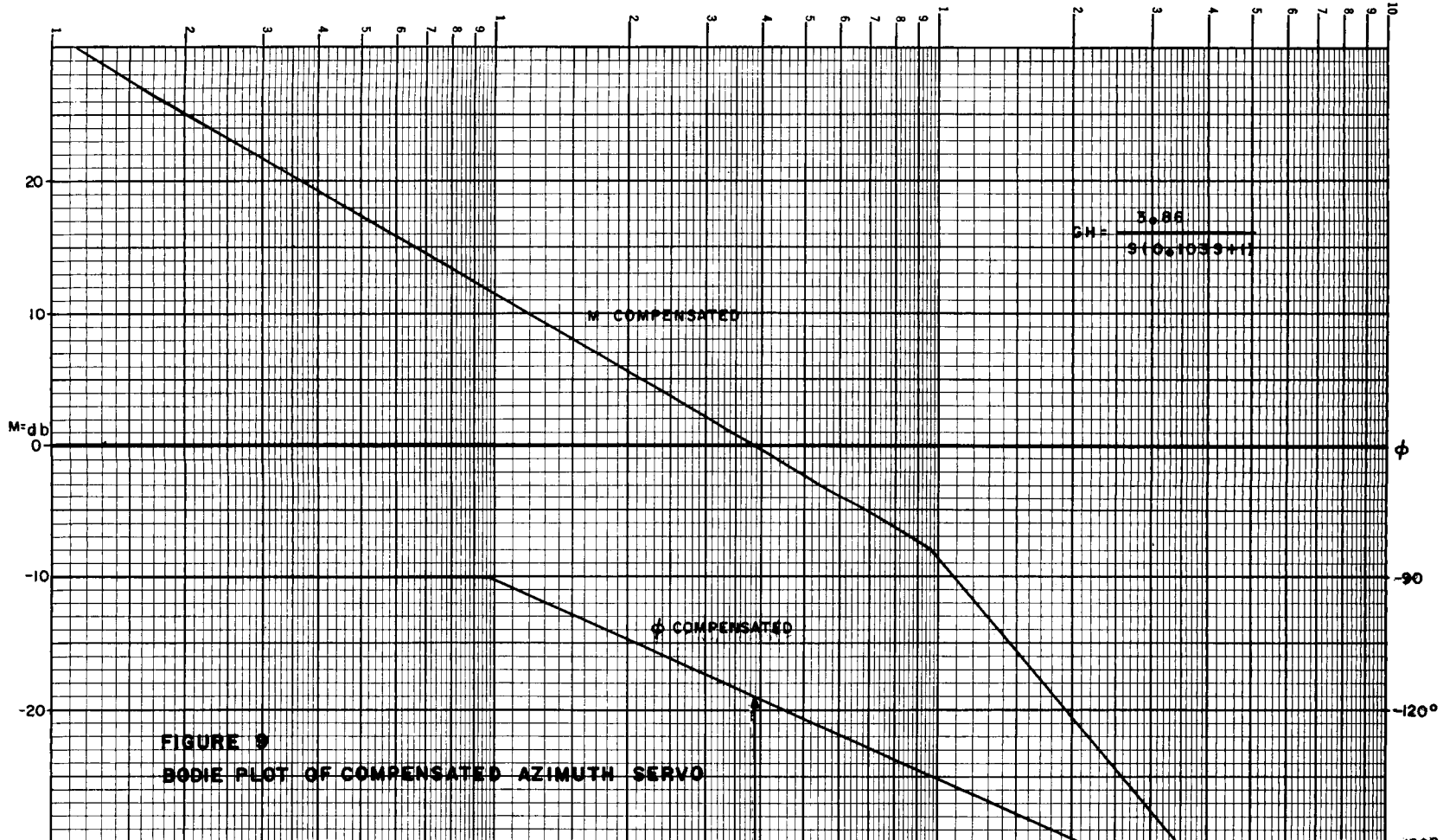

FIGURE 9
BODIE PLOT OF COMPENSATED AZIMUTH SERVO

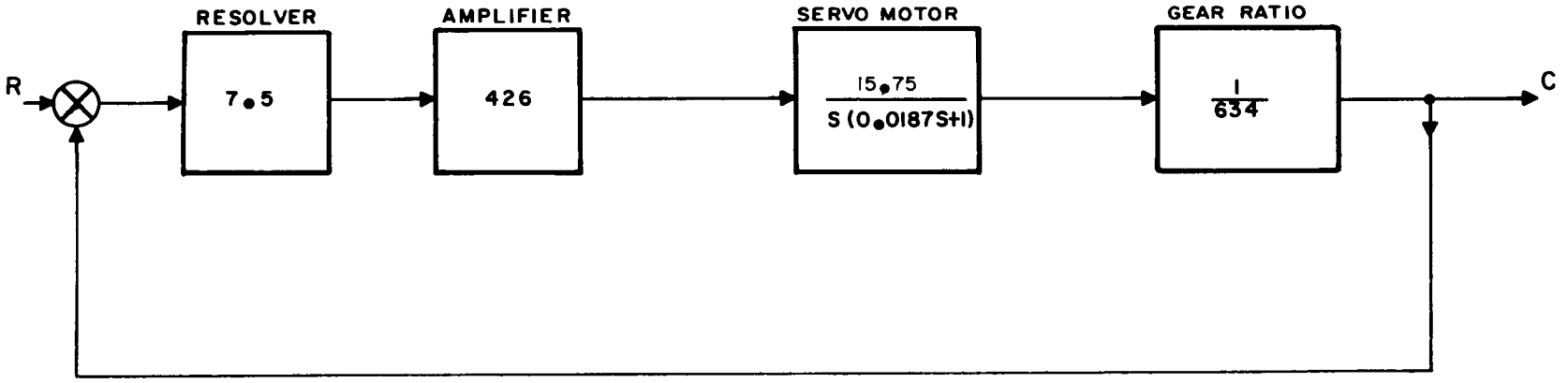

FIGURE 10 AZIMUTH INSTRUMENT SERVO BLOCK DIAGRAM

FIGURE 11

BODE PLOT OF FLUXGATE SERVO LOOP

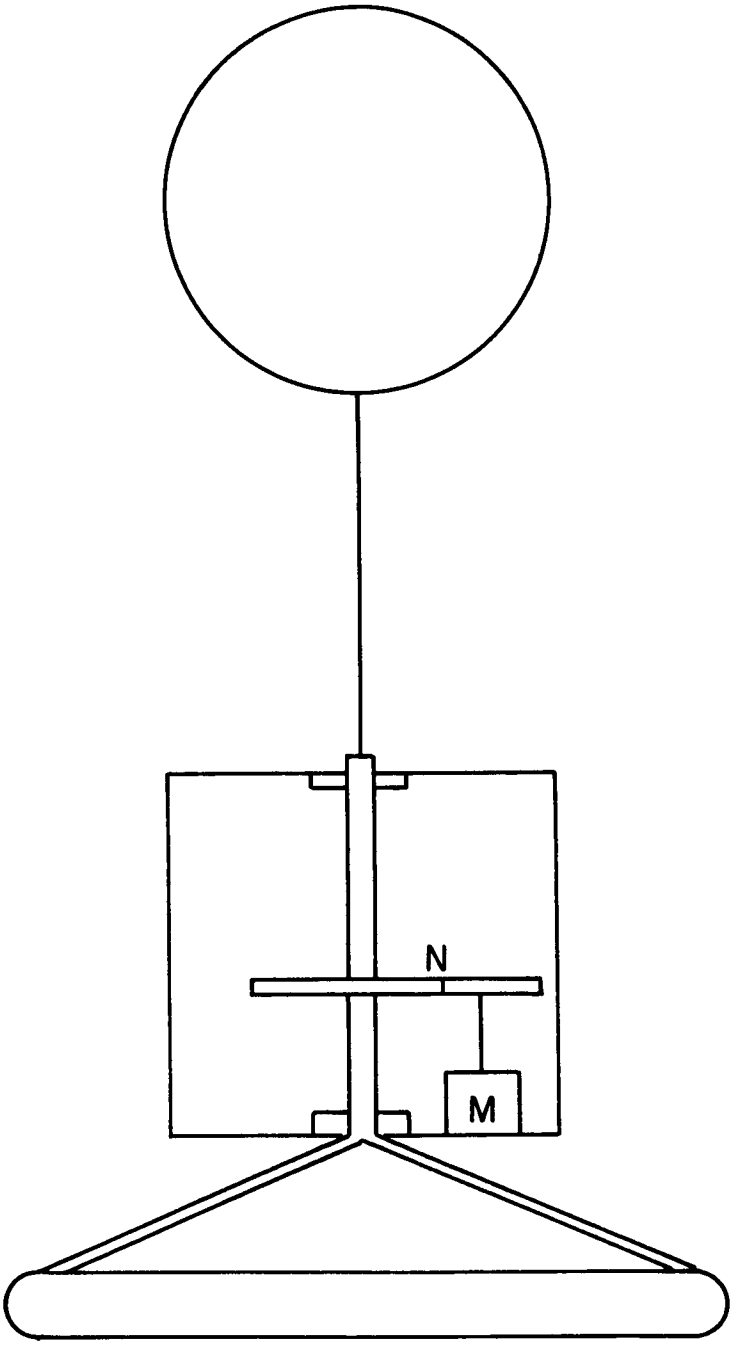

FIGURE 12 BALLOON GONDOLA

$F_S = 0.1$

$N^2 F_E = 38.5$

$$G_{(s)} = \frac{S^2 + .067\,S + 0.1}{S\left[S^3 + 2.626\,S^2 + .0798\,S + .071\right]}$$

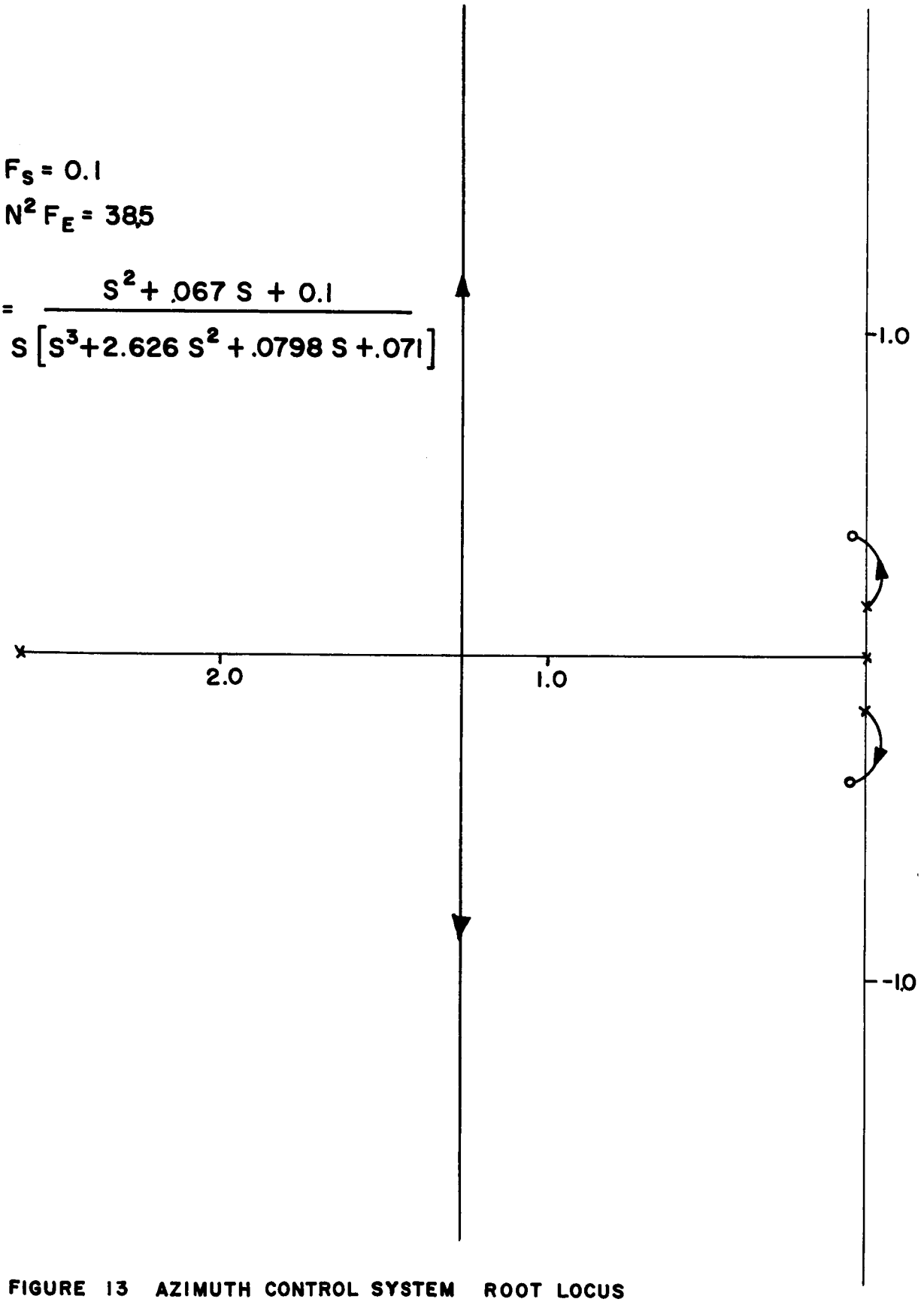

FIGURE 13 AZIMUTH CONTROL SYSTEM ROOT LOCUS

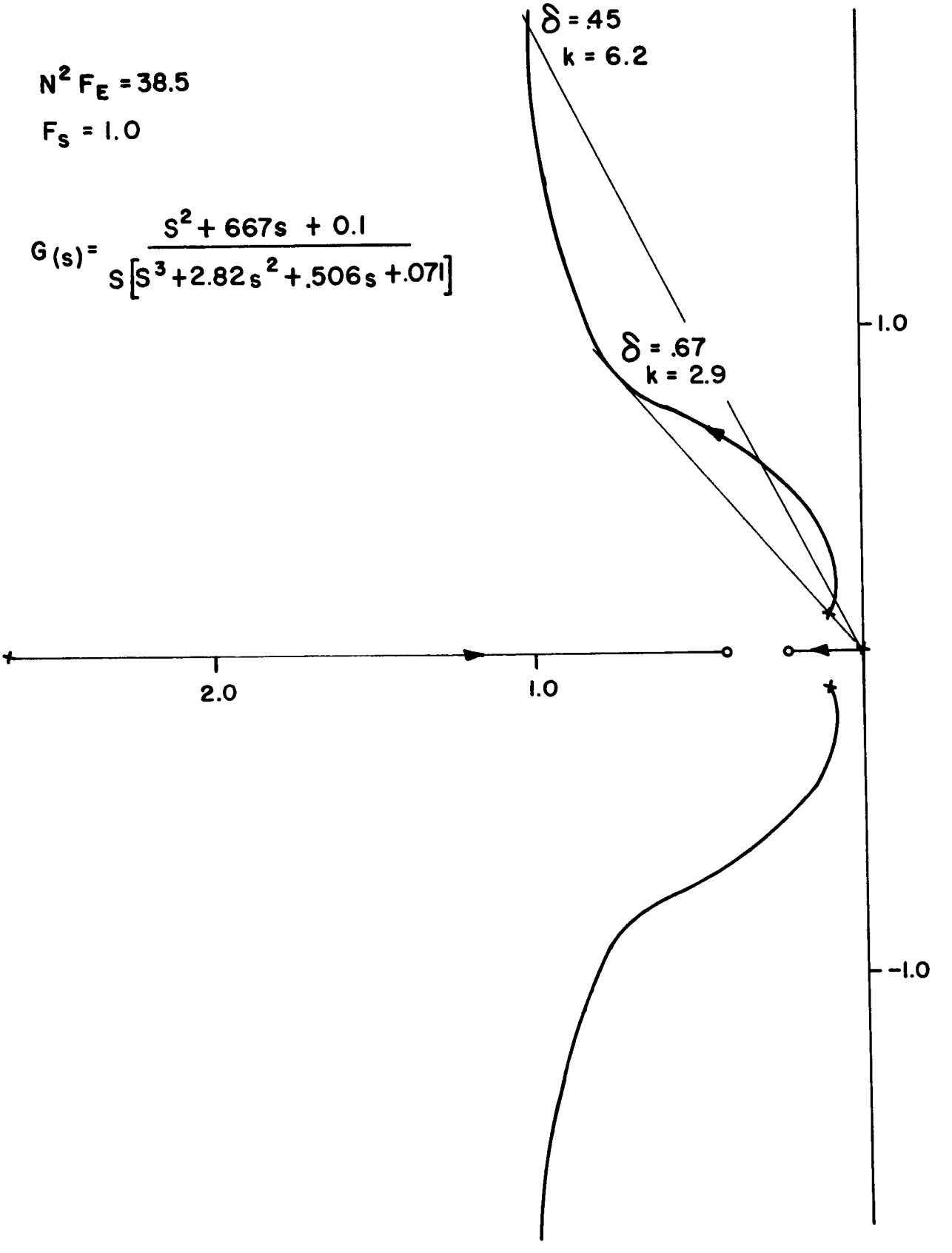

FIGURE 14 AZIMUTH CONTROL SYSTEM ROOT LOCUS

C. Equatorial Computer

Introduction: A celestial tracker on the earth's surface must compensate for the earth's rotational motion. The angular coordinates defining the geographical location of the tracker and the celestial location of the target, determine sets of vector components that vary as the earth rotates. Resolving a vector into its components with electrical induction resolvers that are set with tracker and target coordinates and rotated at earth's rate by a precision timing motor provides azimuth and elevation angles necessary to track the target. The computer under discussion utilizes a boosterless resolver train for the resolution of vector components and a precision timing motor to generate the earth's rotation compensation.

Analysis: The aximuth and elevation angles Ψ, θ that define the position of a celestial point may be determined by resolution of a vector, representing the celestial point in earth coordinates into its components in gondola coordinates. See Figure 15. From Figure 15 it can be seen that the unit vector $\vec{e}_2$ points to the celestial point in question. The problem then is to find the components of $\vec{e}_2$ in the Z_i (i = 1,2,3) coordinate system. When these components ($Z_1Z_2Z_3$) are known, the azimuth and elevation angle may be determined as follows:

$$\Psi = \tan^{-1} Z_3/Z_1 \qquad C1$$

$$\theta = \tan^{-1} Z_2/(Z_1^2 + Z_2^2)^{\frac{1}{2}} \qquad C2$$

The components at $\vec{e}_2$ in the Z_i coordinate system may be determined by a series of orthogonal rotational transformations from an inertial reference to the gondola reference. The inertial reference system $\vec{e}_1$ $\vec{e}_2$ $\vec{e}_3$ is described as follows: $\vec{e}_2$ is a unit base vector originating at the center of mass of the earth and diverted toward the celestial point in question, $\vec{e}_1$ is a unit base vector originating at the center of mass of the earth perpendicular to $\vec{e}_2$ and in the plane formed by and the earth's spin axis, $\vec{e}_3 = \vec{e}_1 \times \vec{e}_2$. To determine the components $Z_1Z_2Z_3$ of $\vec{e}_2$ in the $\vec{Z}_1$ coordinate system rotate about $\vec{e}_3$ through the angle δ to obtain the coordinate system $\vec{x}_1\vec{x}_2\vec{x}_3$.

$$\begin{aligned} \vec{x}_1 &= \vec{e}_1 \cos\delta + \vec{e}_2 \sin\delta \\ \vec{x}_2 &= -\vec{e}_1 \sin\delta + \vec{e}_2 \cos\delta \\ x_3 &= e_3 \end{aligned} \qquad C3$$

or in matrix form

$$\begin{bmatrix} \cos\delta & \sin\delta & 0 \\ -\sin\delta & \cos\delta & 0 \\ 0 & 0 & 1 \end{bmatrix}$$

now rotate about $\vec{x}_1$ through the angle β to obtain the coordinate system $\vec{y}_1$ $\vec{y}_2\vec{y}_3$

$$\begin{aligned} \vec{y}_1 &= \vec{x}_1 \\ \vec{y}_2 &= \vec{x}_2 \cos\beta - \vec{x}_3 \sin\beta \\ \vec{y}_3 &= \vec{x}_2 \sin\beta + \vec{x}_3 \cos\beta \end{aligned} \qquad C4$$

or in matrix form

$$\begin{bmatrix} 1 & 0 & 0 \\ 0 & \cos\beta & -\sin\beta \\ 0 & \sin\beta & \cos\beta \end{bmatrix}$$

Finally rotating about $\vec{y}_3$ through the angle L the $\vec{z}_1\vec{z}_2\vec{z}_3$ coordinate system is obtained. This is the gondola coordinate system, and the magnitude of its components $\gamma_1\gamma_2\gamma_3$ determine the azimuth and elevation in angles of the experiment (See Equations C1 and C2).

$$\begin{aligned}\vec{z}_1 &= \vec{y}_1 \cos L - \vec{y}_2 \sin L\\ \vec{z}_2 &= \vec{y}_1 \sin L + \vec{y}_2 \cos L\\ \vec{z}_3 &= \vec{y}_3\end{aligned} \qquad \text{C5}$$

in matrix form

$$\begin{bmatrix}\cos L & -\sin L & 0\\ \sin L & \cos L & 0\\ 0 & 0 & 1\end{bmatrix}$$

The components of the star unit vector on the final reference system become:

$$\begin{bmatrix}Z_1\\ Z_2\\ Z_3\end{bmatrix}=\begin{bmatrix}\cos L & -\sin L & 0\\ \sin L & \cos L & 0\\ 0 & 0 & 1\end{bmatrix}\begin{bmatrix}1 & 0 & 0\\ 0 & \cos\beta & -\sin\beta\\ 0 & \sin\beta & \cos\beta\end{bmatrix}\begin{bmatrix}\cos\delta & \sin\delta & 0\\ -\sin\delta & \cos\delta & 0\\ 0 & 0 & 1\end{bmatrix}\begin{bmatrix}e_1\\ e_2\\ e_3\end{bmatrix} \qquad \text{C6}$$

$$\begin{bmatrix}Z_1\\ Z_2\\ Z_3\end{bmatrix}=\begin{bmatrix}\cos L & -\sin L & 0\\ \sin L & \cos L & 0\\ 0 & 0 & 1\end{bmatrix}\begin{bmatrix}\cos\delta & \sin\delta & \\ -\cos\beta\sin\delta & \cos\beta & \sin\beta\\ -\sin\beta\sin\delta & \sin\beta & \cos\beta\end{bmatrix}\begin{bmatrix} & 0 & \\ \cos\delta & -\sin\beta & \\ \cos\delta & \cos\beta & \end{bmatrix}\begin{bmatrix}e_1\\ e_2\\ e_3\end{bmatrix} \qquad \text{C7}$$

$$\begin{bmatrix}Z_1\\ Z_2\\ Z_3\end{bmatrix}=\begin{bmatrix}\cos\delta\cos L + \sin L\cos\beta\sin\delta & \cos L\sin\delta - \sin L\cos\beta\cos\delta - \sin L\sin\delta\\ \sin L\cos\delta - \sin L\cos\beta\sin\delta & \sin L\sin\delta + \cos L\cos\beta\cos\delta - \cos L\sin\beta\\ -\sin\beta\sin\delta & \sin\beta\cos\delta \qquad \cos\beta\end{bmatrix}X\begin{bmatrix}e_1\\ e_2\\ e_3\end{bmatrix} \qquad \text{C8}$$

As can be clearly seen, the components of the star unit vector in the inertial coordinate system are

$$\begin{aligned}e_1 &= 0\\ e_2 &= 1\\ e_3 &= 0\end{aligned}$$

The significance of the angles δ, β and L can be seen from Figure 15. δ is the declination of the celestial target. β is made up of the right ascension of the target α, the Greenich hour angle to Aries GHAγ, the longitudinal position of the tracking device λ, and the earth's spin rate, ω_e. From the sketch below it can be seen

$$\beta = \alpha - (\lambda + \omega_e t)$$
$$\omega_e t = \text{GHA}\gamma$$

Essentially, β is the angle between the star meridian and the balloon meridian

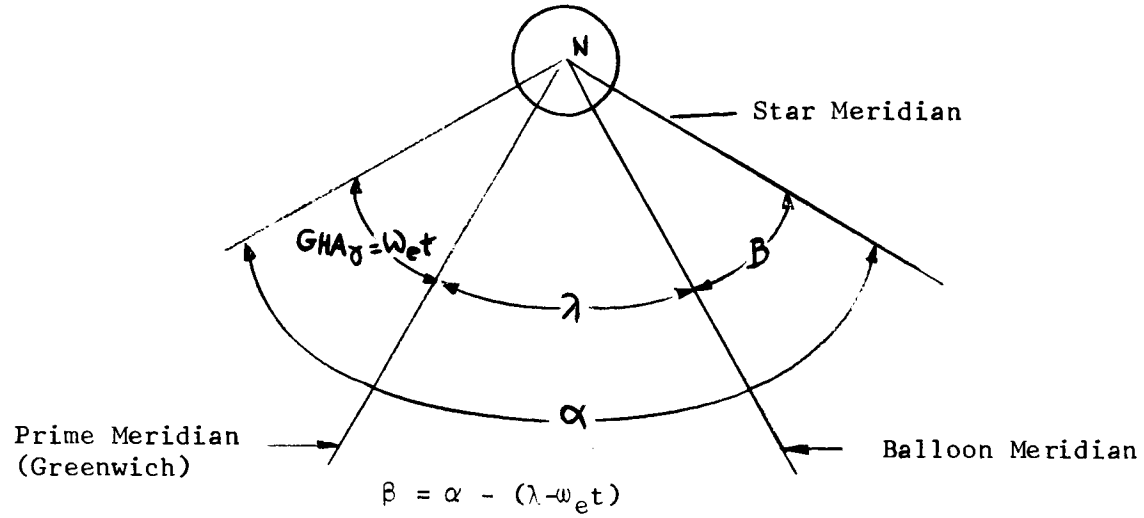

$$\beta = \alpha - (\lambda - \omega_e t)$$

and finally, L is the latitude of the tracking device.
Then

$$z_1 = \cos L \sin \delta - \sin L \cos \beta \cos \delta$$
$$z_2 = \sin L \sin \delta + \cos L \cos \beta \cos \delta \qquad \text{C9}$$
$$z_3 = \sin \beta \cos \delta$$

Mechanization: Equation C9 can be mechanized with a series of a.c. induction resolvers. Induction resolvers are essentially computing transformers with rotating orthogonal primaries (or secondaries). The equations relating output to input of a typical resolver are shown below

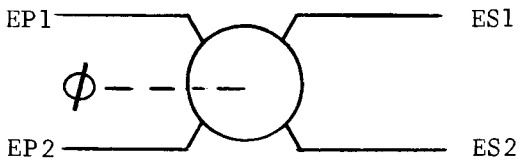

$$ES1 = EP1 \cos \phi - EP2 \sin \phi$$
$$ES2 = EP1 \sin \phi + EP2 \cos \phi$$

By combining the resolvers as shown in Figure 16 the appropriate components can be developed in terms of voltages. The output voltages can be seen to correspond with Equation C9 by making the proper substitutions. Resolvers 4 and 5 are used in an application different than shown in the above sketch. In the case of R4 and R5 the output drives a servo motor which positions the resolver motor until one output is zero. At this position, the other rotor being 90° away, has maximum coupling with the flux vector formed by the inputs (V_5, V_6, V_7, V_8). Its output is therefore proportional to the vector sum of the two inputs. The rotor angular position is the angle between one leg and the hypotenuse of the triangle. These are the angles ψ and θ that are required

to point the experiment to the celestial target. The problem of converting these angles to signals for the servo amplifiers is discussed in the section on servo loop design.

D. Sun Sensor

The sun tracker portion of the Balloon Solar Observatory system is comprised of three major subdivisions: sun presence, elevation, and azimuth. Each subdivision consists of an appropriate sun sensor and its associated electronics.

The sun presence portion of the sun tracker is used to insure that the elevation drive circuitry is activated only when the azimuth is pointing at the sun within 15^{o}, thus preventing the elevation drive from tracking the sun prior to proper azimuth acquisition. This is accomplished by using a photovoltaic solar cell which is shielded to allow an output only when it is pointing at the sun within 15^{o} in azimuth (see Figure 17). The elevation angle meanwhile can be anything from zero to 85 degrees. The sun presence assembly is mounted on the gondola pointing forward (see Figure 20). The output from the solar cell is used to drive a micropositioner relay which in turn appropriately activates the elevation circuits. Since the solar cell is wired directly to the micropositioner relay and since the input resistance of the micropositioner is 50 ohms, the solar cell is being operated in its short circuit mode. In this mode of operation the current available from the cell is about twice the minimum and approximately one quarter of the maximum amount for which the micropositioner was designed, thus insuring positive operation without over driving the circuit.

The elevation portion of the sun tracker consists of two matched photovoltaic cells mounted on a 6^{o} wedge which is located on the camera mounting plate (see Figures 18 & 20). When the wedge apex points at the sun, the cells are illuminated equally and generate equal voltages. Since these voltages are subtracted, a null voltage exists at this time. This D.C. difference voltage is amplified by a Burr-Brown amplifier and chopped at a 400 cps rate by a solid state micro-chopper. The gain of the Burr-Brown amplifier is adjusted to give a gain from sun angle to the output of the sun tracker electronics of 200 Mv/degree, in order to insure a pointing accuracy of 1^{o}. The gain of this circuit can be varied widely to meet changes in requirements simply by changing the values of several components. The amplifier voltage output is limited to ± 3 volts and the associated circuits are sized to limit the output current to four milliamps. This insures that the amplifier is being operated at a maximum power level of only 60% of its rated power handling capacity.

The azimuth sun tracker has two sets of matched photovoltaic cells with each of the sets being mounted on a separate wedge. The two wedges are mounted on the gondola with one wedge pointing forward and one aft. Each azimuth wedge assembly consists of two photovoltaic cells mounted on a 6^{o} wedge. When this wedge points at the sun the cells are equally illuminated and therefore generate equal voltages. However, since the azimuth wedges are mounted on that part of the gondola which does not move in elevation, the azimuth wedge has to point at the sun's position in azimuth

when the sun has any position in elevation from zero to approximately 80 degrees, depending on the latitude, the time of day, and the time of year. In order to minimize the effect of the sun's elevation position on the azimuth tracker output, the azimuth wedge was designed so that it always points at 45^{o} in elevation (see Figures 19 & 20).

The forward and aft pointing azimuth wedges are physically and electrically identical. The cells on each wedge are wired to each other to give their difference voltage, and these differences voltages are added prior to amplification.

In the forward pointing portion of the solar mode, the azimuth motor is arranged to drive in a counterclockwise direction with a positive error signal. If the forward wedge in Figure 19 is wired to produce a positive voltage when cell number two is illuminated more than cell three, and if the aft wedge produces a positive voltage when cell number one is illuminated more than cell four, then the only stable null is with the forward wedge pointing at the sun.

The aft pointing portion of the solar mode is selected by reversing the direction of the motor for a positive error signal. The only stable null under these conditions is with the aft wedge pointing at the sun.

The difference voltages from the azimuth wedges are amplified by a Burr-Brown amplifier and the remainder of the circuitry is identical with that in the elevation portion of the tracker. Offset bias circuits are included in the electronics to balance the output from the system after final assembly.

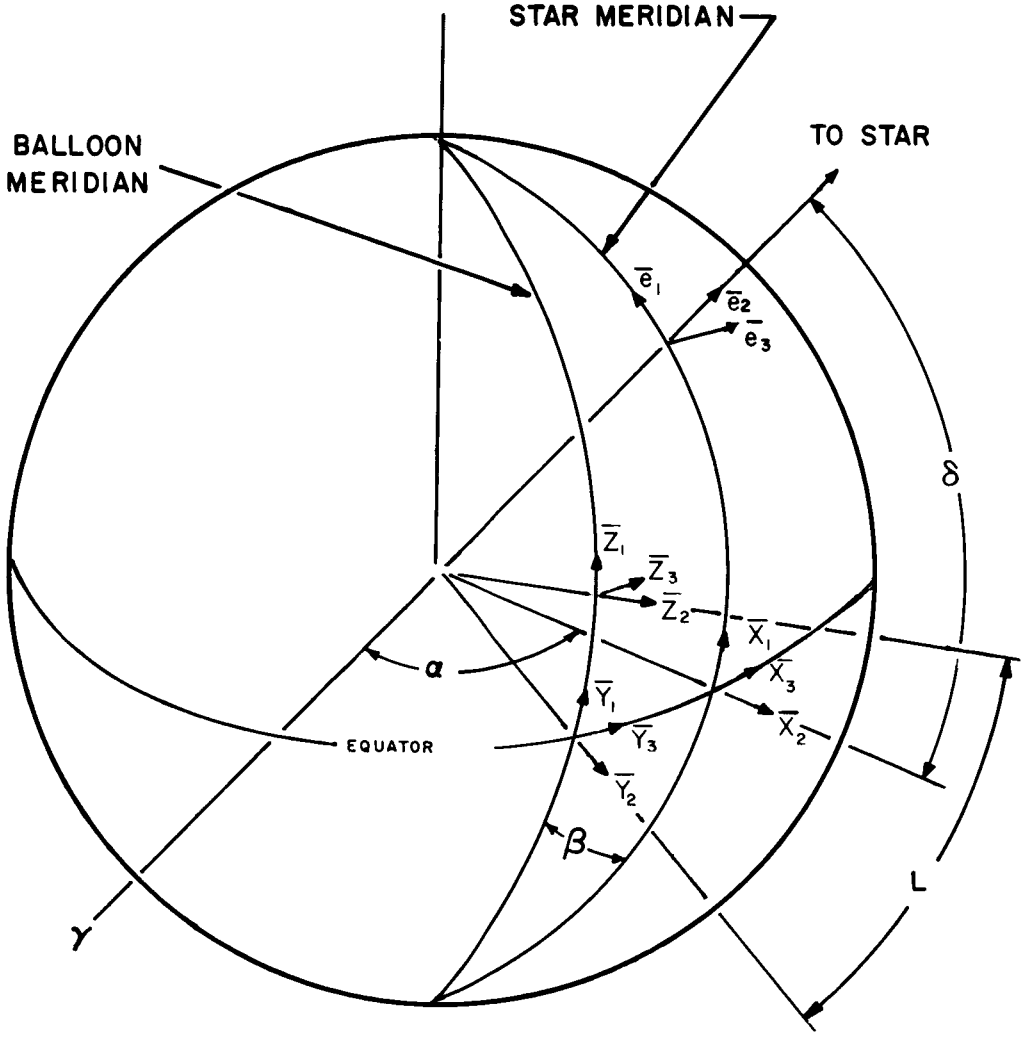

STAR COORDINATES IN THE e_1, e_2, e_3, INERTIAL SYSTEM ARE:

$$\vec{e}_1 = 0$$
$$\vec{e}_2 = 1$$
$$\vec{e}_3 = 0$$

FIGURE 15. STAR/BALLOON COORDINATE TRANSFORMATION

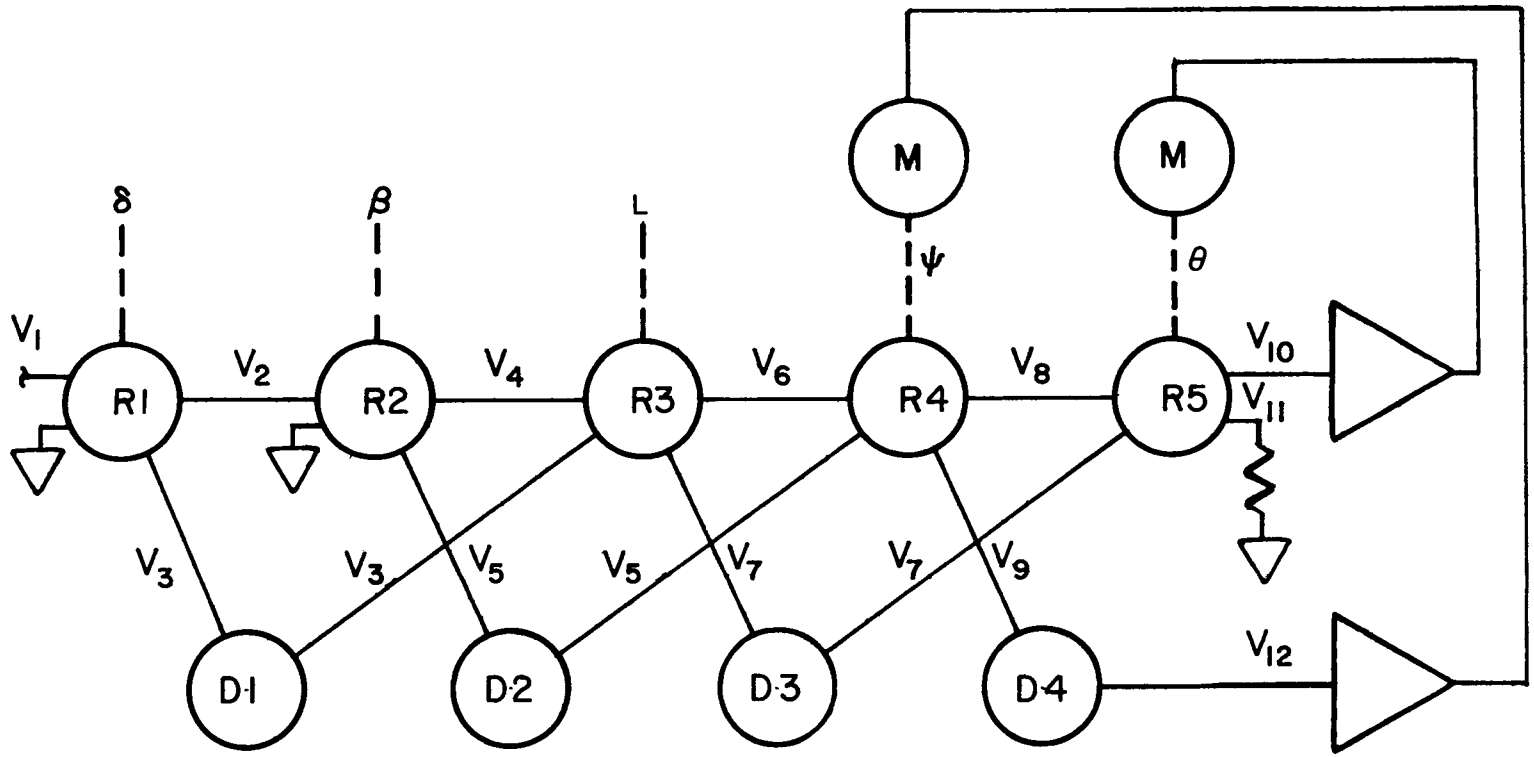

$V_1 = E_v$, v is reference voltage 26v, 400∿

$V_2 = V_1 \cos$

$V_3 = V_1 \sin$

$V_4 = V_2 \cos \beta$

$V_5 = V_2 \sin \beta$

$V_6 = V_4 \cos L - V_3 \sin L$

$V_7 = V_3 \cos L + V_4 \sin L$

$V_8 = V_L \cos \psi - V_5 \sin D$

$V_9 = V_S \cos \psi + V_6 \sin \psi$

Outputs:

$V_{10} = V_8 \cos - V_7 \sin = 0$ at null

$V_{11} = V_7 \cos + V_8 \sin = 0$ at null

$V_{12} = V_9 = 0$ at null

$\tan\theta = \frac{V_8}{V_7}$ $\tan\psi = \frac{-V_5}{V_6}$

FIGURE 16 RESOLVER CHAIN

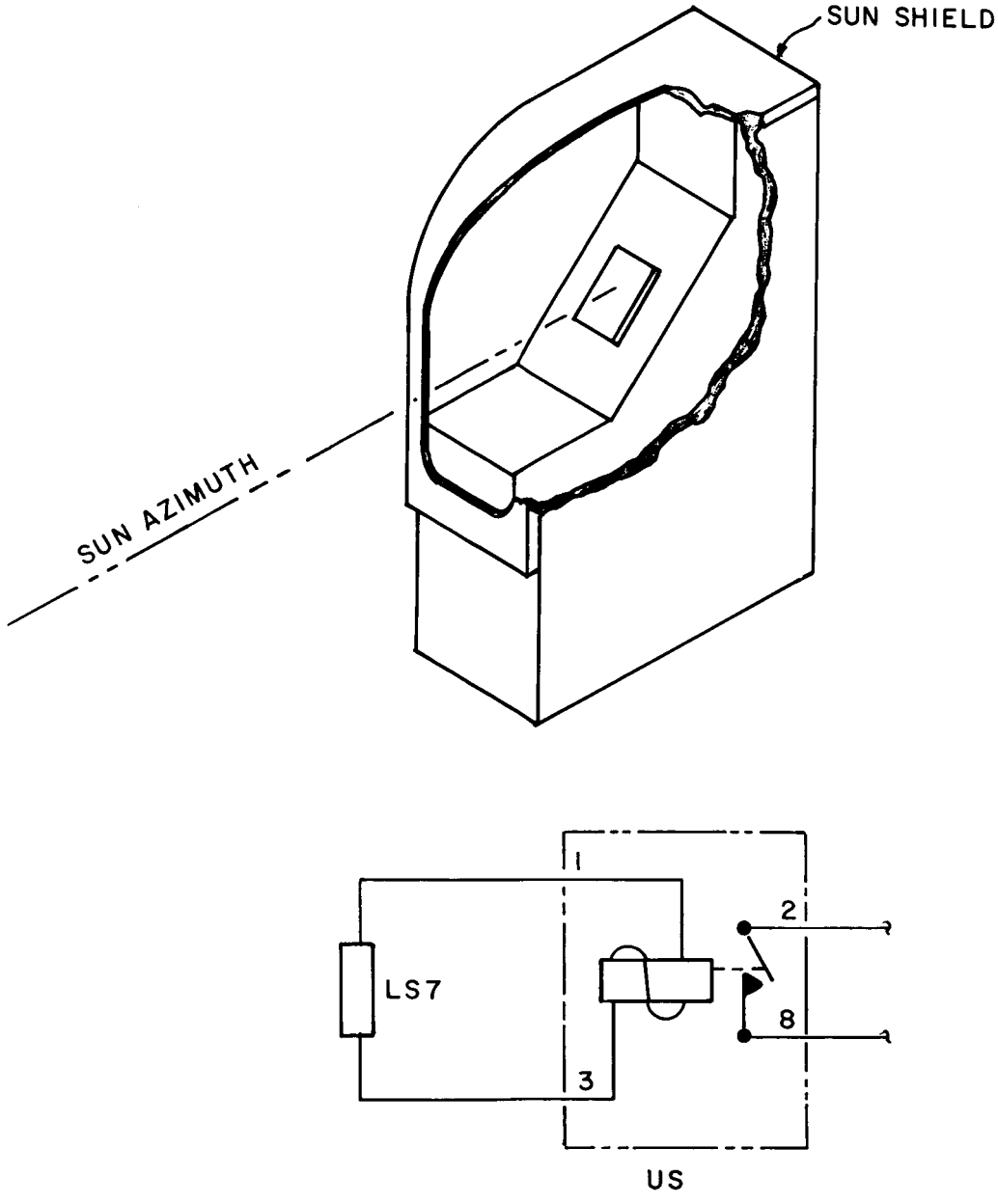

FIG. 17 SUN PRESENCE CELL

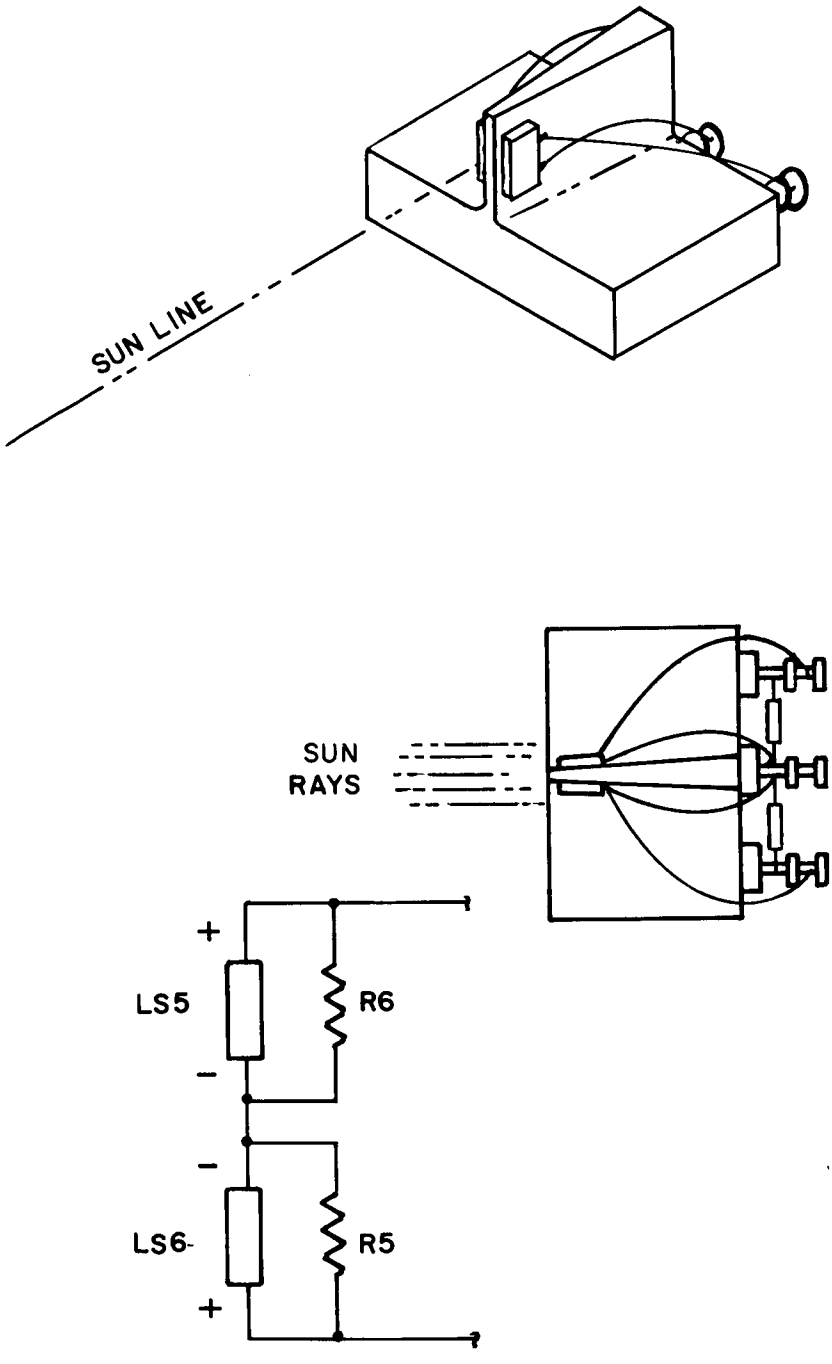

FIG. 18 ELEVATOR WEDGE

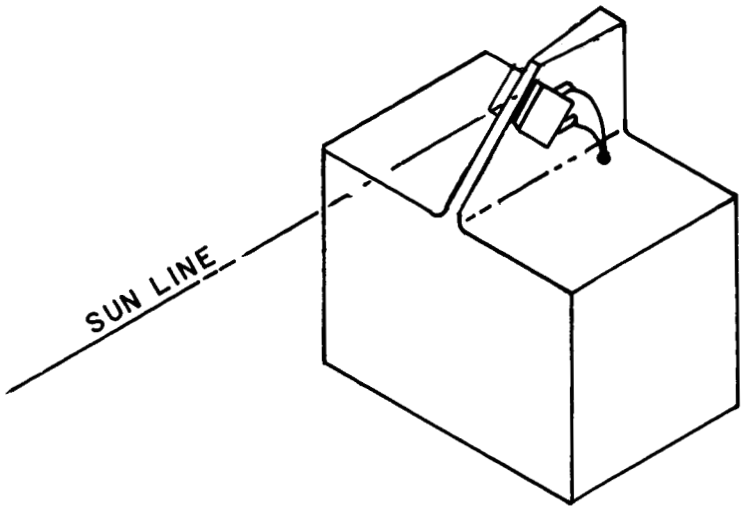

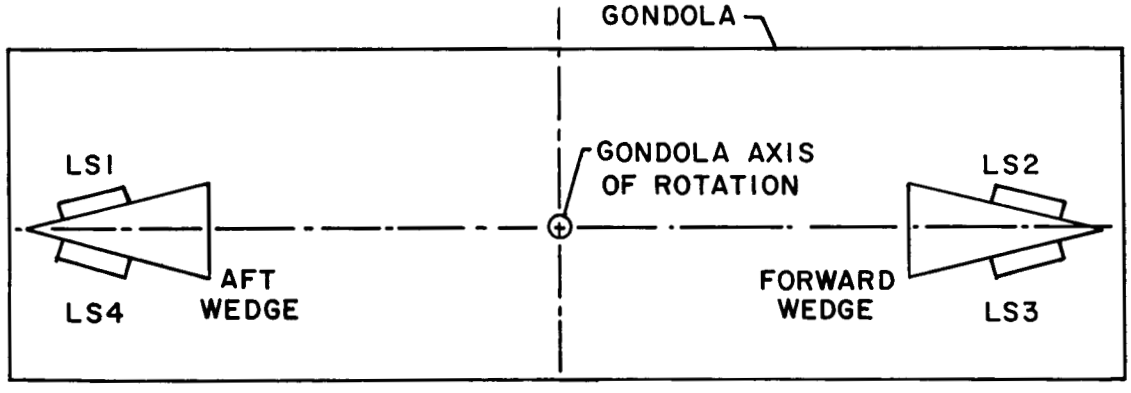

DIAGRAMATICAL TOP VIEW OF AZIMUTH WEDGES ON GONDOLA

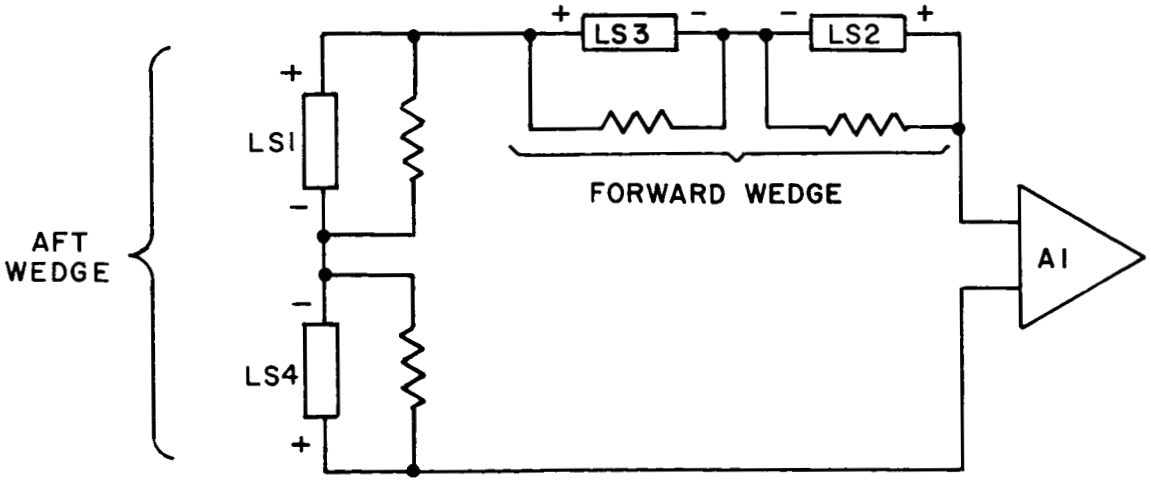

FIG. 19 AZIMUTH WEDGE

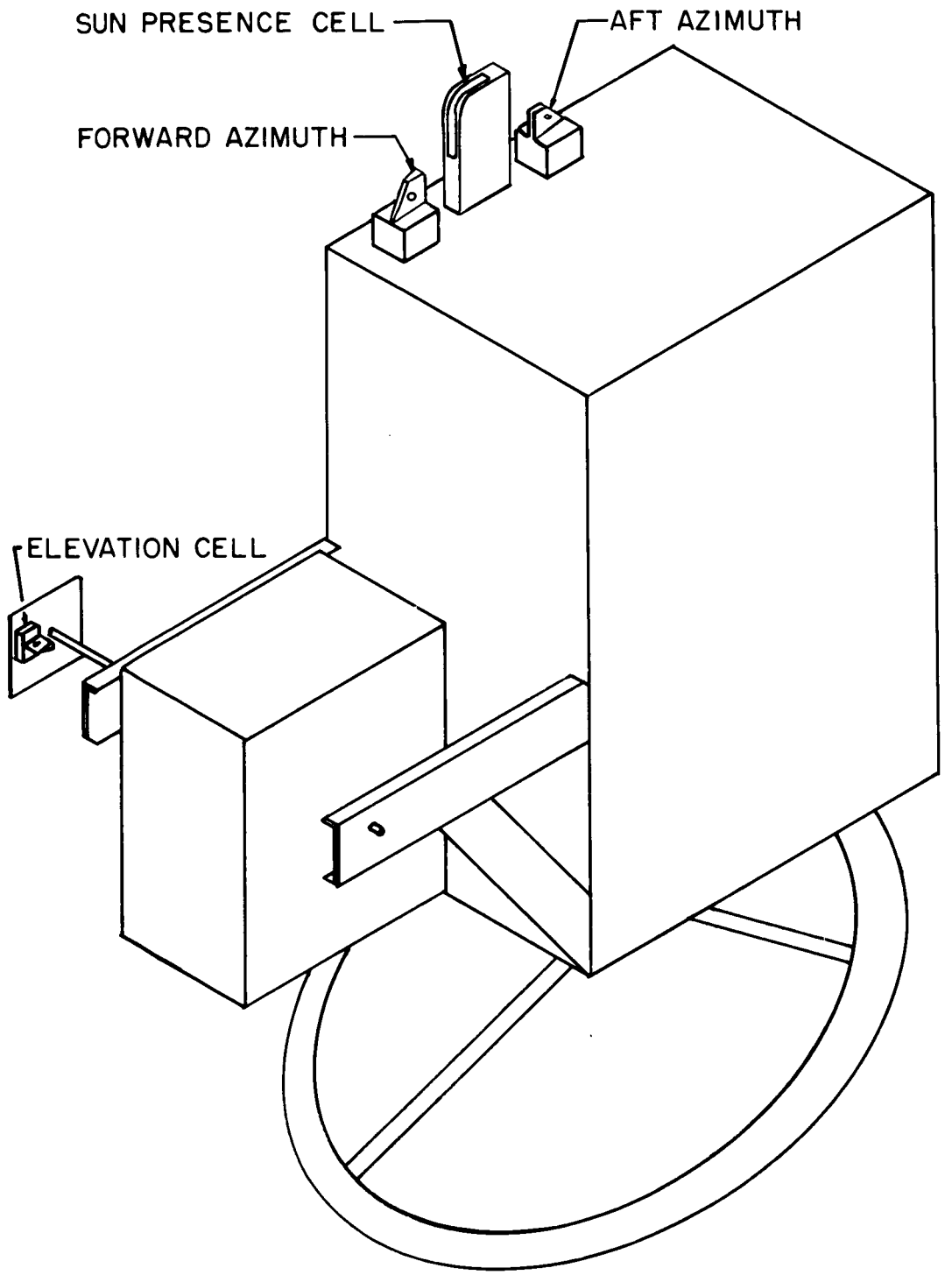
SUN PRESENCE CELL
AFT AZIMUTH
FORWARD AZIMUTH
ELEVATION CELL

FIG. 20

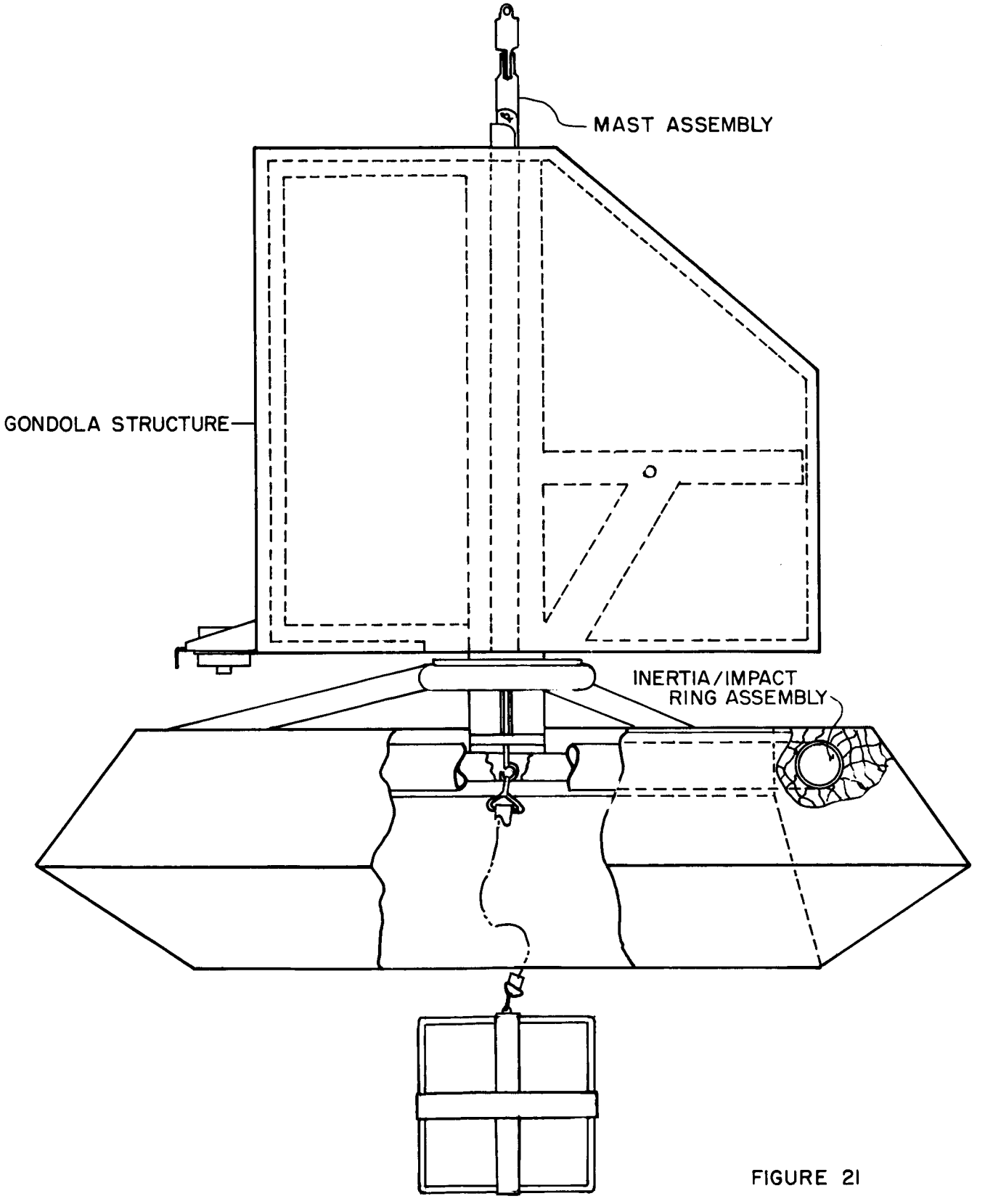
MAST ASSEMBLY
GONDOLA STRUCTURE
INERTIA/IMPACT
RING ASSEMBLY

FIGURE 21

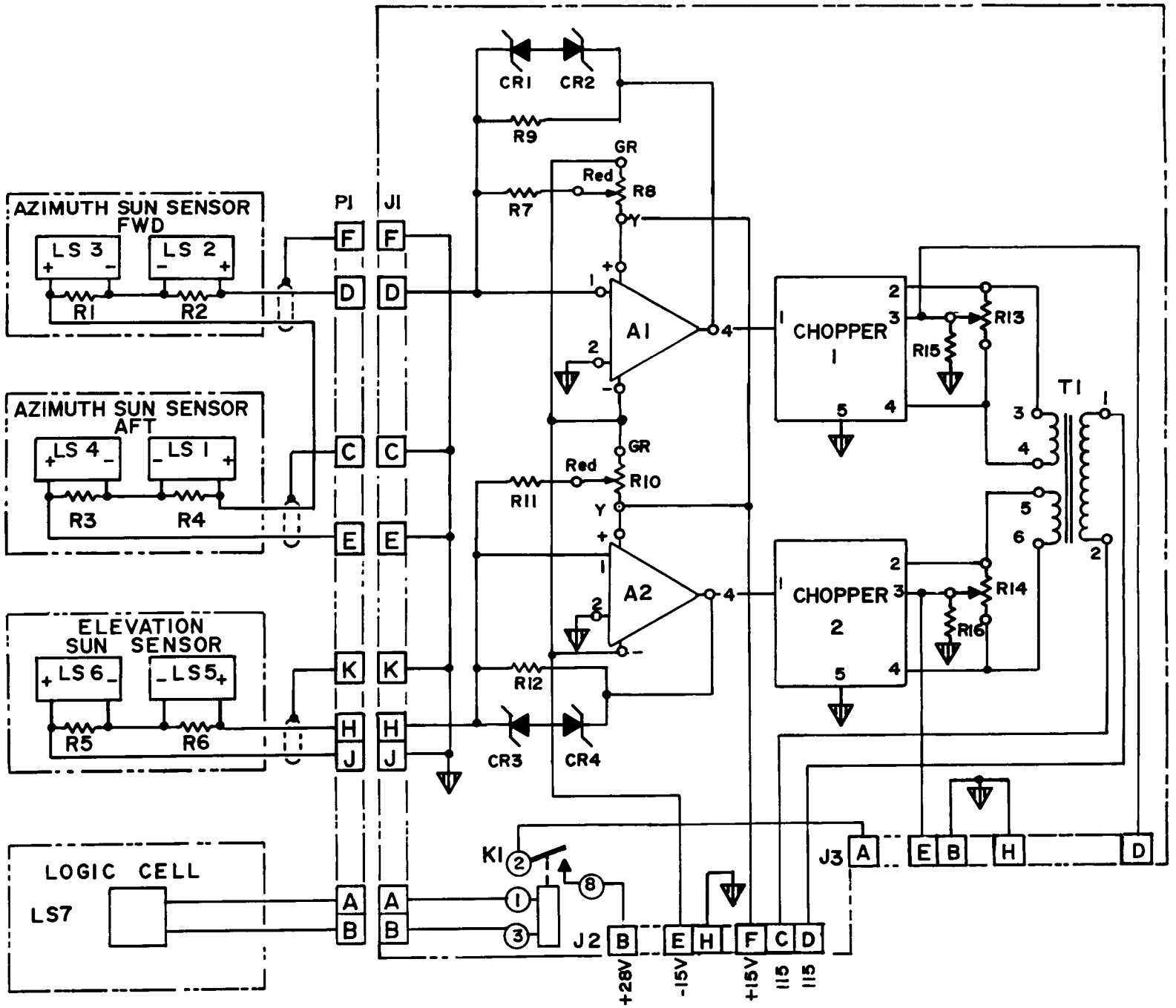

FIGURE 20A SUN TRACKER ELECTRONICS

IV. Structural Mechanical Design

1. Structural/Thermal Design Objectives

The basic structural design criteria for the Balloon Solar Observatory Gondola is described in Paragraphs "A" through "B" below. The sources for establishing this criteria are: (1) Experiment requirements, (2) Mission environment restraints, and (3) Support equipment (Control, recording, and power storage equipment) requirements.

A. Configuration Criteria

The basic dimensional constraints placed on the design of the Gondola structure were determined from the following experiment considerations:

(1) The experiment instrument to be carried on the Gondola will occupy 1 cubic foot of volume.

(2) The experiment instrument must have freedom of rotation about the horizontal and vertical axes of the gondola.

(3) All support equipment shall not occupy more than an additional 4 cubic feet and must be housed within the protective confines of a structural housing. Based on the above stipulations, an overall dimensional envelope (beyond which the gondola structure was not to exceed) of 30 inches in height, 30 inches in length, by 20 inches in width was established.

B. Strength and Rigidity

In addition to staying within the envelope dimensions stipulated above, the gondola must be capable of sustaining its own weight, the weight of the experiment instrument and the weight of all support equipment packages in a balloon lift-off and parachute drop type environment (high acceleration/deceleration). The experiment instrument was estimated to weigh 100 lbs. The support equipment and gondola structure weight was not to exceed 250 lbs. The landing impact environment was estimated to be 7 "G's". For conservatism an additional 3 "G's" has been added to arrive at the total structural environmental factor of 10 "G's". Thus the strength criteria of the primary gondola structure was established such that all components of the primary structure shall be designed to withstand the total payload weight of 350 lbs. multiplied by a 10g environmental factor or 3500 lbs.

The requirement for rigidity was not defined in terms of structural natural frequency, but it was stipulated that the structure shall be sufficiently rigid to insure no amplification of small disturbance forces imparted by the control system or the experiment instrument. This stipulation, without a call-out for structural natural frequency, was not unreasonable since the gondola, suspended from a balloon at 150,000 feet, will be operating in a quasi-steady state environment (appreciably no

external forces acting on the gondola to excite vibration). Although high frequency vibrations induced by the control system could seriously degrade pointing accuracy, in the case of BSO the effects on the pointing requirement are negligible. Therefore, the primary strength consideration was the minimum structural weight commensurate with the required structural strength.

C. Structural Weight & Inertia

From the total payload weight of 350 lbs., an allotment of 70 lbs. was made for the gondola structure; however, because of the mode of operation of the control system, the weight of an inertia ring (to establish counter rotating torque) is also included in the 70 lb. allotment. From control considerations it was desirable to have the inertia of the ring match or exceed the inertia properties of the loaded gondola. As a worst case the ring inertia should not be less than one-half the inertia of the loaded gondola (two to one mismatch). In an effort to establish practical dimensions and weights for an inertia ring, it was dictated that the moment of inertia of the loaded gondola shall not exceed 5 slug ft^2. Based on this, an allotment of 20 lbs. was made for the inertia ring and a maximum practical ring diameter of 4 feet was stipulated. Thus the weight objective for the gondola structure shall be 50 lbs.

D. Mechanical Concept of Operation

As mentioned in Paragraph C above, the gondola control system requires an inertia ring, or wheel, to provide counter rotating torque. Therefore the mechanical design objective is to directly couple the inertia ring to the control system such that this inertia ring absorbs the control motor reaction torque.

E. Shock Mitigation

At the completion of the experiment mission, the gondola will be released from the balloon with the descent controlled by a 28' parachute. With a 350 lb payload the parachute has an average drop velocity of 5 feet/second. The design objective is therefore to provide shock mitigation material at the base of the gondola to absorb the impact energy on landing and thus preserve sensitive experiment equipment and support equipment packages from severe shock.

F. Thermal Control

The temperature environment at 130,000 feet (the mission altitude) is $+20^{\circ}F$ and in itself does not pose any severe thermal problems; however, at this altitude the density of the air is low ($1.06X10^{-4}$ lb/ft^3) and effects from convection heat transfer are therefore negligible. The cooling of components must be primarily by conduction and radiation. Sufficient insulation over the external faces of the gondola will also be required as a thermal barrier against earth albedo and direct solar radiation. This insulation will increase the thermal lag of the gondola and is especially important during the ascent to altitude phase of the mission. During ascent the gondola must pass through a $-60^{\circ}F$ air temperature zone

(from 40,000 ft to 85,000 ft). The thermal design objective was to provide maximum thermal protection at altitude and to provide the minimum temperature excursion commensurate with insulation weight, during gondola ascent.

2. Structural Design

A basic operational scheme was developed which enhanced the operation of the control system and the survival of the equipment, the experiment and the gondola structure during the landing impact environment. This scheme as depicted in assembly drawing Figure 21, consisted of the design and mathematical integration of three separate structural/mechanical assemblies. The first assembly is the Gondola structure which houses the support equipment and the experiment instrument. The second assembly is the mast assembly which supports the gondola and about which the gondola rotates. The tip of this mast assembly is attached to the balloon via the parachute lines. The third assembly is the inertia/impact ring assembly. This assembly provides the counter rotating torque required by the control system and is capable of absorbing a large percentage of the landing impact energy. The inertia/impact ring structure is bolted to the base of the mast assembly. Throughout the design of the above three assemblies, emphasis was placed not only on the proper design for functional operation, but also on minimizing structural weight commensurate with required strength and rigidity.

A. Gondola Structural Assembly

The gondola structural assembly is formed from welded aluminum (6061-T6) primary and secondary structural members. All support equipment loads are cantilevered off the main primary structural members. The functions of the secondary structural members are to provide local mounting points for equipment boxes and thermal insulation, and overall structural rigidity. The function of the primary structure is to support the loads of all equipment boxes and the experiment package; it also transfers these loads (including the 10g environmental factor) to the mast assembly.

To achieve 100% structural effectivity of all the aluminum welded joints, aluminum gusset plates were welded to each joint. The dimension of each gusset was chosen such that the length of each gusset weld exceeds the length of joint weld by a factor of 10. The primary structure was lightened approximately 20% by drilling 3-inch and 2-inch diameter lightening holes along the members which form the primary structure. In locating the position of lightening holes care was taken to insure that the strength was not reduced below that required.

(1) The primary structural members consist of two vertical 5 X 1 3/4 X 1/4 inch channels, 30 inches in length. The base of the channels are welded to a specially designed shaped horizontal bridge channel and are spaced 20 inches apart.

(2) The horizontal bridge channel is specially formed by welding a 7 X 20 X 3/16 inch base plate to two formed flanges as shown on Figure 22. The bridge channel is capped at each end by the weldment of

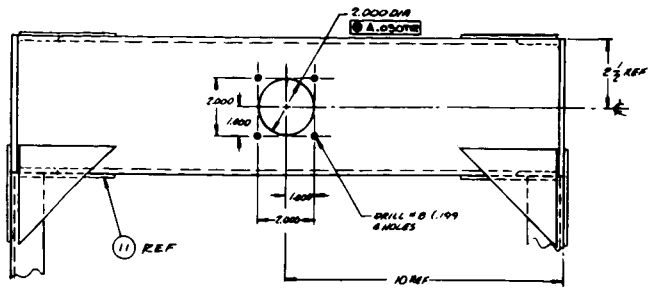
2.000 DIA
Ⓜ A 0.50 M
2.000
1.400
1.800
2.000
DRILL Ø 0.199
4 HOLES
11 REF
10 REF

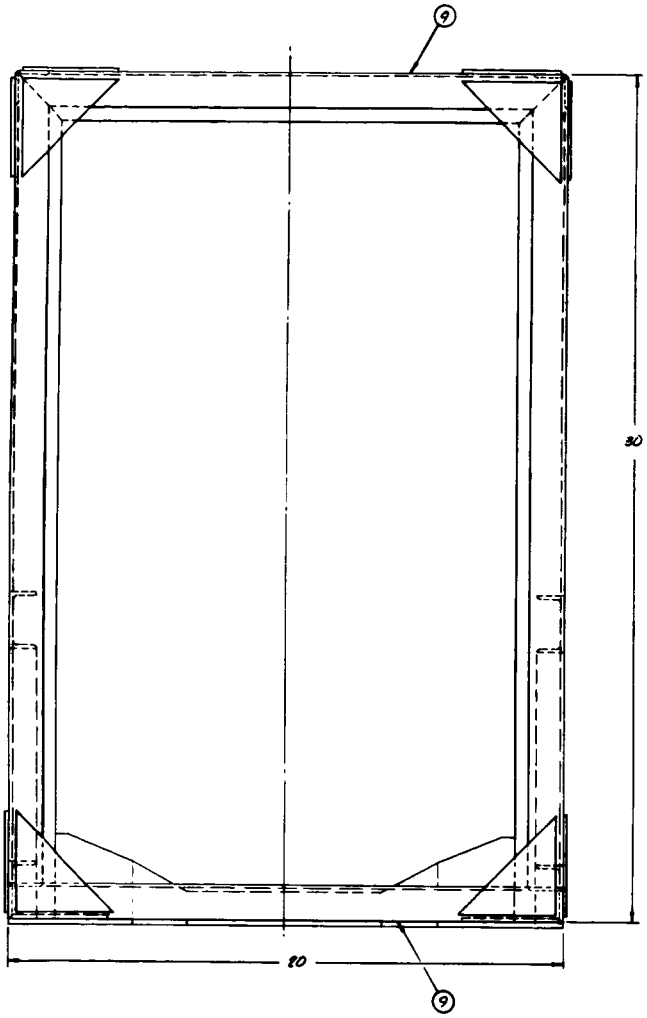
9
30
20
9

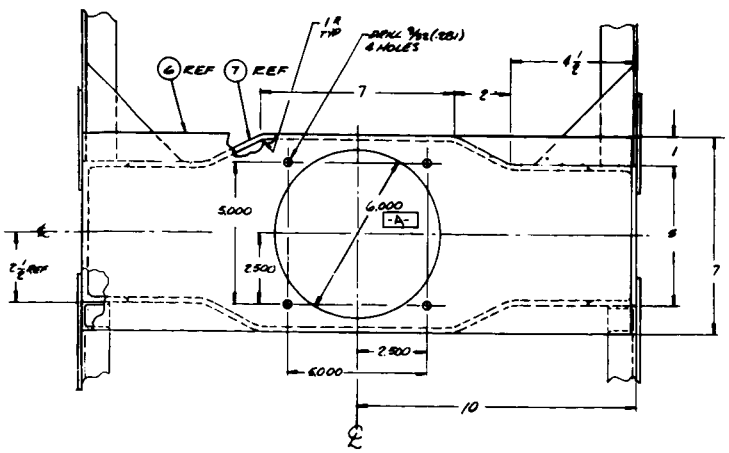
1.0 TYP
DRILL 3/32 (.094)
4 HOLES
6 REF
7 REF
7
2
1 1/2
1
5.000
6.000
-A-
2.500
2.500
6.000
10

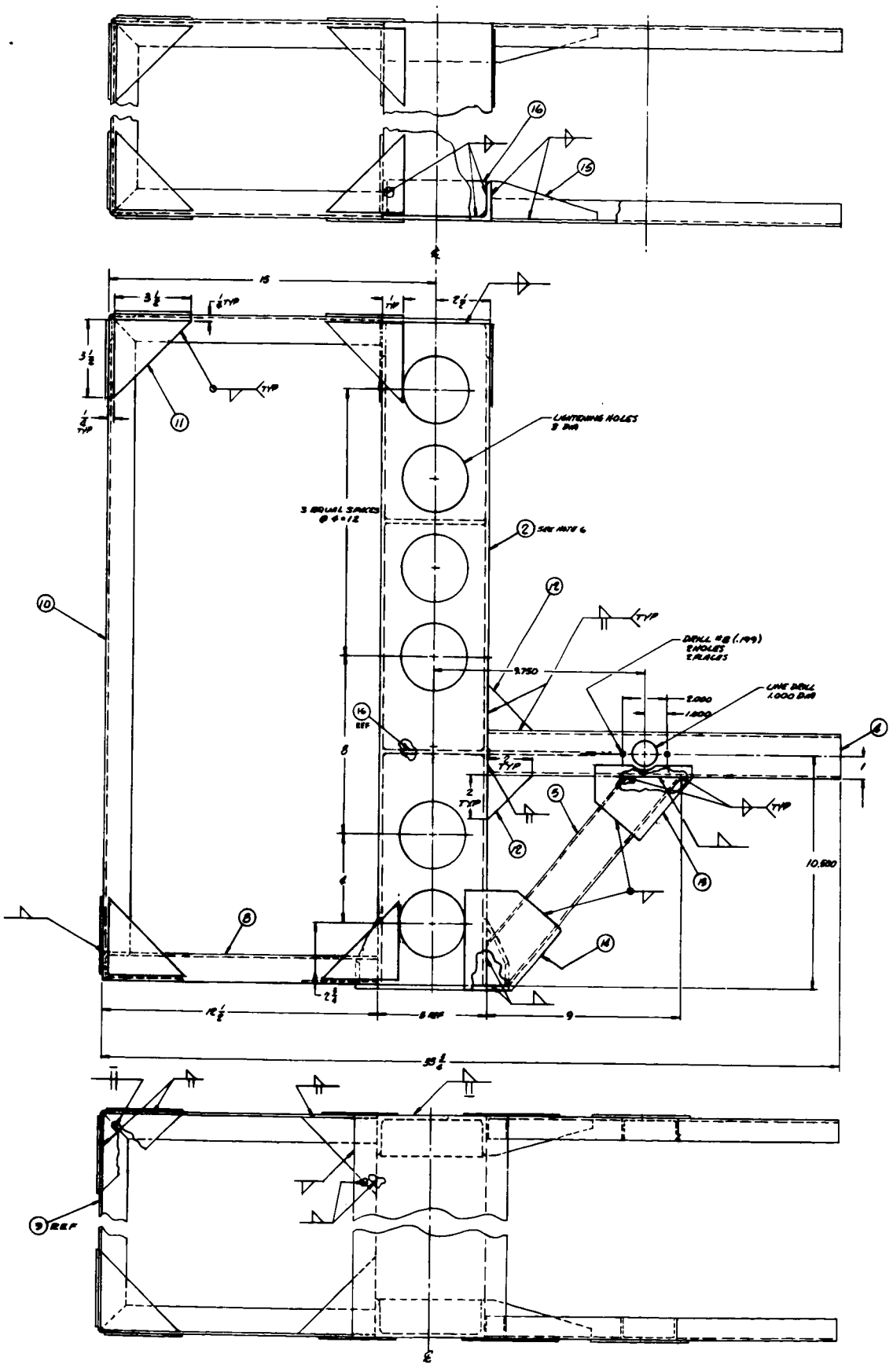
16
15
18
3½
¼ TYP
1 TYP
2½
3½
¼ TYP
11
TYP
LIGHTENING HOLES 3 DIA
3 EQUAL SPACES @ 4=12
2 SEE NOTE 6
12
10
TYP
DRILL #8 (.199) 2 HOLES 2 PLACES
3.750
2.000
1.800
LINE DRILL 1.000 DIA
16 REF
8
4
1
½ TYP
2 TYP
5
TYP
12
13
10.830
8
14
2½
12½
8 REF
9
35¼
9 REF

NOTES: UNLESS OTHERWISE SPECIFIED

1. AFTER WELDING - STRUCTURE IS TO BE STRESS RELIEVED AS FOLLOWS: HEAT TREAT TO 385° ± 15° FOR 18 HOURS. BRING UNIT TO TEMPERATURE STATED AS QUICKLY AS PRACTICABLE, FURNACE SHOULD MAINTAIN CONSTANT TEMPERATURE OF ± 10° FOR TIME SPECIFIED. COOLING RATE TO BE NORMAL IN ROOM CONDITION ENVIRONMENT.
2. FINISHED STRUCTURE TO BE SQUARE TO WITHIN 1/8 MAX IN ALL DIRECTIONS
3. CHEMICAL FINISH: BLACK ANODIZE AFTER WELDING
4. ALL WELDED JOINTS TO BE FREE OF FLUX & WELDING RESIDUE PRIOR TO ANODIZE PROCESS.
5. ALL MACHINE WORK TO BE DONE AFTER HEAT TREAT PROCESS.
6. MODIFY ITEMS 2 & 3 MATERIAL BY CUTTING 2 INCH FLANGE TO 1 3/16

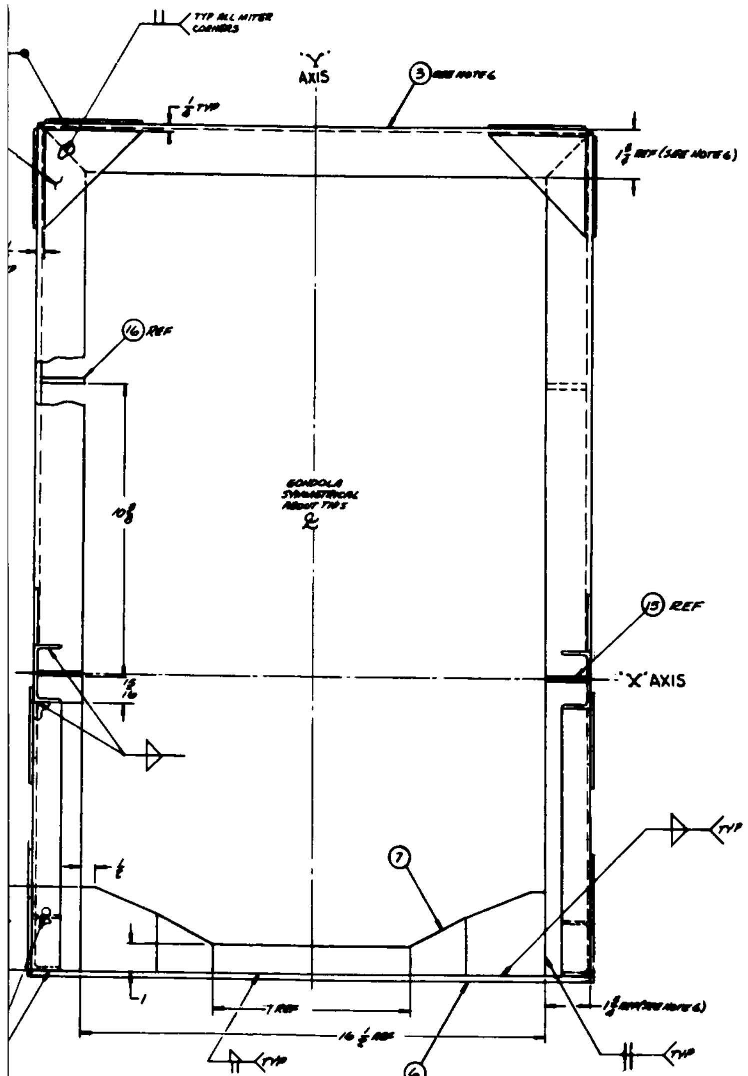

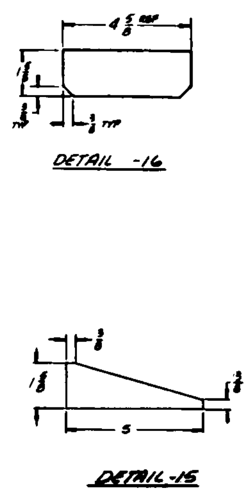

FIGURE 22

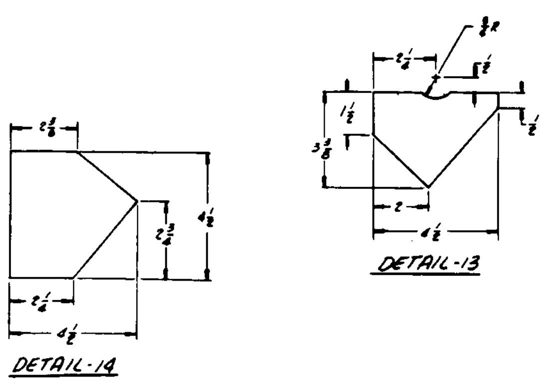

ITEM	REQ'D	PART NO.	DESCRIPTION	MATERIAL	MAT'L SPEC	UNIT WT.
16	4	-16	GUSSET-FLANGE 1 5/8 x 4 ... x 1/8	AL ALY SH	6061-T6	
15	2	-15	GUSSET-CHANNEL 1 5/8 x 5 x 1/8	AL ALY SH	6061-T6	
14	2	-14	GUSSET-LOWER REINFORCING 4 1/2 x 4 1/2 x 1/8	AL ALY SH	6061-T6	
13	2	-13	GUSSET-UPPER REINFORCING 3 3/8 x 4 1/2 x 1/8	AL ALY SH	6061-T6	
12	8	-12	GUSSET-TRIANGULAR 2 x 2 x 1/8 THK	AL ALY SH	6061-T6	
11	24	-11	GUSSET-CORNER 3 1/2 x 3 1/2 x 1/8 THK	AL ALY SH	6061-T6	
10	2	-10	ANGLE 1 1/4 x 1 1/4 x 1/8 x ... (DWG # 77-F)	AL ALY	6061-T6	
9	2	-9	ANGLE 1 1/4 x 1 1/4 x 1/8 x 20 LONG (DWG # 77-F)	AL ALY	6061-T6	
8	4	-8	ANGLE 1 1/4 x 1 1/4 x 1/8 x 12 1/2 LONG (DWG # 77-F)	AL ALY	6061-T6	
7	2	-7	GUSSET-BOTTOM 3 x 17 x 1/16	AL ALY SH	6061-T6	
6	1	-6	PLATE-BOTTOM 7 x 20 x 1/16	AL ALY SH	6061-T6	
5	2	-5	CHANNEL-DIAGONAL (...)	AL ALY	6061-T6	
4	2	-4	CHANNEL-SUPPORT (...)	AL ALY	6061-T6	
3 (SEE NOTE 6)	1	-3	CHANNEL-TOP (5 x 2 x 1/8 WT x 20 LG) REYNOLDS DWG # ...	AL ALY	6063-T6	
2 (SEE NOTE 6)	2	-2	CHANNEL-SIDE (5 x 2 x 1/16 WT x 30 LG) REYNOLDS DWG # 8981	AL ALY	6063-T6	
1	X	...-104010	GONDOLA WELDMENT			

LIST OF MATERIAL

NATIONAL AERONAUTICS AND SPACE ADMINISTRATION
GODDARD SPACE FLIGHT CENTER

622.5

GONDOLA WELDMENT
A508 BALLOON

NEXT ASSEMBLY: GI-A508-1104005
SCALE: HALF
DRAWING NO.: GI-A508-1104010
SHEET 1 OF 1

the 5" vertical channels. Also, at each end of the bridge channel, the secondary structural base members tie into the primary structure. For strength, rigidity, and weld effectivity, both horizontal and vertical gusset plates have been welded to these joints. The center of the bridge channel base plate has a 6" diameter clearance hole. The gondola structure pivots about the centerline of this hole. A bearing retainer plate (see Figure 23) is bolted to the underside of this bridge channel base plate. The lower mast assembly bearing is pressed into this bearing retainer plate with the mast assembly passing through the 6" hole. The weight of the entire payload is therefore transferred from the vertical 5" channels to the horizontal bridge channel. From the horizontal bridge channel the load is then transferred through the bearing retainer plate, to the lower mast assembly bearing and finally to the mast assembly.

(3) The top of the two 5" channels are capped with a 5 X 1 3/4 X 1/4 inch cross channel. The top mast secondary structural members are tied into the structure at these capped corners and the joints are reinforced with welded vertical and horizontal gussets. The center of this cross channel as a 2" diameter hole. The mast assembly passes through the centerline of the hole. From the underside of the cross channel, in line with the hole, is bolted the upper bearing retainer plate (see Figure 24). The purpose of the upper mast assembly bearing is to hold the mast assembly in the correct alignment position. When the mast assembly is inserted from the base of the gondola through the center of the gondola structure, the mast assembly shaft will slide through the inner face of the upper bearing - thus positioning the mast assembly shaft with respect to the gondola. Note should be made that this upper bearing is capable of transmitting tangential and normal forces to the cross channel, but will not transmit vertical thrust forces imposed by the payload weight. The bearing which transmits the principal thrust forces is the lower mast assembly bearing.

(4) The loading diagram for the gondola primary structure is shown below:

SIMPLIFIED LOADING DIAGRAM FOR SECTIONED GONDOLA STRUCTURE (ENVIRONMENTAL FACTOR INCLUDED)

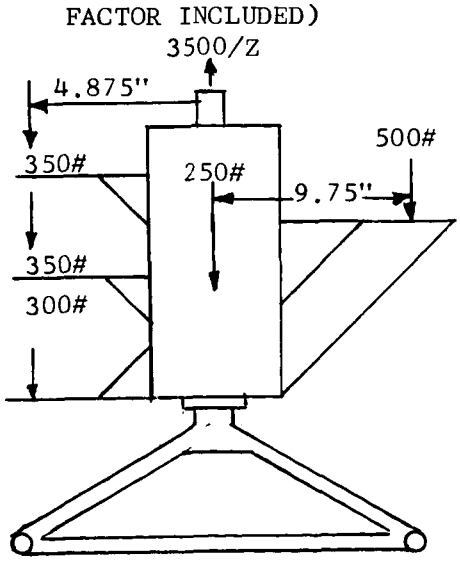

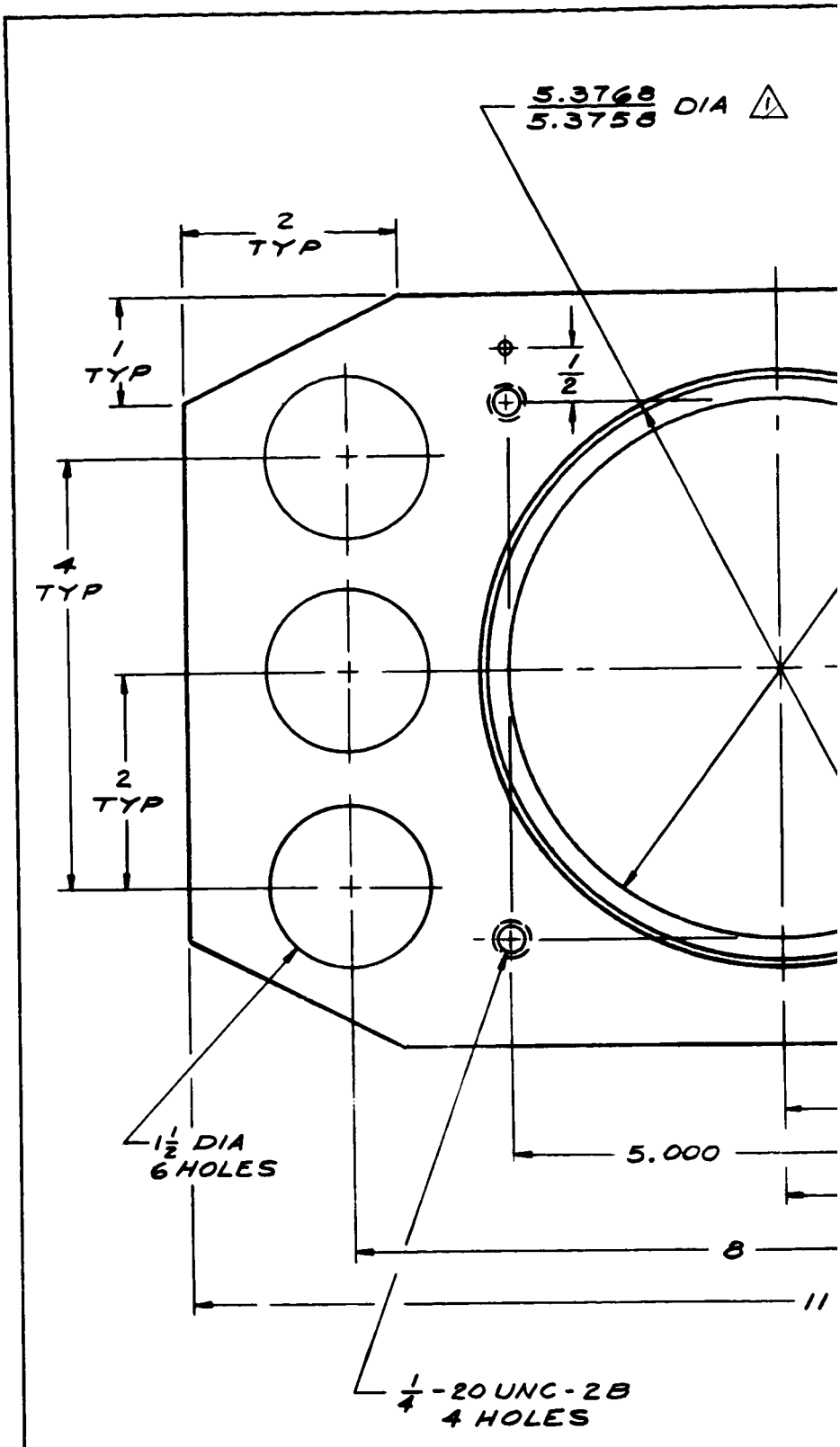

MAT'L:
AL ALY PLATE
2024-T4 (OPTIONAL 6061-T6)
FINISH:
BLACK ANODIZE 125/
MACH FINISH ALL OVER √

REVISIONS			
SYM	DESCRIPTION	DATE	APPROVAL

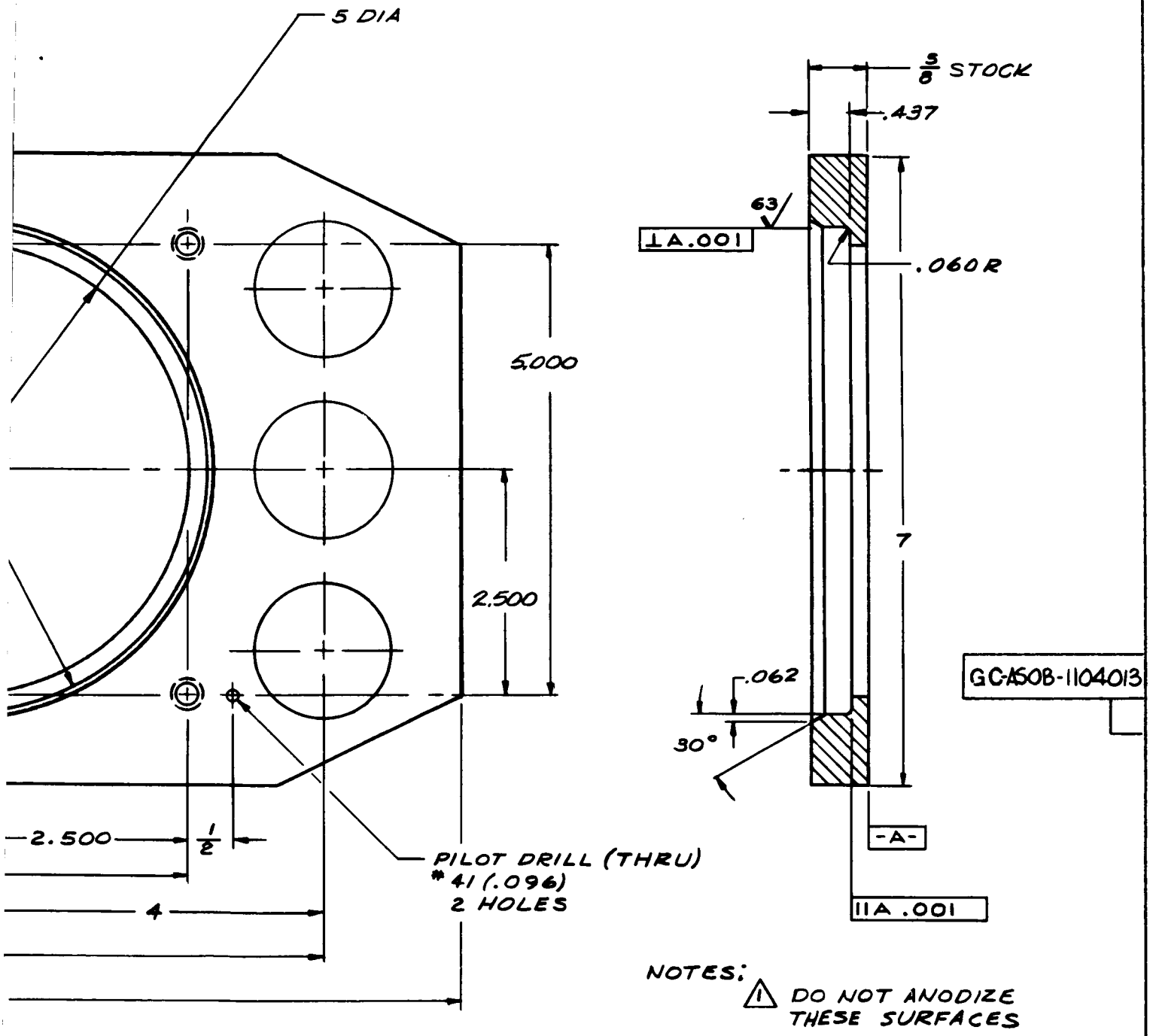

NOTES:

1. ⚠ DO NOT ANODIZE THESE SURFACES

FIGURE 23

REQD	PART NO.	DESCRIPTION	MATL	MATL SPEC	UNIT WT.

LIST OF MATERIAL

UNLESS OTHERWISE SPECIFIED
DIMENSIONS ARE IN INCHES
TOLERANCES ON:
FRACTIONS ±1/64 DECIMALS ± .005 ANGLES ± 2°

NAME	INIT	DATE
DESIGNER		
DRAWN Ed Lewis	EL	8-13-63
CHECKED Zapura	EJ	9/20/63
APPROVED W. NAGEL	WN	9/24/63
APPROVED D.B. Fallstrom		9/24/63

GJ-ASOB-1104005
NEXT ASSY | USED ON

BEARING PLATE LARGE ASO BALLOON

NATIONAL AERONAUTICS AND SPACE ADMINISTRATION
GODDARD SPACE FLIGHT CENTER
GREENBELT, MARYLAND

GC-ASOB-1104013

SCALE FULL | INIT 0°

CODE 622 | SHEET 1 OF 1

SIMPLIFIED LOADING DIAGRAM FOR TOTAL STRUCTURE

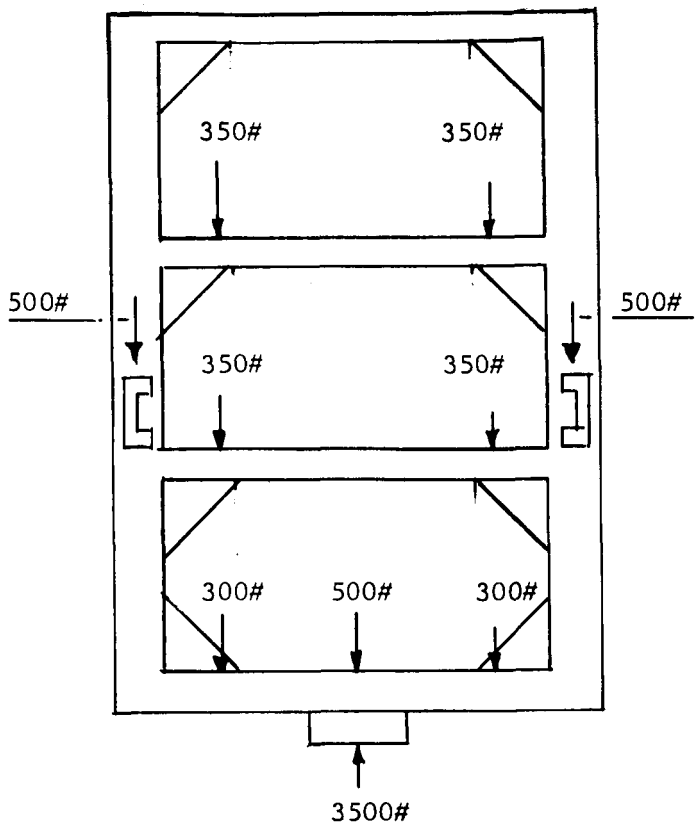

(5) Although a complete stress analysis of the entire structure was not performed, the sizing of all primary structural members was based on local stress analyses using the above loading diagram. These stress calculations were based on the assumption that all support equipment and experiment instrument loads are cantilevered from the 5" channel structure. Stress checks for the channel structure have been made for failure in bending, collapse of flanges, and shear failure at the critical lightening hole sections. The cantilever equipment support beams were analyzed for shear failure, bending failure and deflection. The special horizontal bridge channel was examined for bending and shear stress failure. This analysis follows:

(a) Stress Analysis of Horizontal Bridge Channel

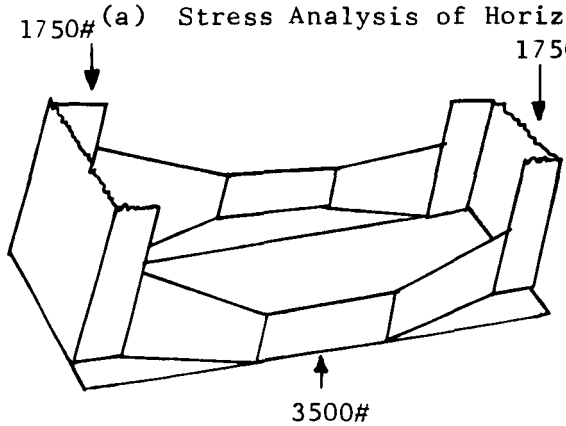

R_1 = 1750#
R_2 = 1750#
W = 3500#
l = 20 inches
Q = Shear Force
M = Bonding Moment
f = Deflection

NOTES:

1. ⚠ DO NOT ANODIZE THESE SURFACES

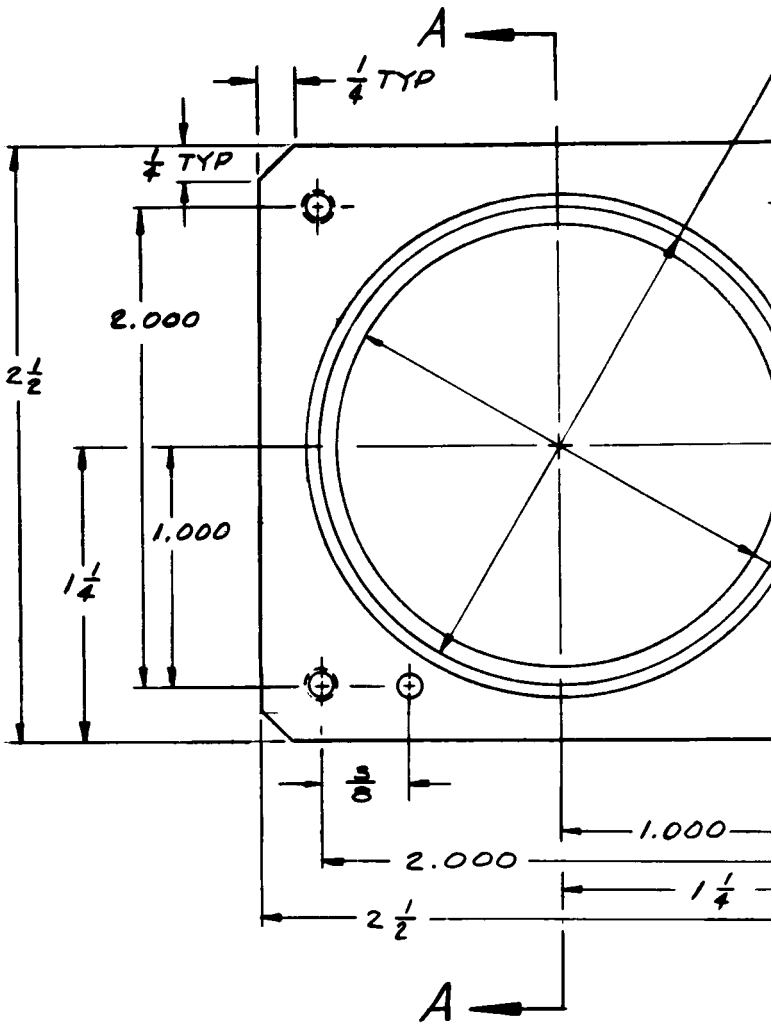

MAT'L:
AL ALY PLATE
2024-T4 (OPTIONAL 6061-T6)

FINISH:
BLACK ANODIZE

MACH FINISH ALL OVER 125√

REVISIONS			
SYM	DESCRIPTION	DATE	APPROVAL

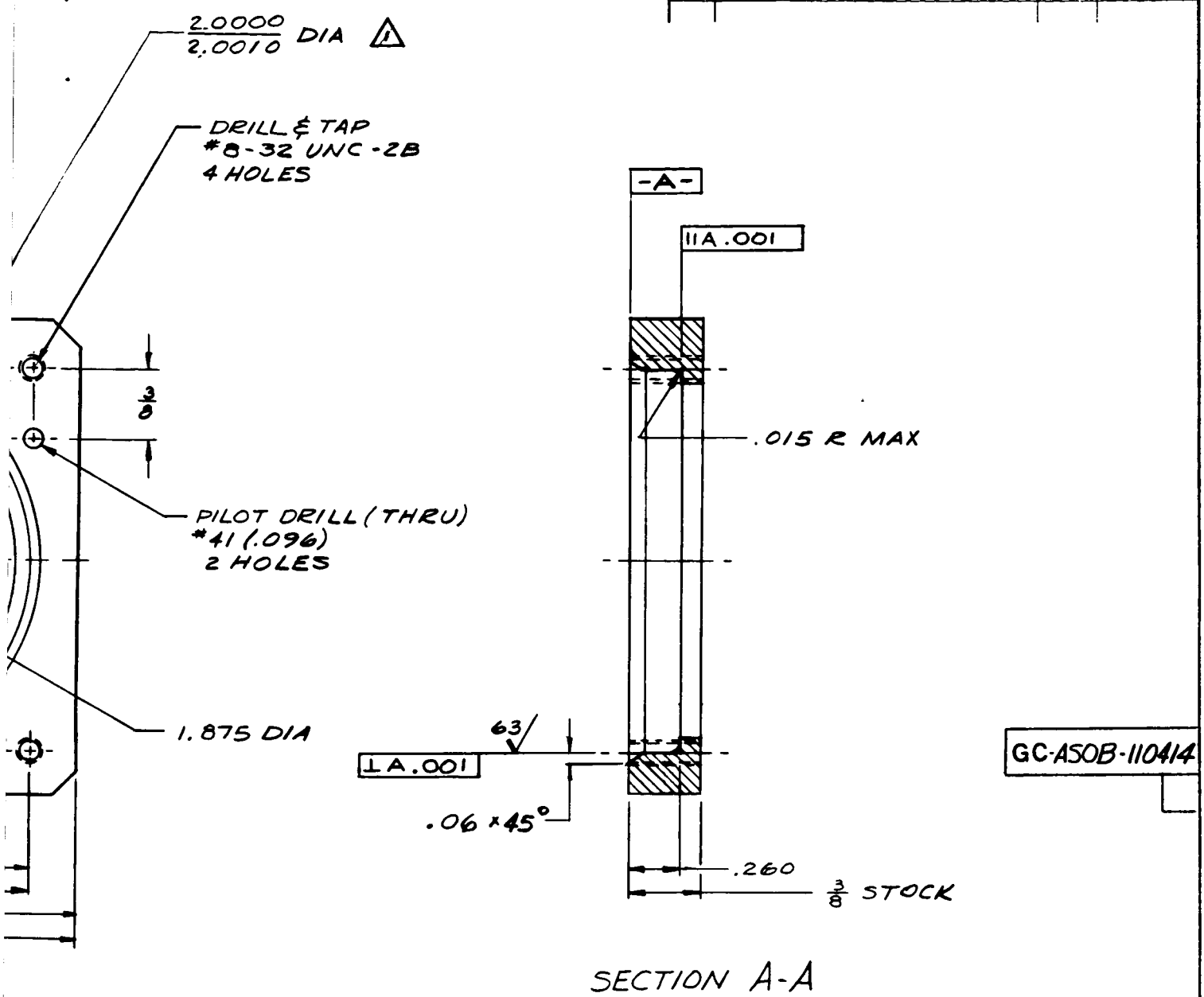

SECTION A-A

FIGURE 24

REQD	PART NO.	DESCRIPTION	MATL	MATL SPEC	UNIT WT.
		LIST OF MATERIAL			

UNLESS OTHERWISE SPECIFIED	NAME	INIT	DATE		
DIMENSIONS ARE IN INCHES	DESIGNER			BEARING PLATE SMALL ASO BALLOON	NATIONAL AERONAUTICS AND SPACE ADMINISTRATION GODDARD SPACE FLIGHT CENTER GREENBELT, MARYLAND
TOLERANCES ON:					
FRACTIONS ±1/64 DECIMALS ± .005 ANGLES ± 2°	DRAWN Ed Lewis	EL	8-26-63		
	CHECKED Capuano	EJ	9/9/63		
	APPROVED W. Nagel	WN	9/11/63		GC-ASOB-1104014
GJ-ASOB-1104005	APPROVED RG Fulton		9/26/63		
NEXT ASSY	USED ON	SCALE 2:1		CODE 622	SHEET 1 OF 1

Simplified Lower Bridge Channel Loading Diagram

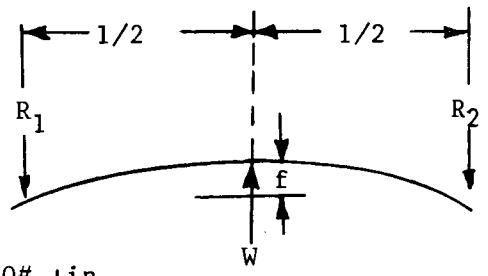

$R_1 = \frac{W}{2}$, $R_2 = \frac{W}{2}$

$M_x = \frac{W_x}{2}$

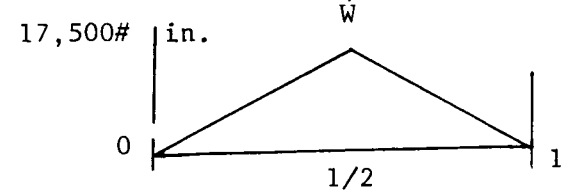

$M_{max} = \frac{Wl}{4}$, a+x = 1/2

$Q_x = \pm \frac{W}{2}$

$f = \frac{Wl^3}{EI48}$ (MAX)

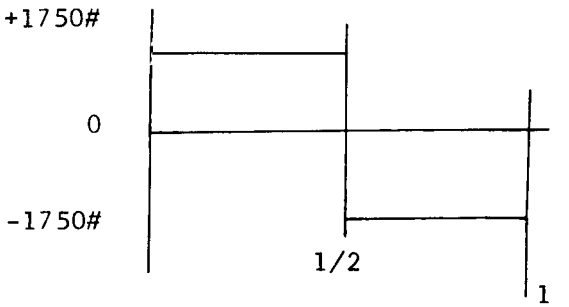

M_{max} = 17,500# in

Q_x = 1750

$f = \frac{Wl^3}{EI48}$

In solving for the section inertia I of the composite structure, the dimensions for I are chosen

$I = 1/3\ (5"XC_1^3 - (4\ 5/8")\ X\ h^3 + 2\ X\ (3/16")\ C_2^3)$

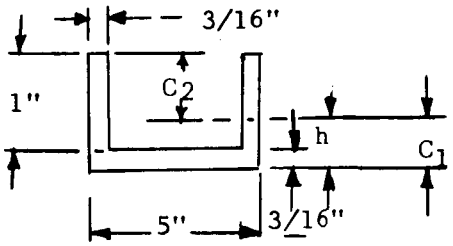

C_1 = .398 inches

C_2 = 1-.398 = .602"

h = .023"

I = .160 in^4

Solving for maximum bending stress

$$6 = \frac{MC}{I} \qquad 6_{max} = \frac{M_{max}C}{I} = 43{,}500\#\ in^2$$

Max bending stress for 6061-T6 is 35,000#/in^2. Therefore, the bridge channel will fail under maximum load. To overcome this weakness a bearing retainer plate (Figure 23) is added to distribute the load (W).

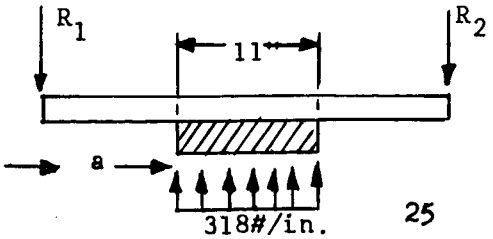

W=W/11=3500#/11=318#/in

a = 10-5.5 = 4.5 in

$M_{max} = R_1(a + R_1/2W)$

M_{max} = 12,700# in.

NOTES:

1. DO NOT ANODIZE THESE SURFACES

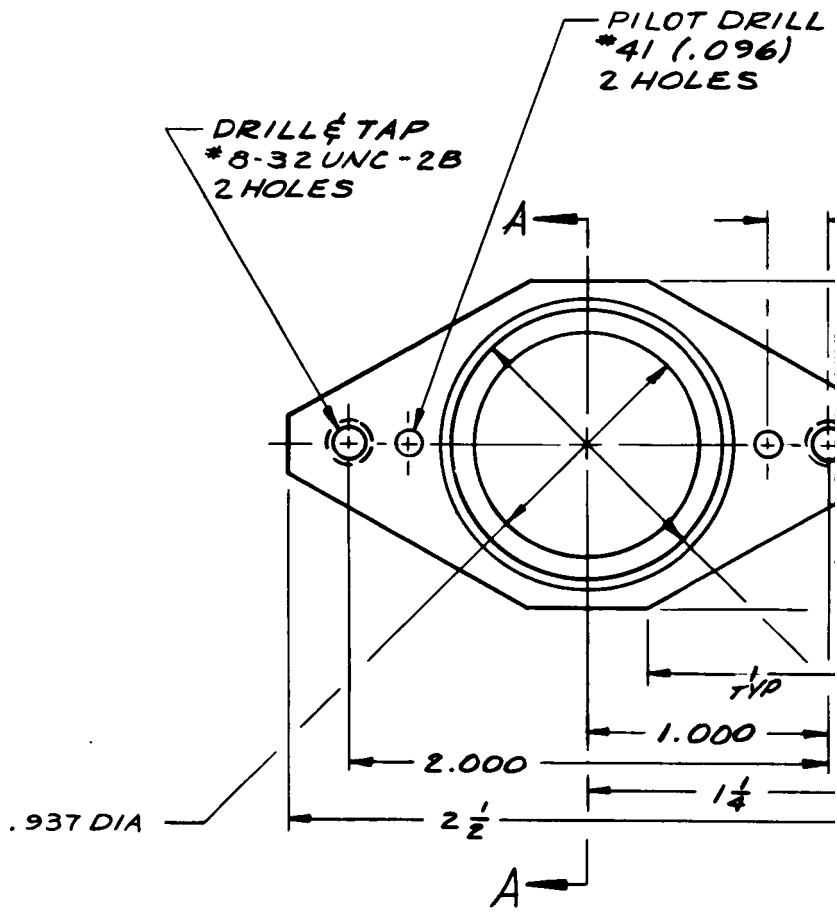

MAT'L:
AL ALLY PLATE
2024-T4 (OPTIONAL 6061-T6)

FINISH:
BLACK ANODIZE

MACH FINISH ALL OVER 125√

REVISIONS			
SYM	DESCRIPTION	DATE	APPROVAL

(THRU)

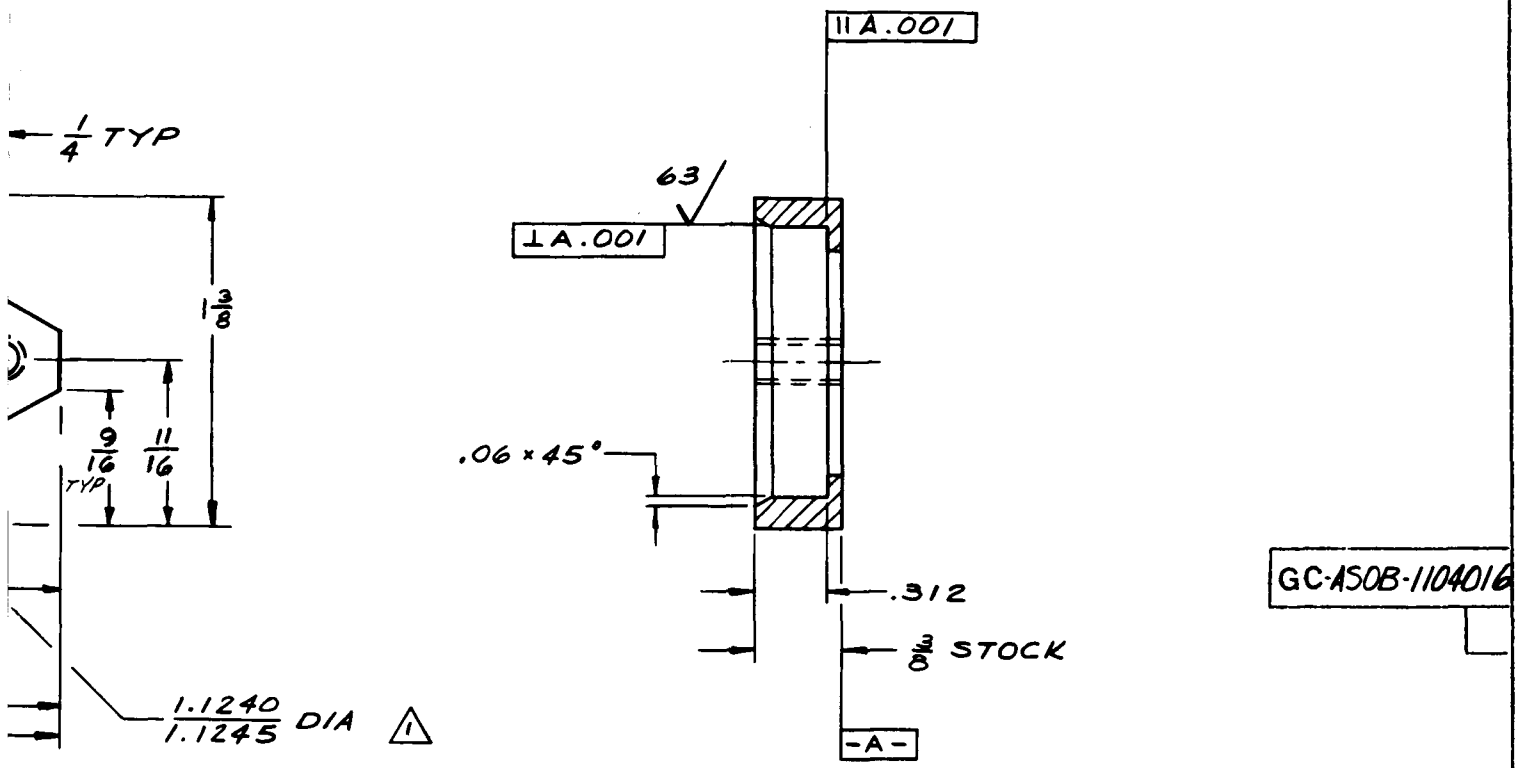

SECTION A-A

FIGURE 25

REQD	PART NO.	DESCRIPTION	MATL	MATL SPEC	UNIT WT.

LIST OF MATERIAL

UNLESS OTHERWISE SPECIFIED
DIMENSIONS ARE IN INCHES
TOLERANCES ON:
FRACTIONS ±1/64 DECIMALS ± .005 ANGLES ± 2°

	NAME	INIT	DATE
DESIGNER			
DRAWN	Ed Lewis	EL	8-26-63
CHECKED	E. Carlson	EJ	9/18/63
APPROVED	W. NAGEL	W.N.	9/24/63
APPROVED	P.G. Feldman	PGF	9/29/63

GJ-ASOB-1104005
NEXT ASSY | USED ON

BEARING PLATE ELEVATION
ASO BALLOON

NATIONAL AERONAUTICS AND SPACE ADMINISTRATION
GODDARD SPACE FLIGHT CENTER
GREENBELT, MARYLAND

GC-ASOB-1104016

SCALE 2/1 | CODE 622 | SHEET 1 OF 1

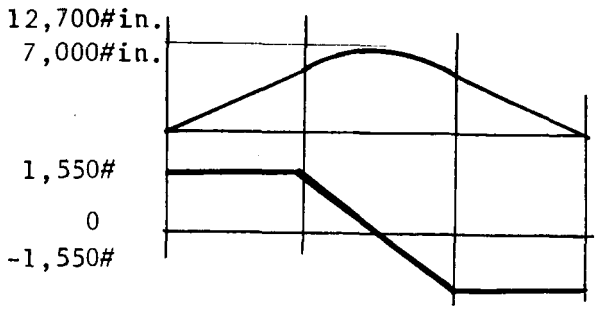

$6_{max} = M_{max}C/I$

$6_{max} = 31,600\#/in^2$

Factor of Safety = 1.11

(b) The design is now satisfactory, but the margin of safety appears to be small. However, it should be pointed out that the I, inertia, value used did not take into account the section Inertia of the 5/8 inch thick bearing retainer plate. Nor does the .160 value take into account the fact that the flange dimension of the bridge channel increases from 1" minimum to 3". Both of the above factors will substantially increase the safety factor. In predicting the maximum value of deflection the above factors are taken into consideration. A revised value for section inertia of .2 $inches^4$ is used in the deflection equation

$$f_{max} = \frac{Wl^3}{48EI} = .292 \text{ in}$$

f_{max} = .292 inches
(point load)

As a further check for deflection, the bridge channel is assumed to be uniformly loaded over the entire length

$$f_{max} = \frac{5WL^3}{384EI} = .182 \text{ in}$$

(uniform load)

The true deflection falls somewhere between these two values - .182 to .292 inches.

Checking for shear stress

Q_x = shear force = 1750#

A_x = shear area = 2(3/16x1) + 5x3/16

$A_x = 1.3055 \text{ in}^2$

$6_{shear\ max} = 1750 = 1,350\#/in^2$

Allowable shear stress = $20,000\#/in^2$.

Shear is therefore not critical.

(6) The experiment instrument is supported between two channels 16.25 inches in length and 2 inches in width. These two channels originate at the 5" channel primary structure and extend horizontally outward. At their origins the two support channels are welded to the primary structure and the weldment area is reinforced by vertical gusset plates to prevent vertical shearing. To increase the lateral rigidity of the channels, internal webb gussets were welded to the center line of each 2" channel.

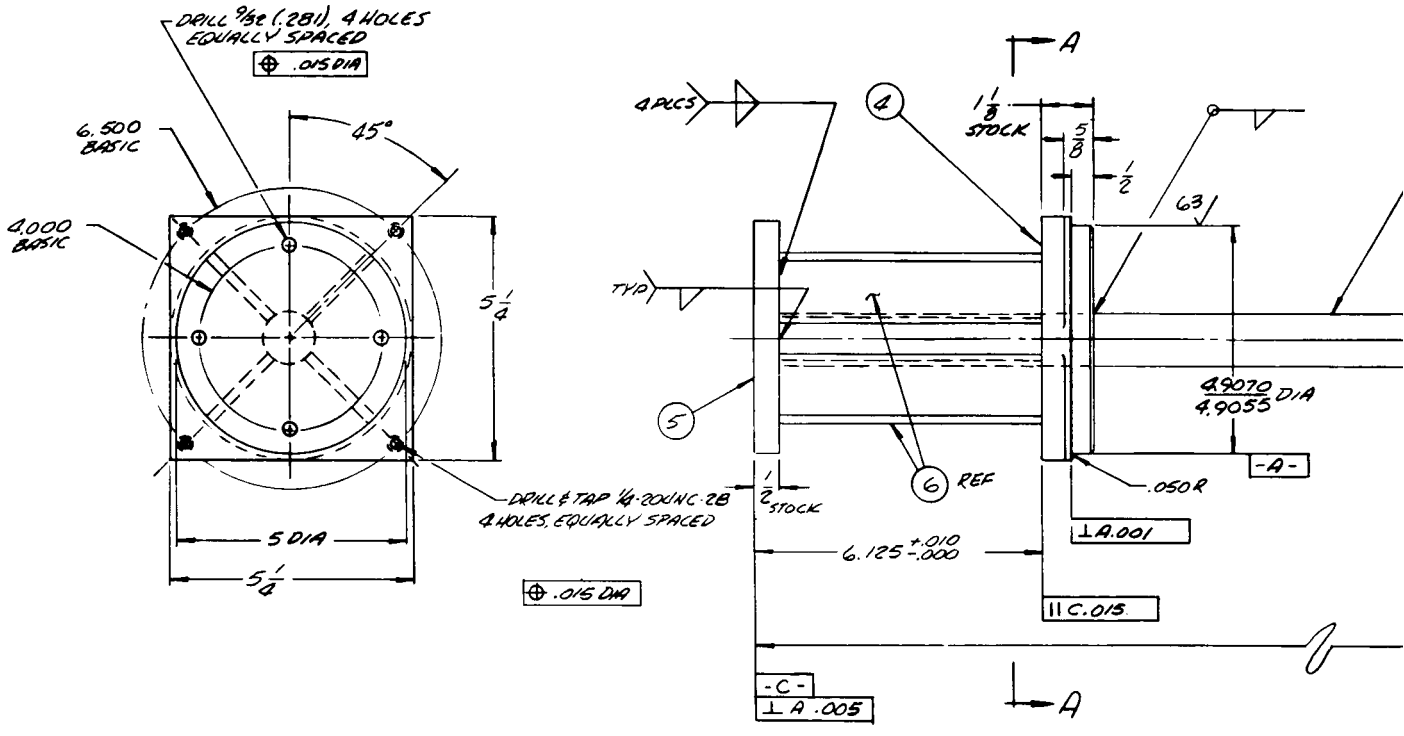
DRILL 9/32 (.281), 4 HOLES EQUALLY SPACED
⊕ .015 DIA
6.500 BASIC
45°
4.000 BASIC
5 1/4
5 DIA
5 1/4
DRILL & TAP 1/4-20 UNC-2B 4 HOLES, EQUALLY SPACED
⊕ .015 DIA
A
4 PLCS
4
1 1/8 STOCK
5/8
1/2
63
TYP
5
6 REF
1/2 STOCK
.050 R
4.9070 4.9055 DIA
-A-
⊥A.001
6.125 +.010 -.000
11 C.015
-C-
⊥A .005
A

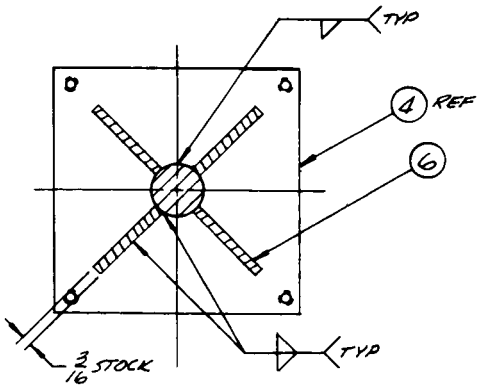
TYP
4 REF
6
3/16 STOCK
TYP

SECTION A-A

NOTES: UNLESS OTHERWISE SPECIFIED

1. STOCK SIZES MAY BE ALTERED FOR EASE OF FABRICATION
2. ALL MACHINED SURFACES 125 MAX
3. ALL WELDING TO BE DONE PRIOR TO MACHINING.
4. MACHINED CORNER RADII .015 MAX
5. CHEMICAL FINISH: ANODIZE-BLACK

REVISION LETTER	PART NO.	REVISIONS	CHECKED BY	DATE
A		.843 DIA WAS .875 DIA	Ed Lewis	2-25-64

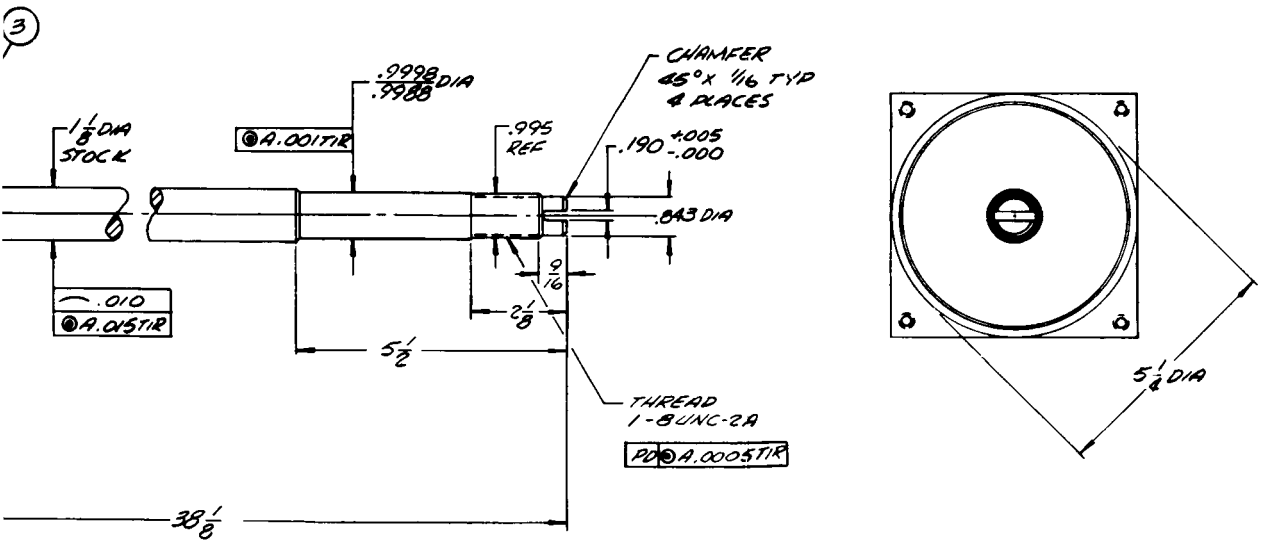

FIGURE 26

ITEM	REQ'D	PART NO.	DESCRIPTION	MAT'L	MATL SPEC
6	4	-6	SUPPORT WEB 3/16 THK X 1 1/8 X 5 5/8 SHEET	AL ALY	6061-T6
5	1	-5	BASE 1/2 THK X 5 DIA PLATE	"	"
4	1	-4	BEARING PLATE 1 1/8 THK X 5 1/4 X 5 1/4	"	"
3	1	-3	SHAFT 1 1/8 DIA X 38 1/8 LG ROD	AL ALY	6061-T6
2					
1	X	GD-A50B-1104011	GONDOLA MAST		

LIST OF MATERIALS

DESIGNED		8/27/68
DRAWN	E. Lajeunesse	8/21/63
CHECKED		8-27-63
APPROVED		8-27-63
APPROVED		8/27/63

NATIONAL AERONAUTICS AND SPACE ADMINISTRATION
GODDARD SPACE FLIGHT CENTER
622 DIVISION

TOLERANCES
UNLESS OTHERWISE SPECIFIED
ANGULAR DIMENSIONS ±2°
FRACTIONAL DIMENSIONS ±1/64
DECIMAL DIMENSIONS ±.005

UNLESS OTHERWISE SPECIFIED, MACHINE FINISH √

GONDOLA MAST
ASOB BALLOON

NEXT ASSEMBLY	SCALE	DRAWING NO.
GJ-A50B-1104005	1/2	GD-A50B-1104011

SHEET 1 OF 1

These critical gusset plates extend to the flange and webb sections of the 5" channel (primary structure) and are welded to these sections. In this fashion, both lateral rigidity and structural integrity are achieved.

At mid-point along the length of the two 2" channels are bolted the experiment pivot bearings. The experiment support shaft passes through these bearings and the experiment instrument pivots about them. Both alignment and strength of these bearings are critical. Misalignment can result in abnormally high and non-uniform frictional forces which resist the rotational effort of the control system. The weight of the experiment instrument is transmitted through the bearing retainer plate (Figure 25) to the channels. Thus failure of the bolts holding the bearing retainers to the channels is catastrophic. The following are shear stress and bearing stress calculations for retainer plate and bolts:

Check for Shear Stress Failure at Experiment Support Bearing Plate and the Structure

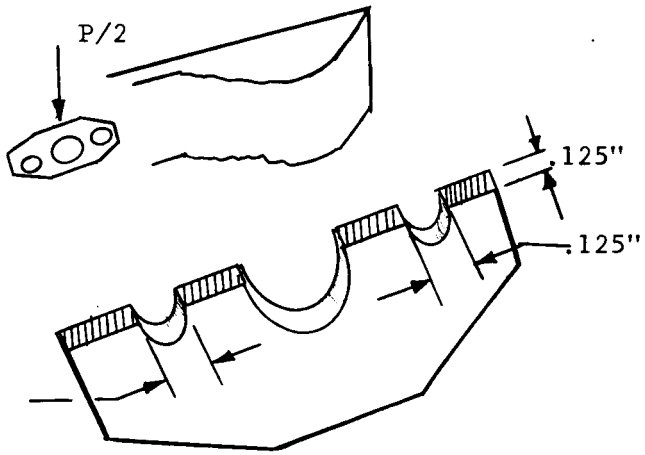

Stress Area = .125X.125

A_s = .0156

A_s = .0156

Allowable Load=874.0 lb

Load P, applied through shaft

P=60lb/2 = 30 lb.

For 10g acceleration

P = 300 lbs.

Safety Factor = 2.91

Directly beneath the experiment instrument bearings, the 2" channels are braced by 2x1x.125x13 inch supporting channels structurally tied to the base of the primary structure. Thus a truss structure is formed to support the experiment payload. For payload landing protection, the horizontal 2" channels extend out 9" beyond the center line of the experiment instrument bearings.

(7) Critical alignment of the bearings is achieved when the gondola structure undergoes final machining of the bearing surfaces. Prior to this time the entire gondola structure has been stress relieved (by heat treatment) to insure dimensional stability. When the machining operation of the bearing flats has been completed the gondola structure remains "jigged" on the vertical milling table and the bearing retainer plates are positioned in their respective locations on the gondola structure. With the bearing retainer plates in position, the alignment holes and retainer plate bolt holes are drilled through the gondola structure. Finally, alignment pins are pressed into the alignment holes. If the situation ever necessitates removing and reinstalling the bearing retainer plates, then care should be taken that new alignment pins are pressed into the bearing retainer plate and structure prior to tightening the bearing retainer plate bolts.

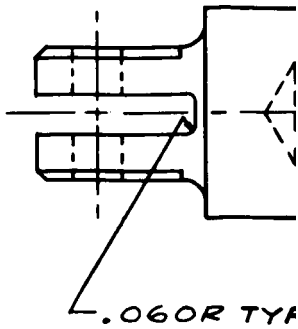

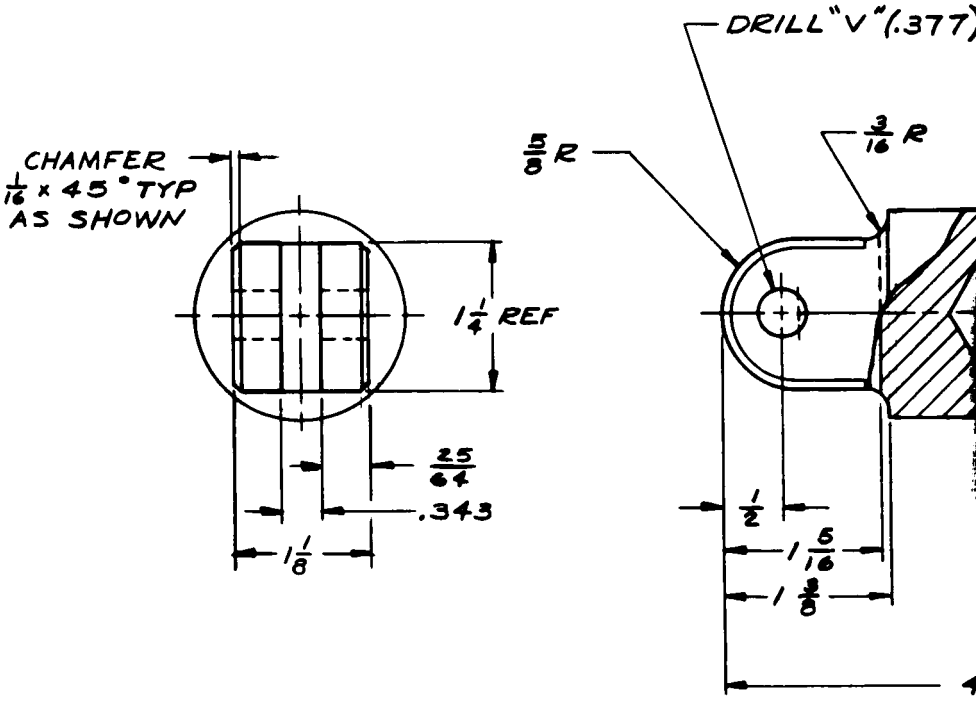

MAT'L:
AL ALY BAR
2024-T4 (OPTIONAL 6061-T6)

FINISH:
BLACK ANODIZE

MACHINE FINISH 125 √ ALL OVER

NOTES:
1. DO NOT ANODIZE THESE SURFACES

REVISIONS			
SYM	DESCRIPTION	DATE	APPROVAL

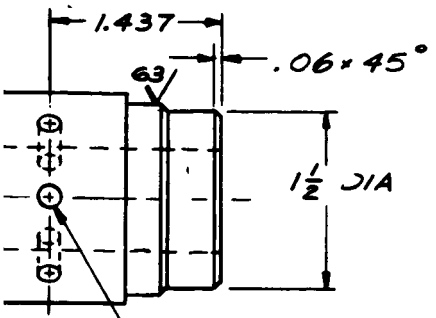

DRILL & REAM $\frac{.1895}{.1905}$ THRU ⚠1

4 HOLES EQUALLY SPACED ABOUT ONE HALF THE PERIMETER OF 1.750 DIA

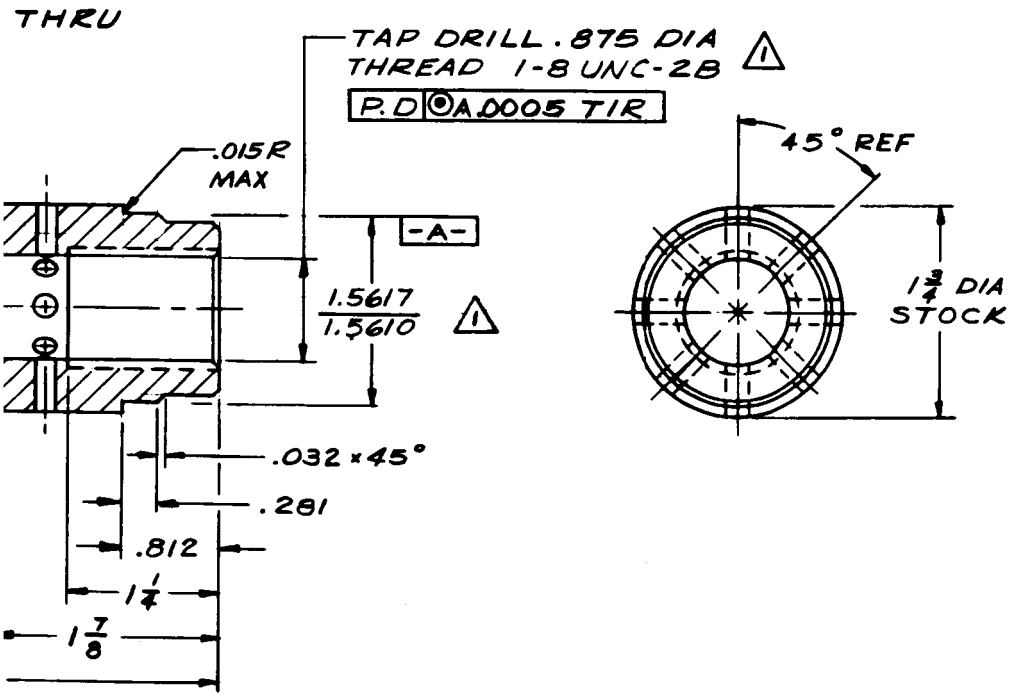

GC-ASOB-1104030

FIGURE 27

REQD	PART NO.	DESCRIPTION	MATL	MATL SPEC	UNIT WT.

LIST OF MATERIAL

UNLESS OTHERWISE SPECIFIED	NAME	INIT	DATE
DIMENSIONS ARE IN INCHES	DESIGNER		
TOLERANCES ON:			
FRACTIONS ±1/64 DECIMALS ± .005 ANGLES ± 2°	DRAWN ED LEWIS	EL	9-20-63
	CHECKED [illegible]	EJ	9/20/63
	APPROVED W. NAGEL	WN	9/24/63
1104005	APPROVED [illegible]	[illegible]	9/25/63
NEXT ASSY / USED ON			

BEARING CAP

ASO BALLOON

NATIONAL AERONAUTICS AND SPACE ADMINISTRATION
GODDARD SPACE FLIGHT CENTER
GREENBELT, MARYLAND

GC-ASOB-1104030

SCALE FULL | WT. | CODE 622 | SHEET 1 OF 1

B. The Gondola Mast Assembly

The mast assembly is formed from welded 6061-T6 aluminum round and flat stock. The entire assembly is heat treated after welding and black anodized after the finish machining operation. The mast assembly consists of a shaft structure, a 5" bearing and lower bearing plate, and a special slevis/bearing nut (see Figure 26).

1. The base of the shaft structure is structurally reinforced. Approximately 33" from the base of the mast assembly the shaft is machined down to 1" in diameter. The main control system gears are seated on the 1" shaft diameter. The 1" shaft diameter section continues out to the .995" diameter threaded section at the top of the shaft. Thus all driving gears can be slipped onto the mast assembly from the forwarded end of the shaft structure. The 2 1/8" threaded/slotted section at the top of the shaft is the most critical design aspect of the mast assembly. At the threaded section the mast assembly attaches to the parachute lines and hence all loads are ultimately transferred through the threads to the clevis/bearing nut. Based on the bellow stress calculations 1-8UNC-2A threads were selected to be machined on the end of the aluminum shaft. In addition to machining threads on the end of the shaft structure, a 9/16" deep (.190" diameter) open end slot has been machined at the top of the shaft. The purpose of the slot is to provide a locking capability for the clevis/bearing nut.

2. Stress Analysis of Critical Mast Attachment Screw Threads

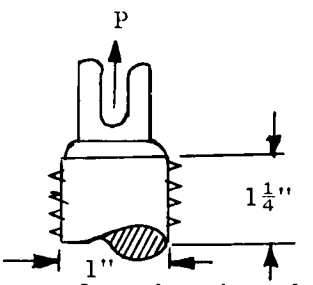

Tension Failure

The total stress area for the threads is given by the equation

$$A_s = 3.1416 \frac{(E_m + K_m)^2}{4}$$

Where

A_s = Stress area

E_m = Mean pitch diam.

K_m = Mean minor diam.

Pitch diameter Max. = .9168"
Pitch diameter Min. = .9100"

E_m (Mean pitch diam.) = 1.8268/2 = .9134"

Minor diameter Max. = .8446"
Minor diameter Min. = (.8446-h_b) in.

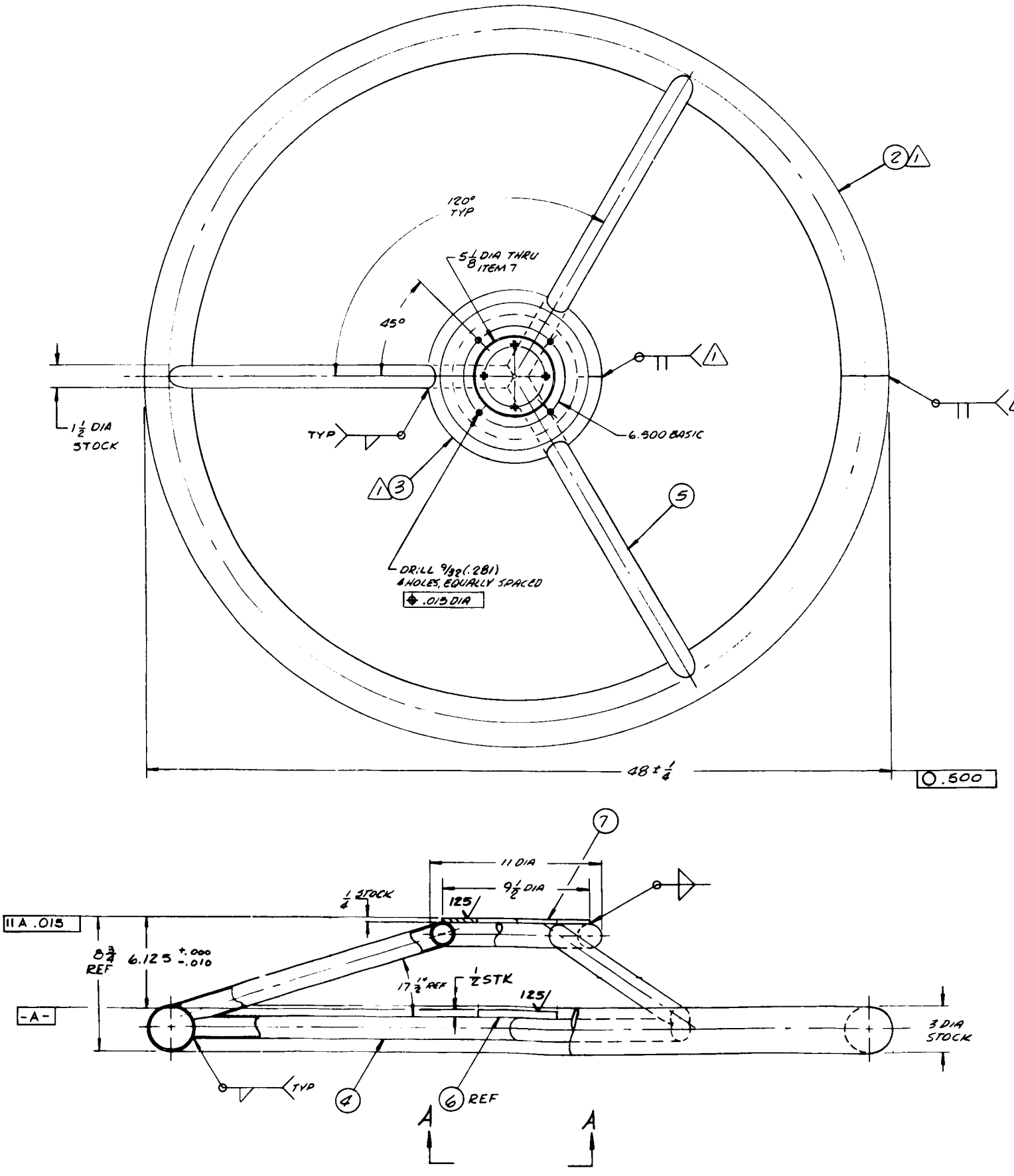
120° TYP
5 1/8 DIA THRU ITEM 7
45°
1 1/2 DIA STOCK
TYP
6.300 BASIC
DRILL 9/32 (.281) 4 HOLES, EQUALLY SPACED
.015 DIA
48 ± 1/4
.500
11 DIA
9 1/2 DIA
1/4 STOCK
125
11 A .015
8 3/4 REF
6.125 +.000 -.010
17 1/2 REF
1/2 STK
-A-
3 DIA STOCK
TYP
REF
A
A

NOTES: UNLESS OTHERWISE SPECIFIED:

1. ITEMS 2 & 3 MAY BE FABRICATED FROM TWO OR MORE SECTIONS
2. CHEMICAL FINISH: BLACK ANODIZE
3. ALL WELDING TO BE DONE PRIOR TO MACHINING.

REVISIONS			
SYM	DESCRIPTION	DATE	APPROVAL

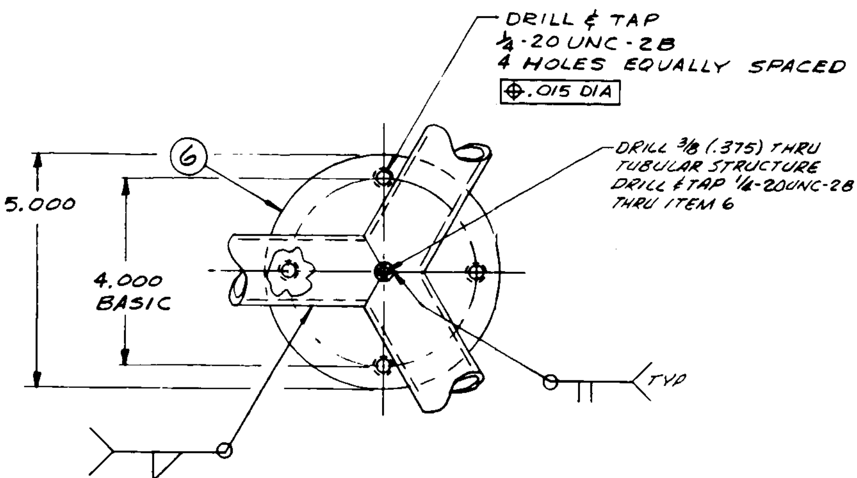

VIEW A-A
AT ℄ AXIS
SCALE: 1/2

GD-ASOB-1104012

FIGURE 28

ITEM	REQD	PART NO.	DESCRIPTION	MAT'L	MAT'L SPEC	UNIT WT.
8						
7	1	-7	PLATE-TOP 1/4 THK x 9 1/2 DIA	AL ALY	6061-T6	
6	1	-6	PLATE-BOTTOM 1/2 THK x 5 DIA			
5	3	-5	STRUT-DIAGONAL 1 1/2 OD x 1/8 WT x 18 LONG TUBE			
4	3	-4	STRUT-BOTTOM 1 1/2 OD x 1/8 WT x 21 LONG TUBE			
3	1	-3	RING-SUPPORT 1 1/2 OD x 1/8 WT x 30 LONG TUBE			
2	1	-2	RING 3 OD x 1/8 WT x 141 1/2 LONG TUBE	AL ALY	6061-T6	
1		GD-ASOB-1104012	INERTIA RING			

LIST OF MATERIAL

UNLESS OTHERWISE SPECIFIED
DIMENSIONS ARE IN INCHES
TOLERANCES ON:
FRACTIONS ±1/64 DECIMALS ±.005 ANGLES ±2°

	NAME	INIT	DATE
DESIGNER			8/27/63
DRAWN	C. Lafuna		8/22/63
CHECKED	ZELL		8-27-63
APPROVED			8-27-6
APPROVED			8/2

GJ-ASOB-1104005
NEXT ASSY | USED ON

INERTIA RING ASOB BALLOON

NATIONAL AERONAUTICS AND SPACE ADMINISTRATION
GODDARD SPACE FLIGHT CENTER
GREENBELT, MARYLAND

GD-ASOB-1104012

SCALE 1/4 & NOTED | WEIGHT 25.6# | CODE 622 | SHEET 1 OF 1

Pitch = 1 inch/8 threads = .1250

h_b = .6495 x Pitch = .08118 in.

Minimum Minor Diameter = .7634

Mean Minor Diameter = (.8446 + .7634)/2

= .8040 in.

$$A_s = 3.1416 \frac{(.9134 + .8040)^2}{4}$$

A_s = .57913 in^2

Max. allowable tonsile stress for aluminum is 35,00psi. Therefore, to fail in pure tension the maximum allowable load

P = 35,000 x .57913 = 20,269 lb.

Expected load of 350 lbs. and 10g safety factor = 3,500 lb.

Design achieves a safety factor = 5.79

For failure in Thread Shear

A_s = 3.1416(.9134+.8040)/2 Pitch/2 x (no. of threads)

A_s = .1686 in^2/thread

There are 8 threads/in

For $1\frac{1}{4}$" there are 10 threads

A_s = 1.686 in^2

Yield strength conservative 10,000psi

Max allowable load 10,000/1.686 = 5,930 lb.

Actual load 350 x 10 = 3500 lb.

Safety factor = 1.69

3. The clevis/bearing nut (see Figure 27)is machined from 6061-T6 aluminum. This nut has three main machined sections and three corresponding functions. The first machined section is the clevis. Through the center of the clevis passes a 3/8" diameter steel pin. The pin links a parachute line clevis plate to the mast assembly clevis/bearing nut. The second machined section is the female thread/lock pin holes section. 1-8UNC-2B threads are machined into the .875 diameter slot in the base of the nut. The depth of the slot is 1.875". The depth of the threads is 1.25". In the thread free region of the slot four holes, equally spaced about the circumference of the nut, are drilled perpendicular to the center line of the slot. Thus when the nut is screwed onto the shaft structure, it can be locked in place by setting a pin through any one of the four holes and the slotted section of the shaft structure. The third machined section is the external bearing surface section. The lower external surface and the nut is machined to a diameter of 1.5610", +.007, -.0. As this clevis/bearing nut is tightened,

the lower body of the nut slides into the inner race of the upper mast assembly bearing. This bearing is already locked in position by the upper mast bearing retainer plate. Thus when the clevis/bearing nut slides into the inner race, the mast assembly shaft is accurately positioned with respect to the gondola assembly. Since the tolerance call out between the inner bearing race and the external clevis/bearing nut surface necessitates a light press fit, there is virtually no play between the mast assembly and the gondola structure. From the standpoint of accurate pointing and control this is a very desirable feature. Once the clevis/bearing nut is screwed down tightly (with hand pressure only) a 316-stainless steel pin is positioned through the clevis/bearing nut and through the slotted shaft. With the pin in position, rotation of the clevis nut with respect to the mast assembly shaft is not possible. In this manner precision type smooth rotation of the gondola structure about the mast assembly is achieved.

Stress Analysis for Clevis and Clevis Pin Shear Failure

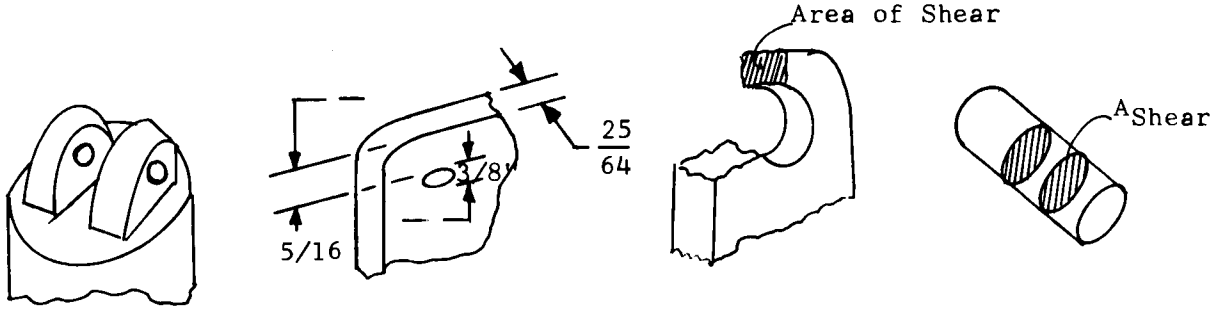

Shear Failure of Clevis

The minimum (conservative) shear stress area,

A_s = 5/16 in. x 25/64 in. = .122 $in.^2$

Total concentrated load = P/2

P/2 = 1750 lb.

Total shear stress = P/2 x $1/A_s$

= 14,300psi

The maximum kinetic energy of a 400lb balloon system falling at 25ft/sec is 3,850 ft-lbs ($E_{max}=\frac{1}{2}MV^2/G$). For a conservative approximation the value of 4,000 ft-lbs of energy shall be used. Now assume that an energy absorbent such as Styrofoam #1 is used to absorb this impact energy. This material has a shock absorbent capability of 7.2 in-lbs per cubic inch of material. The present ring design is 12.5 ft in circumference and has a cross sectional tube diameter of 3". Hence, to absorb 4,000 ft-lb of energy the volume of Styrofoam attached to this ring must be 6,666 in^3.

$$\frac{4000\text{ft-lb}}{7.2\ \frac{\text{in-lb}}{\text{in}^3}} \times 12\ \frac{\text{in}}{\text{ft}}$$

function of the lower tubular ring is twofold. First, the mass of the tube itself provides a large percentage of the desired counter rotating inertia (1.75 slug-ft^2). Second, the tubular ring section provides a stable platform base for the gondola structure and a means for attaching the impact energy absorbent material.

The function of the shock mitigation material which is epoxied to the lower ring section and is part of the inertia/impact ring assembly is twofold. First, it absorbs the gondola landing impact energy. Second, the weight of the mitigation material provides additional inertia to the assembly. For example, 4 lbs. of material will result in approximately .75 increase in ring inertia slug-ft^2 increase in ring inertia. When this inertia is combined with the inertia of the ring (1.758 slug-ft^2) the minimum required inertia of 2.5 slug-ft^2 is achieved for the inertia/impact ring assembly. Thus the design objective is fulfilled. In actuality the inertia of the mast assembly which is extremely small (.02 slug-ft^2) should also be added to the total counter rotating inertia.

The resulting thickness of foam is 21.3 inches (based on necessary volume of absorbent material and effective cross sectional area of ring).

Now that a volume of material has been selected, the next consideration to examine is the resulting impact deceleration. It is desirable that this value does not exceed -10g's. Hence, a determination of optimum impact area follows:

$\sigma A = F = ma$

$a = -10g's$

$F = 4{,}000$ lbs

σ for styrofoam #1 = 6,000 lbs/ft^2

Therefore the impact area must not be greater than .666 ft^2 (4000/6000). This means the impact material width must not exceed .666/12.5 ft = .64", to keep the deceleration below 10g's.

For 6061-T6 al. allowable (yield) shear stress = 20,000psi
Safety factor = 1.4

Shear stress of clevis pin

The shear stress area of the steel pin,

$$A_s = \frac{D^2}{4} = \frac{3.14x(3/8)^2}{4}$$

$$A_s = .1115 \text{ in.}^2$$

Total concentrated load on one end of pin = 1750 lb.

Total pin shear stress

$$\frac{P/2x1}{A_s} = 15{,}650\text{psi}$$

For 316 stainless steel bolts yield shear stress allowable = 30,000 psi

Safety factor = 1.92

C. The Inertia/Impact Ring Assembly

The inertia/impact ring assembly is formed from extruded 6061-T6 tubular aluminum and 6061-T6 flat stock (see Figure 28). After welding, the ring assembly is heat treated and then undergoes "finish" machining. The entire assembly is then black anodized and finally impact energy absorbent material (shock mitigation material) is epoxyed to the base of the ring assembly.

The inertia/impact ring assembly is composed of an upper and lower tubular ring section. Each ring section is structurally interconnected. The outside dimension of the lower ring section is 48" in diameter. The

V. Testing

Introduction

The objective of the test program was to verify the feasibility of design concepts to be used in the system. Although tests of the entire gondola are planned, it was felt desirable to run limited tests early in the development. The two major categories of tests performed were thermal-vacuum environmental tests of the control subsystem components and non-environmental development tests of various portions of the system. Some of these tests were performed with the assistance of the GSFC Test and Evaluation Division. Discussions of the tests in the two categories follow.

Environmental Tests

Thermal-vacuum tests were run to evaluate the environmental capabilities of the components used in the control subsystem. All components of the subsystem were tabulated, and test setups were conceived to test each type of component. The test setups were such that some of the flight operations could be verified.

An environmental schedule was prepared which simulated a balloon ascent to 130,000 feet and subsequent four hour flight. An attempt was made to run all tests according to this thermal-vacuum schedule.

The following components were tested:

1. Connectors
2. Servo Components
3. Programmer Components
4. Fluxgate Compass
5. Electronics and Camera (A camera and switching electronics system was developed to provide accurate position information for the experimenters toward the end of the balloon system development.)

The remainder of this section is a discussion of these tests. The components tested are listed, the procedure is summarized, and the results are noted. For more detailed information on a test, reference must be made to the actual data sheets (not included in report).

Test 1: Connectors

Components Tested

1. Connector (Cinch DE 9P)
2. Connector (Winchester type - 9 pin)
3. Relay (Elgin-Advance Relays-DPDT MV-2C-600P-16)

Procedure

The circuit is connected so that 130 volts AC, and 35 volts DC, are between wires passing through the connectors. The 35 volts is used to energize the relay, which in turn connects the 130 volts to an inductive load. The relay is energized at a pressure simulating 80,000 feet (21mm). This simulates the operation of the launch-recovery relay in the actual subsystem. At a pressure simulating the operational altitude (130,000ft), the relay is energized and de-energized several times.

Results

The test was successful with no evidence of arcing. The environmental schedule was not followed, and no thermal simulation was attempted. However, pressures as low as 1mm were maintained for about one-half hour. The relay was successfully operated at a pressure simulating 80,000 feet, and several times thereafter.

Test 2: Servo Components

Components Tested

1. Motor-Generator (Kearfott RB04-5H)
2. Servo-Amplifier (Kearfott C703148001)
3. Resolver (Reeves R-150)
4. Resolver Transformer (Microtran M8097)
5. Bias Transformer (Microtran M8063)
6. Barometric Switch (Gorn GB-300-NA71-1)
7. Gearhead (Metron Instrument Co-2025:1)
8. Relay (Allied 6PDT JH-18D)
9. Relay (3) (Two Potter Brumfield DPDT SC11DA, One Elgin DPDT MV 2C-200D-16)
10. Capacitor (3) (Aerovox-200 Farad P123ZNB)
    (Vitimin Q-91P15494S4)
    (Vitimin Q-91P33394S5)
11. Resistor ($\frac{1}{2}$ watt; 240K)

Procedure

The circuit is connected so that the resolver is made to null at all 90^{o} positions, by commands external to the chamber. This simulates the look up, down, and"horizontal" functions in the actual subsystem. Nulling at 180^{o} to a given position is also possible by command. This simulates the "back azimuth" function in the actual subsystem. The circuit is energized at a pressure simulating 90,000ft by the barometric switch, at which time the resolver rotates to a null at the first commanded position. The resolver position is observed by means of a dial, and the generator output is recorded.

Results

The test was successful with no evidence of improper functioning. The pressure portion of the environmental schedule was successfully followed, but there was little confidence in following the temperature portion. (This was caused by improper calibration of the thermo-couple in the vacuum chamber thermal control system.) Observation of the chamber thermal control system indicated temperature cycling was occuring, however.

The barometric switch properly actuated at an indicated pressure of 20mm, and the resolver was driven to the command null position. Subsequent to this, various commanded nulls were achieved including "back azimuth" positions. At the end of the test, the barometric switch properly de-energized the circuit at an indicated pressure of 32.4mm. Some hysteresis in the barometric switch was discovered in this test.

Test 3: Programmer Components

Components Tested

1. DC Motor and Gearhead (A.W. Haydon M5818 Chronometrically governed)
2. Cam (PIC Design Corr.)
3. Cam Micro Switch
4. DC Motor (A.W. Haydon, Chronometrically governed)
5. Switch stack (A.W. Haydon, Eleven cam switches)

Procedure

The DC motor, M5818, is connected to rotate the PIC cam which actuates the cam micro switch. The actuation of the cam micro switch in turn applies voltage to the switches in the switch stack. The PIC cam is set so that the cam micro switch energizes the switch stack after 75 minutes (which corresponds to a simulated altitude of 80,000ft) and de-energizes the switch stack after 5 hours (simulating the end of a balloon flight). The swtich stack cams are rotated continuously (1/5 rpm) during the entire test by the other DC motor. The test setup closely simulates the operation of the cams and switches during an actual flight. During the test, the operation of all cams is recorded.

Results

The desired test environment was more nearly achieved on this test than any heretofore. Temperature extremes were very nearly confirmed by a thermometer within the chamber, and the pressure portion of the environmental schedule was followed. The switch stack cams were energized by the cam micro switch at the proper time, and the recording of the switch outputs confirmed their proper sequencing. The switch stack was properly de-energized after 5 hours and 1 minute had elapsed. This accuracy in setting the PIC cam is somewhat indicative of what may be expected in the flight unit.

Test 4: Fluxgate Loop

Components Tested

1. Fluxgate Compass (Benidx type 15019, Serial #310500)
2. Control Transformer (CT)(Bendix type AY-500-6-A1)
3. Electronics Card (Bendix type SA 229)
4. Transformer 115V/2.8V, 400cps (Micro-tran)

Procedure

The fluxgate is placed at some random orientation, and the CT shaft is positioned to give a nulled output from its rotor windings. The nulled condition is disturbed by a piece of iron rotating past the fluxgate every 4 seconds. (A magnet can also be passed by the fluxgate to disturb the nulled condition.) The disturbance of the null condition is recorded using a phase sensitive demodulator and the SA 229 electronics card (400cps output). The same pattern of null disturbance is looked for under various environmental conditions, to determine whether or not environmental effects are occuring. The test setup is not energized until a pressure simulating 80,000ft is attained so that flight conditions can be duplicated.

Results

The test was run on three separate occasions, because environmental effects were noted each time the test setup was initially energized at 21mm, -67°F. The environmental schedule was followed for each test, up to the point of energizing the setup. While the temperature portion was not followed precisely, the desired temperature was achieved at least by the time the system was energized. After the environmental problem was noted on the first attempt to run the test (using a piece of rotating iron), the fluxgate was returned to Bendix Company (Eclipse-Pioneer) for incorporation of a fluid having better thermal characteristics (less viscousity change with temperature changes). Upon receipt of the unit with the new fluid, the test was again attempted unsuccessfully (using a piece of rotating iron). A third run of the test was made in the presence of a Bendix representative, in hope of discovering how serious the environmental effects being observed were. Initially using a piece of rotating iron and noting the null disturbance pattern changing greatly from the atmospheric condition, pattern, it was decided to use a magnet to create the disturbance for pattern comparison. The magnet approach showed that the fluxgate would null at the proper position under environmental conditions, given sufficient time, even though the null disturbance pattern using the piece of rotating iron could not be repeated. The conclusion was that the rotating iron test was too sensitive in that it did not allow time for the fluxgate to return to null before being disturbed by the iron again. To test this theory, the rotating iron was stopped just after disturbing the fluxgate, and the overshoot of the null was noted similar to that observed under atmospheric conditions, only slower. The fluxgate also nulled at the proper position, showing this capability. The conclusion is that the fluxgate will have a change in its frequency response at low temperatures (more sluggish), but that it should still be an adequate piece of equipment for the balloon mission.

Test 5: Electronics and Camera

Components Tested

1. Static Inverter (Arnold Co.)
2. Filter (115 volts, 400 cps, square wave to 20 and 3 volts, 400 cps, sine wave - built in-house)
3. Aircraft Camera and IMC Stepper Motor (Size 11)
4. Camera Electronics (Built in-house)

Procedure

This test setup is of two functionally different portions of the control subsystem - the static inverter and filer, and the camera and its electronics. Outputs of the 28 volt DC, static inverter are loaded as follows: 115 volts, 400 cps output to the filter and ±15 volts DC, outputs to an appropriate load circuit. The camera, loaded with film, is connected to its electronics. The film is marked to verify at the end of the test that all frames would have been exposed. All equipment is placed into operation, and performance is monitored and recorded as the environmental schedule is followed.

Results

On the first attempt to run this test, the camera electronics failed, but the static inverter and filter portions operated properly. A subsequent thermal test of only the camera electronics revealed a transistor biasing resistor problem which was corrected. A second test of the camera and its electronics, following the thermal-vacuum schedule once again resulted in the camera mechanism failing, but the proper operation of the camera electronics was verified. A thermal test of only the camera uncovered a lubricant problem which was corrected by replacing the lubricant with versalube. A third test, following the thermal-vacuum schedule, demonstrated that the camera could withstand minus 70°F for about 1 1/3 hours, before mechanism failure. This result was felt sufficient to verify capability of the camera to withstand expected flight environment. Thus, the overall test of these two functional portions of the subsystem was considered successfully completed.

Non-Environmental Tests

These tests were run to evaluate critical portions of the system where thermal vacuum environmental capabilities were not in question. The following tests were run:

1. Fluxgate Compass Frequency Response
2. Fluxgate Compass with Square Wave Input
3. Equatorial Computer Low Level Vibration Tolerance
4. Shroud Lines, Spreader Ring, and Mast Strength Test

The remainder of this section is a discussion of these tests, using the same format as for environmental tests. Again, for more detailed information on a test, reference must be made to the actual data sheets.

Test 1: Fluxgate Compass Frequency Response

Components Tested

1. Fluxgate Compass (Bendix type 15019, Serial #310500)
2. Control Transformer (CT) (Benidx type AY-500-6-A1)
3. Electronics Card (Bendix type SA 229)

Procedure

This test was to determine the frequency response of the fluxgate compass, with associated CT and electronics, used for magnetic north sensing in the azimuth control loop. In this loop, the device must accurately indicate electrically its physical orientation relative to magnetic north, under dynamic conditions.

Figure 29 shows how the compass, with associated CT and electronics, is tested. Recording of the error, ϵ, (on a CEC recorder and photo recording memo-scope) indicates the electrical output of the fluxgate, including any effects of the CT and electronics, since the $\pm 3^{o}$ physical displacement does not exceed the linear range of the null output characteristic of the CT or the electronics. The physical input orientation of the fluxgate is recorded using a linear potentiometer. The sinusoidal displacement of the fluxgate about its null position, needed for frequency response determination, is provided by a centrifuge table and linkage. (The potentiometer recording of this happens to be 90^{o} out of phase with the electrical output of the fluxgate, because of the position of the potentiometer in the mechanical linkage.) Frequencies from 0.5cps to 16cps are used.

Results

Figure 30 shows photographs of data at two extremes of the test frequencies (1cps and 16cps). From data such as these, measurements were made, and the frequency response computed using the equation:

$$\text{Gain (db)} = 20 \log \frac{\theta_o(j\omega)}{\theta_i(j\omega)}$$

The results of these computations are plotted in Figure 31, which shows gain (db) and corresponding phase angles at various frequencies. It is seen on the graphs that the magnitude ratio is attenuated as much as 1.2 db at 2cps and that the phase lag angle becomes as large as 21^{o} at 16cps. It is concluded that the dynamic characteristics of the fluxgate compass, with associated CT and electronics, are well within the range required by the ASO Balloon azimuth control loop.

Test 2: Fluxgate Compass with Square Wave Input

Components Tested

1. Fluxgate Compass (Bendix type 15019, Serial #310500)
2. Control Transformer (CT) (Bendix type AY-500-6-A1)
3. Electronics Card (Bendix type SA 229)

Procedure

This test was to determine the feasibility of using a 400cps square wave signal, in place of sine wave, to energize the fluxgate compass. The fluxgate compass is connected to the associated CT and electronics and energized with the square wave, while the output of the electronics is monitored by a recorder and oscilloscope. This is repeated with the fluxgate compass energized with an equivalent magnitude sine wave. Output of the fluxgate electronics with the two inputs are compared.

Results

The output of the electronics was found to be attenuated by a factor of approximately 8.6 when the square wave input was used. Also, large spikes on the output were noted. It is concluded that the square wave input is not satisfactory for energizing the fluxgate compass.

Test 3: Equatorial Computer Low Level Vibration Tolerance

Component Tested - Equatorial Computer Package

Procedure

This test was to verify the quality of workmanship on this package. The package is first inspected to verify its suitable condition for the test. It is then mounted on a vibration test facility and subjected to low level, low amplitude vibration over a range of frequencies. The condition of the package is again inspected.

Results

No noticeable changes to the Equatorial Computer Package occurred during this test. It is concluded that the workmanship is adequate for withstanding low level vibration.

Test 4: Shroud Lines, Spreader Ring, and Mast Strength

Components Tested

1. Shroud Lines
2. Spreader Ring
3. Lower Spreader Plate Assembly
4. Mast Bearing
5. Mast

Procedure

This test was to verify the ability of the above components, when assembled in their normal flight configuration, to withstand expected loads. The assembled components are suspended by an overhead crane and then the mast is attached, through a scale, to the floor. A tension of 3,000 pounds is then applied by means of the overhead crane.

Results

The assembled components withstood the tension without effect. It is concluded that the mechanical design of the components is adequate.

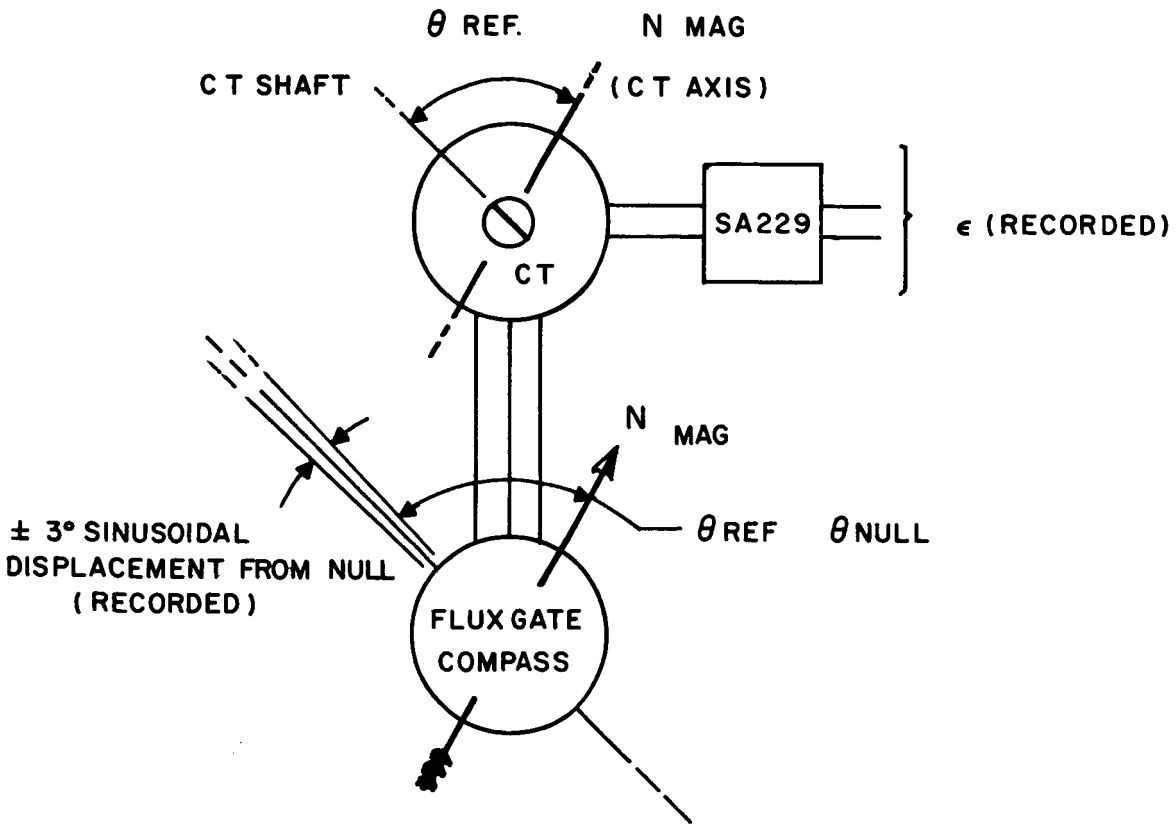

FIGURE 29 FLUXGATE TEST SET-UP

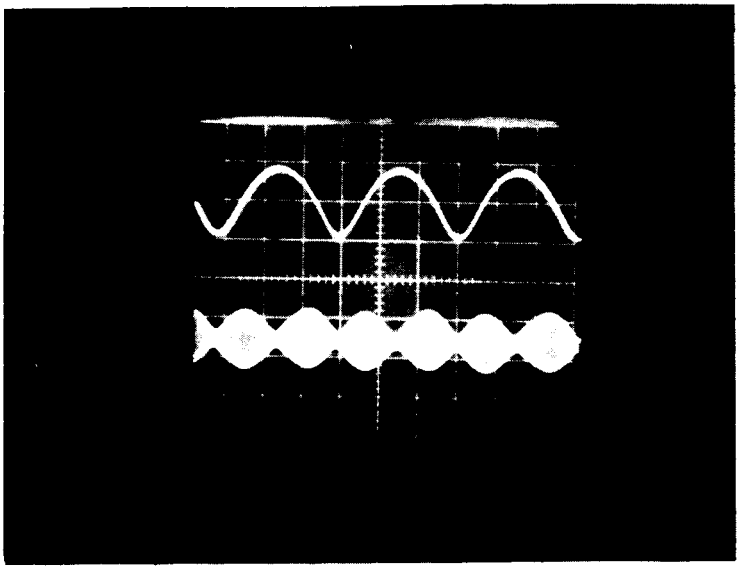

$\theta_i (\pm 3^\circ)$

(SCALE:)
θ_o (3.74 deg/cm)

1 CPS

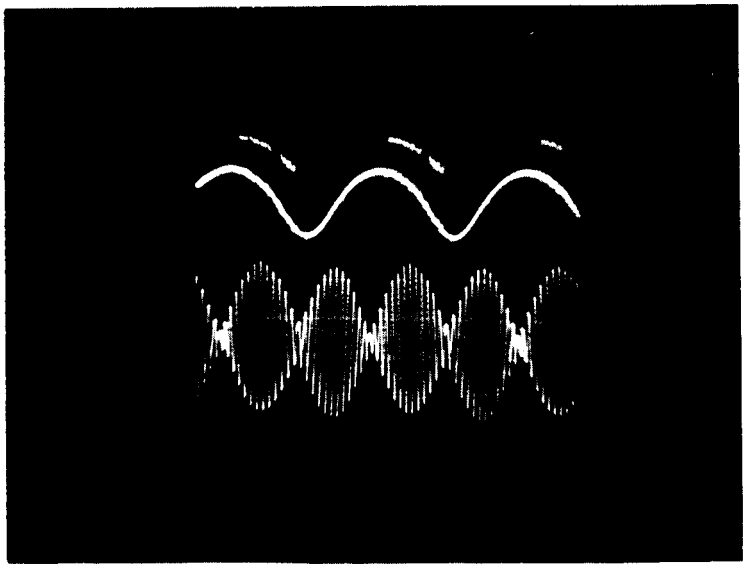

$\theta_i (\pm 3^\circ)$

(SCALE:)
θ_o (1.50 deg/cm)

16 CPS

FLUXGATE
TEST DATA

FIG.30

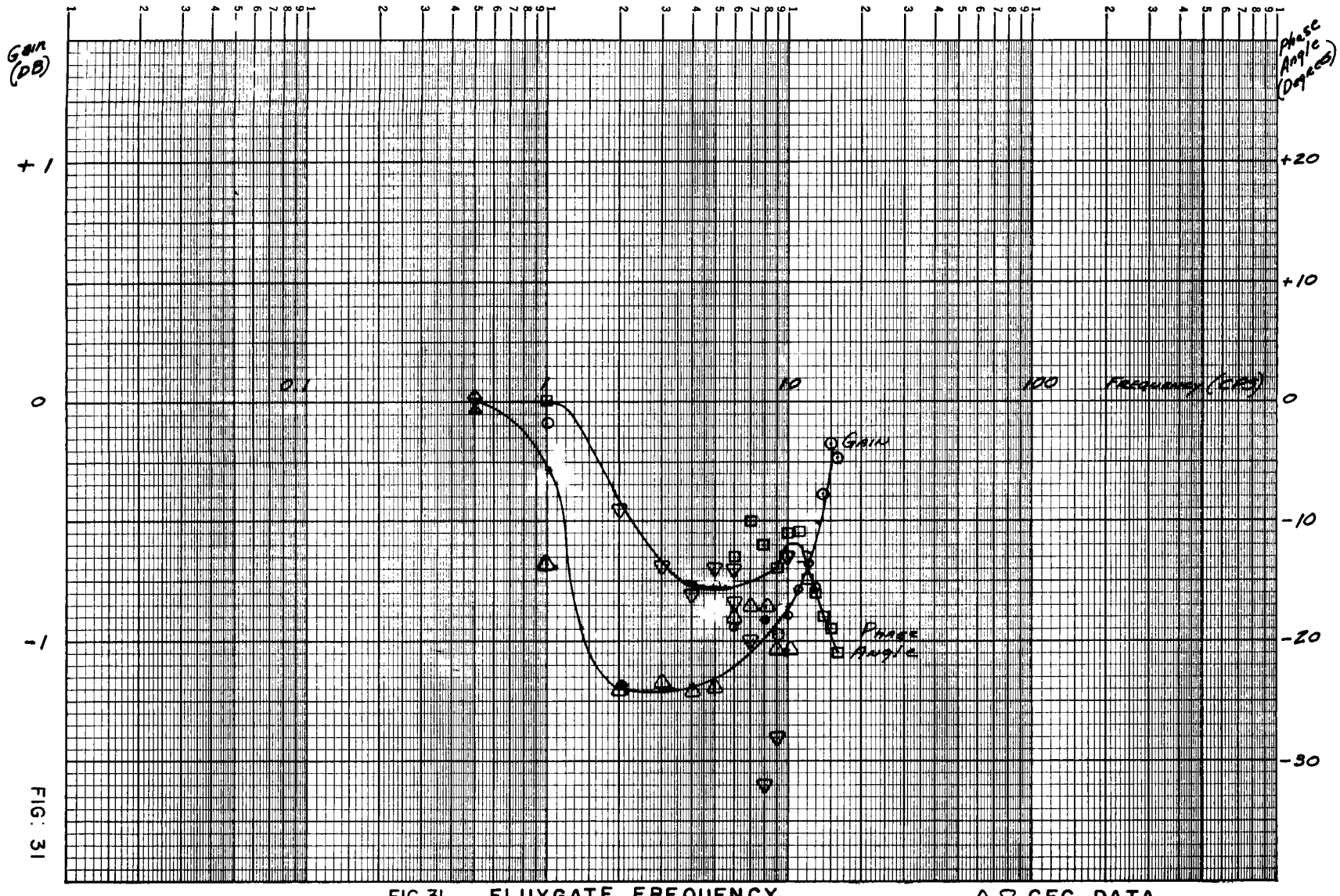

FIG. 31

FIG. 31 FLUXGATE FREQUENCY RESPONSE

△ ▽ CEC DATA

○ □ MEMO-SCOPE DATA

APPENDIX A - TELEMETRY

A strip chart recorder is being flown aboard the gondola to record the important system parameter as a function of time. This information will aid in data reduction and will help determine the cause of any malfunctions that may exist during the flight. A stepping switch alternately applies each of the voltages to be measured to the recorder to effect the necessary time sharing. Thus a single strip chart provides 12 channels of time shared data.

The quantities that will be recorded are elevation position, the temperature inside and on the gondola, the experimenters 6 volt and 28 volt batteries, the control systems 28 volt, and 3 volt batteries and 115 volt and 3 volts AC and +15 volts DC from the static inverter.

The meter input resistance is 4.6 ohms and full scale meter movement requires 100μa. The signal conditioning required for each parameter will be detailed below. The nominal reading for each parameter was chosen to spread the data over the strip chart to facilitate reading. The various circuits are shown diagramatically in Figure A-1.

A potentiometer is driven by the elevation resolver and is energized from the 28 volt DC battery. The wiper voltage from the pot is applied to channel two of the recorder thru the stepping switch. A series resistor is sized to limit the current to 100μa with full pot voltage.

Temperature

A resistance temperature detector is used in a bridge circuit which is sized to give 0μa at -40°C and 100μa at +50°C. In order to measure such a wide range with meaningful resolution it was necessary to use a bridge circuit rather than a voltage divider. If it is found in the future that the temperature variations are small, it will be possible to eliminate the bridge circuits. In order to ground one side of the bridge output it was necessary to energize the circuit with a center tapped supply which required the use of separate batteries. These are mounted on the telemetry rack behind the telemetry box. The circuitry for each temperature channel is identical.

The signal from the inside temperature indicator is routed to channel four on the recorder and the signal from the outside temperature indicator is applied to channel eight.

Experimenter Batteries

The experimenters six volt battery will be monitored on channel five. The voltage will be applied through an 81.1 K ohm resistor to limit the 6 volt reading to 70μa. The 28 volt battery will be monitored on channel six and that voltage will be routed through a 369.4 K ohm resistor to limit that reading to 75μa.

Control System DC Voltages

The 28 volt DC battery is recorded on channel three with a nominal reading of 60μa and the 3 volt DC battery is recorded on channel eleven with a nominal reading of 36μa.

Static Inverter Voltages

The +15 volt DC output from the static inverter is monitored on channel one. It is applied through a 300K ohm resistor to limit its nominal current reading to 50μa. The 115V AC from the static inverter is rectified, filtered, and applied to channel nine through a resistor which limits the nominal reading to 70μa. Also, the 3 volt AC output of the resolver filter is rectified and applied to channel seven through a limiting resistor which is sized to give nominal reading of 90μa.

The recorder, stepping switch, and the voltage conditioning electronics are all mounted on one rack. This facilitates the possibility of choosing different parameters to be monitored in the future.

APPENDIX B - POWER SUPPLY

Electrical power for the balloon system is provided by a 28V DC battery pack consisting of 19 series connected "silvercel" batteries. The nominal capacity of this battery pack is 40amp-hrs., at a 4amp discharge rate. The cells are enclosed in an air-tight aluminum box with a relief valve provided to prevent an internal pressure build-up as the batteries are discharged. Silver zinc batteries were selected for their high watt-hour output per pound of battery weight.

Also, part of the power supply is an inverter-converter which supplies 115vac, 400cps power for the servo motors and ±15vdc for the sun sensor electronics. A separate 28vdc battery pack and 12vdc center tap battery are being furnished by the experimenter but are not part of the system power supply. A power distribution schematic is shown in Figure B-1.

The combined AC and DC power requirement for the system is broken down as follows:

AC

Servo motor ref. voltage	10.5 watts
Compass & Amplifier	.018 watts
Resolver Reference	1.0 watt
	11.7
	50% Inverter Eff. = 23.4 watts

DC

Timer Motor	5 watts
Servo Amplifiers - 10.5 avg. 22.5 max.	10.5 watts
Compass Amplifier	.056 watts
Relays 1.68 watts/relay	8.5 watts
Sun Sensor Electronics	1.5 watts
Camera Electronics	2.0 watts
	27.5 watts

The maximum duration of any flight should not exceed 12 hours, of which at least 2 hours would be required for the launch-recovery phase. The power required during this phase is only 6.5 watts. Therefore, the maximum power required is $10(50.9) + 2(6.5) = 522$ watt-hours, which is within the capacity of the battery pack.

The entire gondola, except the inertia ring, will be covered with two layers of 1" styrofoam. This should prevent the batteries from reaching such a low temperature during ascent as to reduce the battery output.

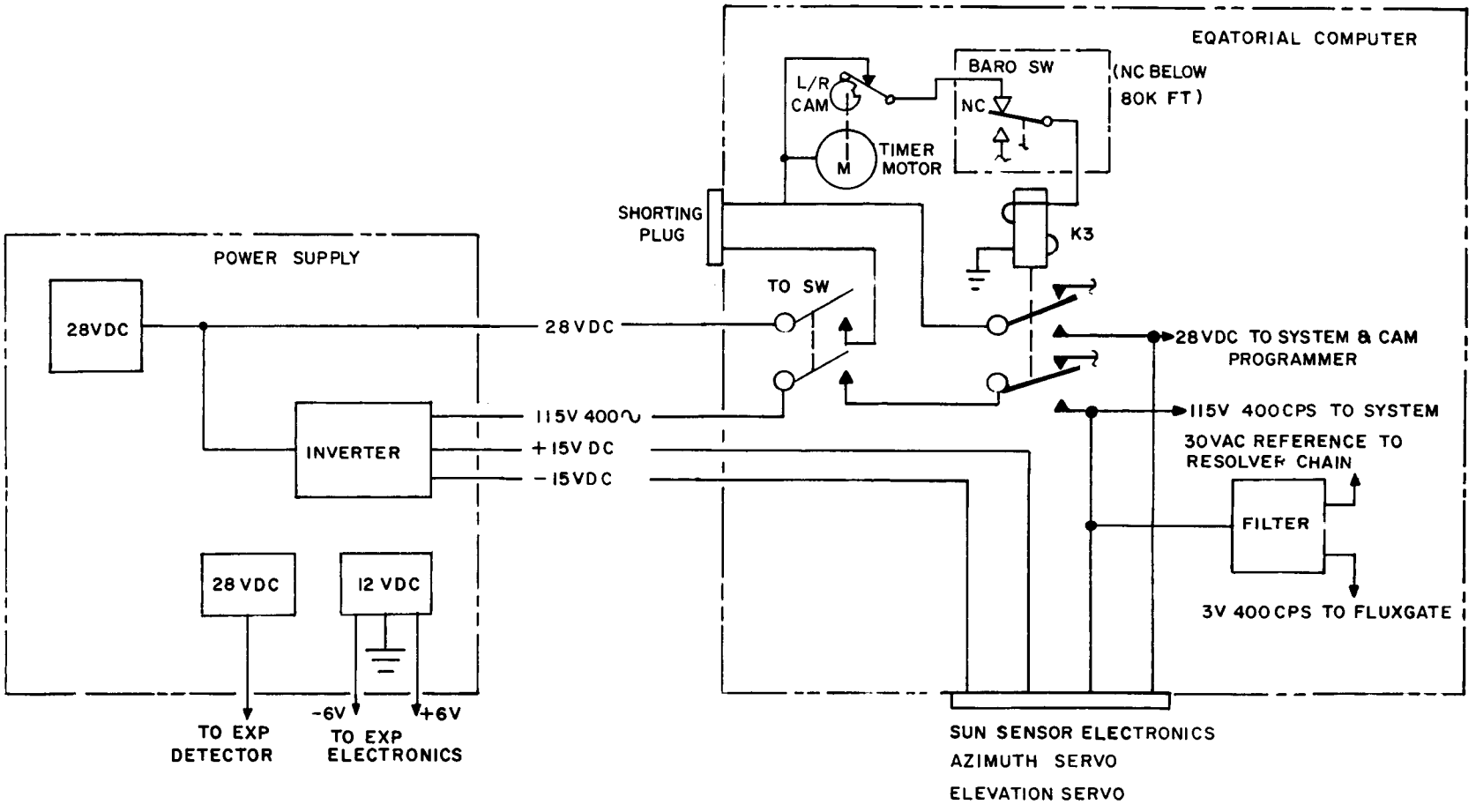

FIGURE B-1 POWER DISTRIBUTION SCHEMATIC

400 Cycle Sine Wave Filter

The 400cps power requirements for the balloon are 115V for the servo motors, 30V for the resolver chain and 3V for the fluxgate compass. These latter two voltages must be sine waves with less than 5% Harmonic Distortion. It was found that considerable weight could be saved by exciting the servo motors with square wave excitation (at a slight decrease in efficiency), by using a square wave inverter instead of a sine wave inverter. This then required designing a small square to sine wave filter to supply the sine wave voltages required.

The filter was designed by the Space Power Technology Branch at Goddard and is shown in Figures B2 and B3. The filter uses series and parallel tuned circuits resonant at 400cps. The circuit was tested for regulation and stability over a temperature range of -10°C to +60°C. The regulation was within ±10% and the distortion was less than 5%. For flight, the filter will be ecco-foam potted.

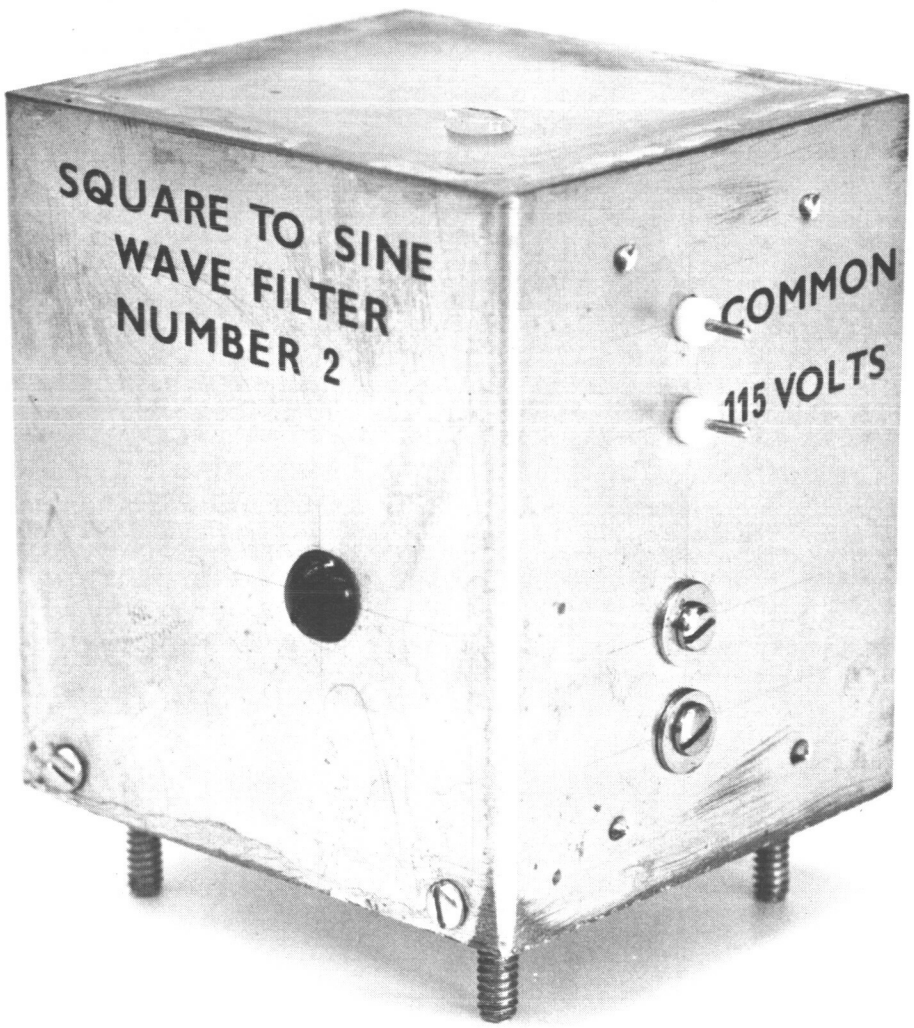

FIGURE B3

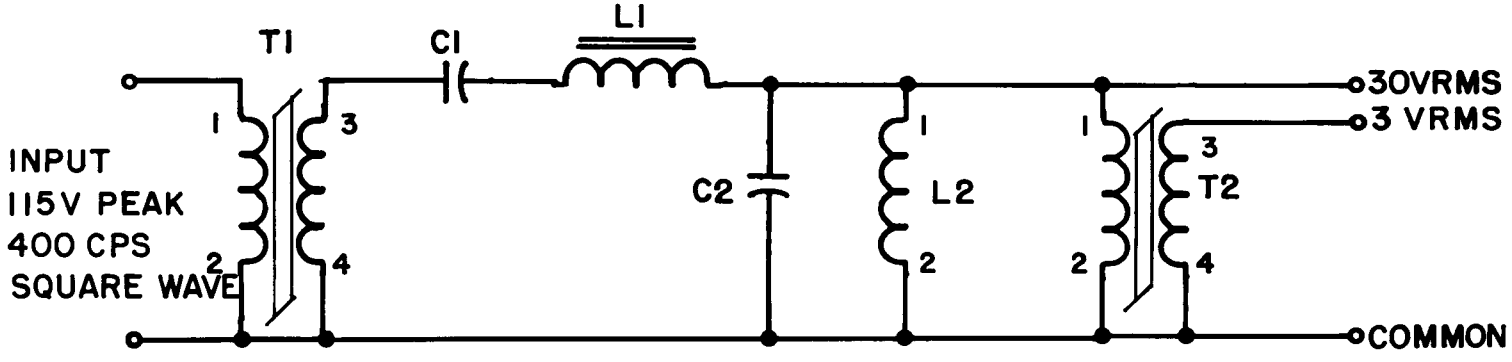

FIGURE B2. SQUARE-TO-SINE WAVE FILTER

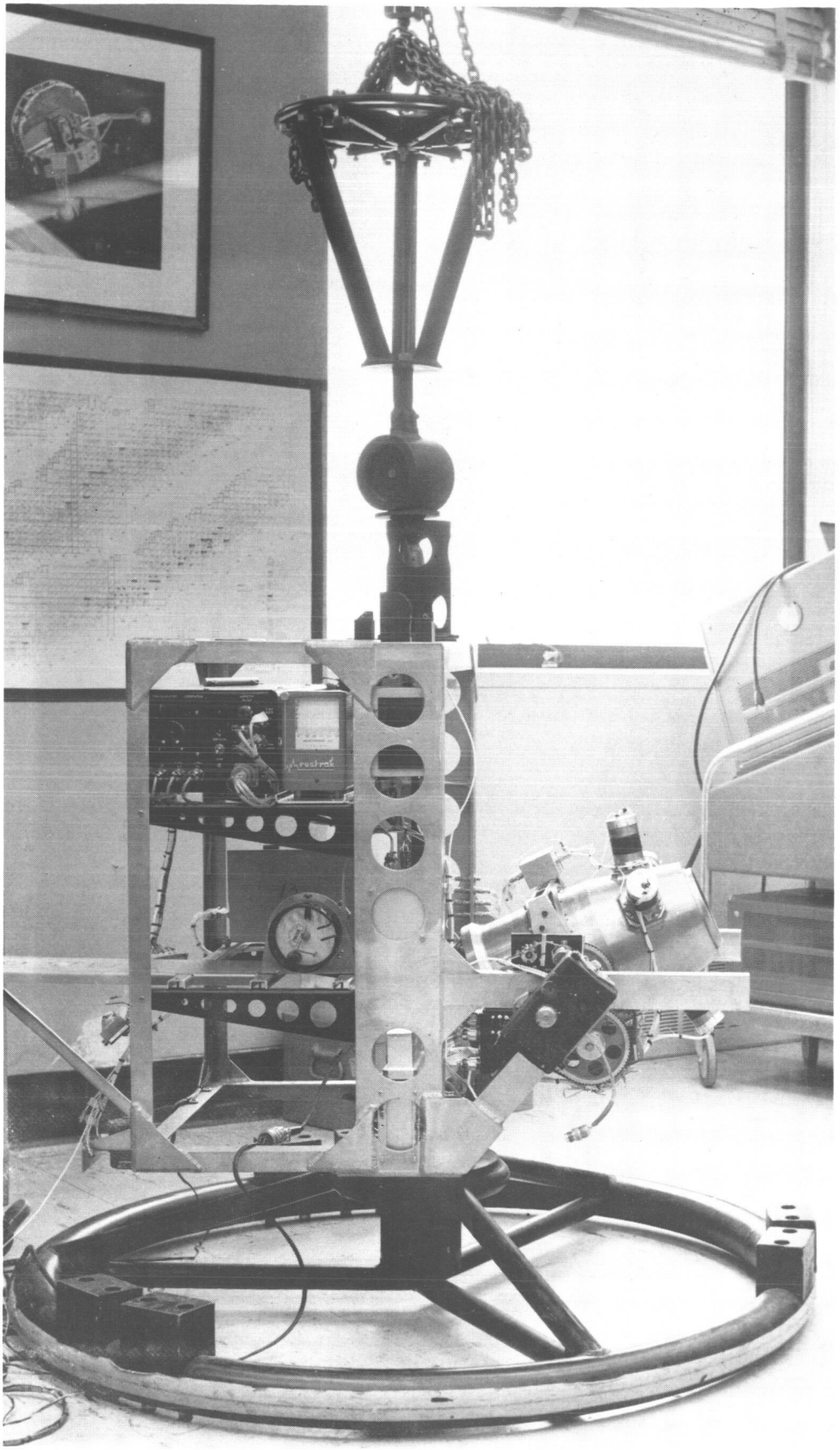

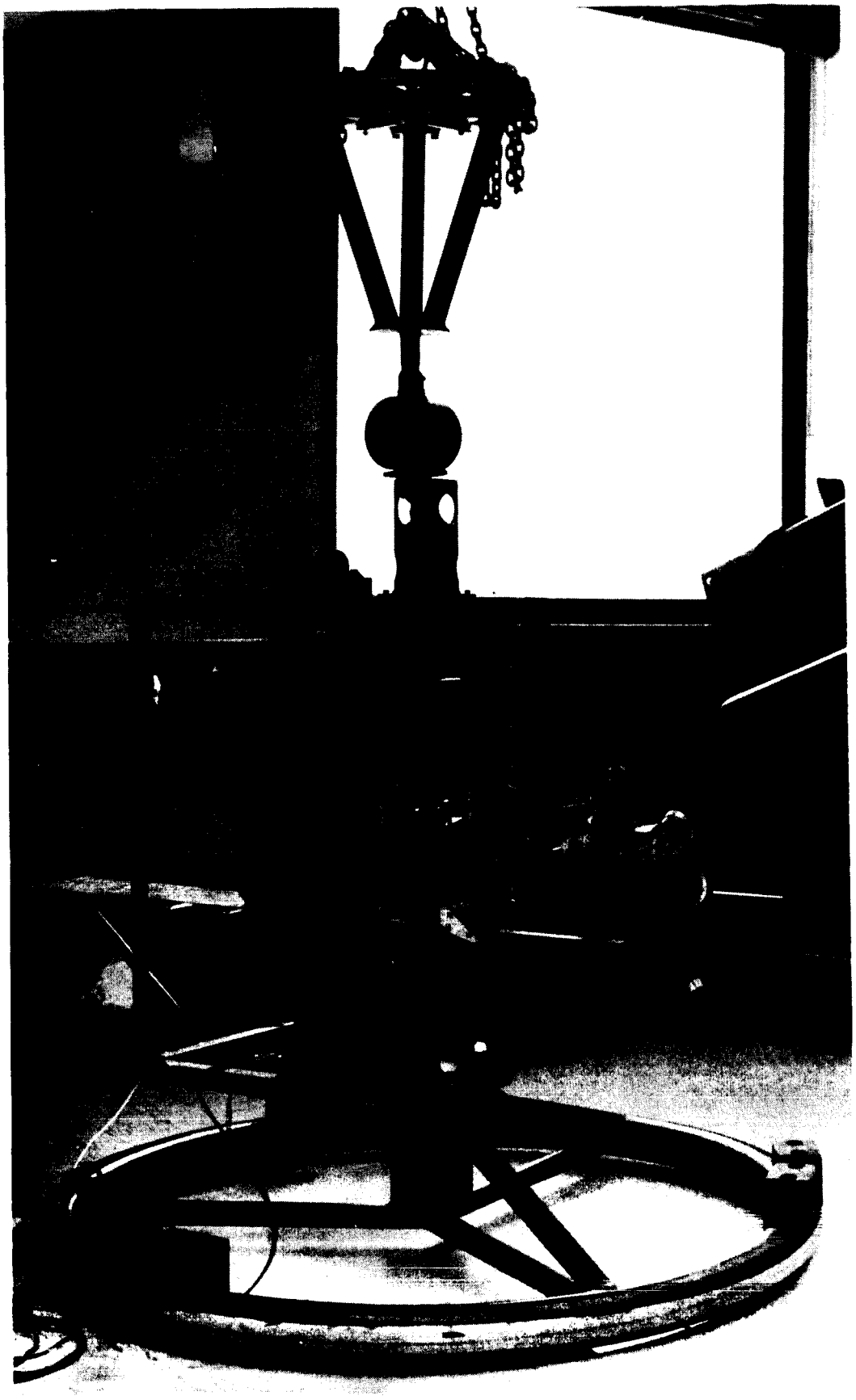

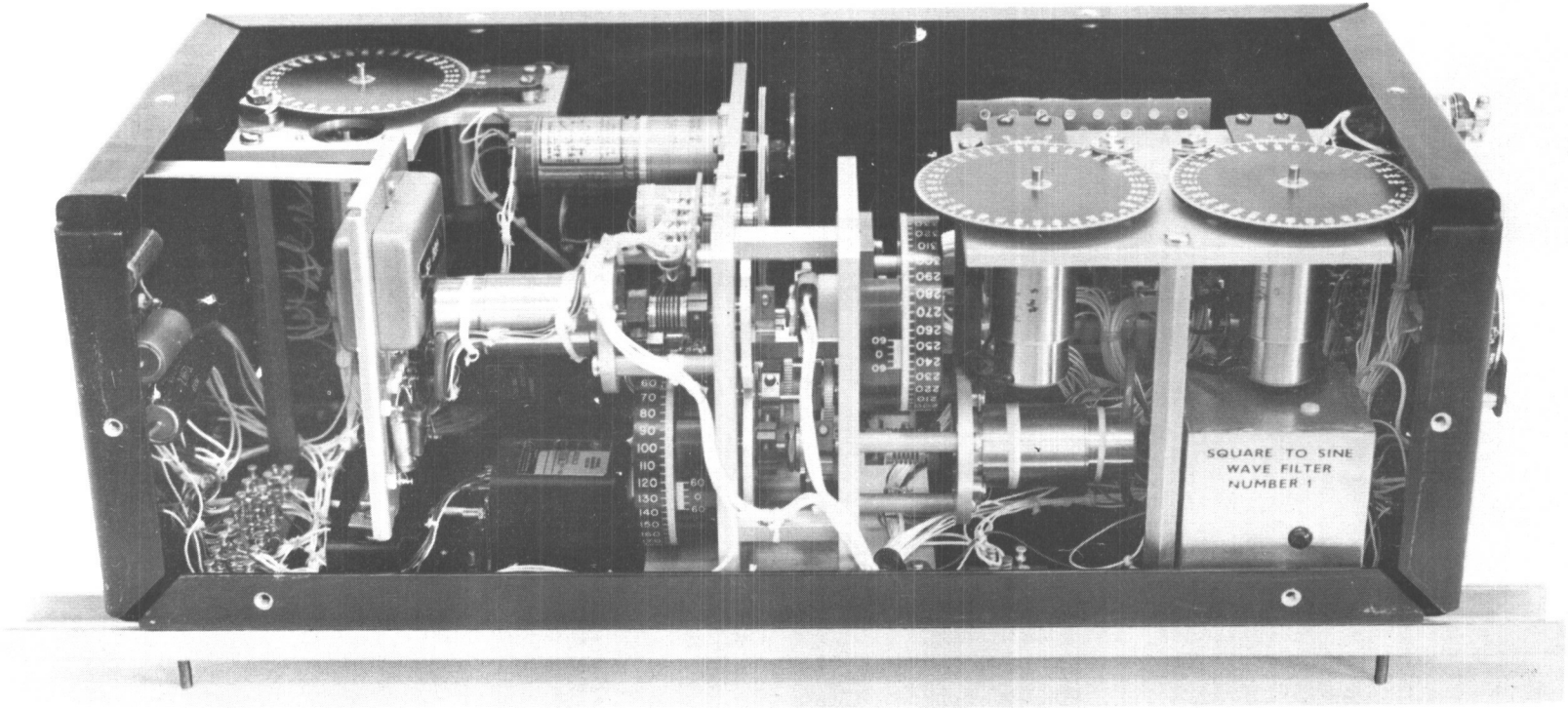
SQUARE TO SINE
WAVE FILTER
NUMBER 1